Stellingen

behorende bij het proefschrift van P.H.F. Morshuis

1. Mensen die alles te snel begrijpen zullen nooit iets leren.

2. Een goed uitgevoerd experiment kan niet mislukken. Het resultaat bevestigt of weerlegt een hypothese, waarbij weerlegging evenveel waarde heeft als bevestiging.

3. De aantasting van een isolatiemateriaal grenzend aan een holte wordt ingezet door "pitting" ontladingen. Zie paragraaf 3.4 van dit proefschrift.

4. De toestand van het grensvlak tussen gas en isolatiemateriaal bepaalt het ontladingsmechanisme in een holte. Zie paragraaf 4.2.1 van dit proefschrift.

5. Het ontwerp van een computermodel van een fysisch proces moet een "tool" zijn, geen doel.

6. Het kopieerapparaat dat in eerste instantie het tot stand komen van de democratische besluitvorming op de universiteit heeft gestimuleerd, is thans eerder schadelijk dan bevorderend.

7. Het verstrekken van een openbaarvervoerkaart aan studenten die geldig is voor stadsbussen en -trams is een grote blunder en weer een bewijs dat de fiets als vervoermiddel niet serieus wordt genomen.

8. De enorme assortimentsuitbreiding van de supermarkten is een voorbeeld van de verrijking van onze samenleving door migranten.

9. Voor de Nederlandse Spoorwegen is een vaste klant een lastige klant.

10. Ook wie geen vlieg kwaad doet slaat soms twee vliegen in één klap.

11. De beste stellingen zijn die, waarbij de lezer zich ergert dat hij niet zelf op de gedachte is gekomen.

PARTIAL DISCHARGE MECHANISMS

Mechanisms leading to breakdown, analyzed by fast electrical and optical measurements

81, Figure 4.14	*the stainless steel table has to be connected to the negative pole of the voltage source instead of to the positive pole*		
82, Figure 4.15	*change + and - in the right hand figure*		
96, eqn (5.9)	$\sigma(z+z')$	→	$\rho(z+z')$
102, line 13	see ?	→	see Figure 5.9
106, line 4	see also Chapter 4, page ?.	→	current.
144, eqn (A.2)	$\delta Q_l = C_{lk} V_k$	→	$\delta Q_l = -C_{lk} V_k$
144, eqn (A.4)	$\delta Q_l = C_{lk}/C_{kk} \delta q$	→	$\delta Q_l = -C_{lk}/C_{kk} \delta q$
144, eqn (A.5)	$C_{kl} \cdot V_l^0 + C_{kk} \cdot V_k^0 = 0$	→	$-C_{kl} \cdot V_l^0 + C_{kk} \cdot V_k^0 = 0$
144, eqn (A.6)	$C_{kl}/C_{kk} = -\left(V_k^0/V_l^0\right)$	→	$C_{kl}/C_{kk} = +\left(V_k^0/V_l^0\right)$

ERRATA

page			
6, Table 1.1	[?]	→	[56]
6, caption	IV	→	III
26, line 14	Technology [?].	→	Technology.
34, line 14	[?].	→	[59,60]
36, line 5	[?].	→	.
36, line 14	[?]	→	[89]
36, line 16	[Kärkaïnen]	→	[44]
41, line 4	see ?	→	see Figure 3.31
42, line 1	section 2.6, Figure 2.10	→	section 2.3, Figure 2.8
43, line 3	Figure 3.14b and Figure 3.14c	→	Figures 3.14a-d
47, line 7	see **3.2.2**	→	**3.3.2**
52, line 12	in Figure 3.23, Figure 3.26.	→	photograph in Figure 3.26.
61, line 29	background radiation	→	background and cosmic radiation
64, eqn (4.12)	$\mu = \gamma\exp[(\alpha-\eta)h]$	→	$\mu = \gamma\{\exp[(\alpha-\eta)h]-1\}$
67, eqn (4.19)	$\frac{\alpha}{\alpha-\eta}$	→	$\frac{\alpha-\eta}{\alpha}$
68, caption Fig 4.5	[Pfaue]	→	[70]
78, caption Fig4.11	[ ].	→	.

PARTIAL DISCHARGE MECHANISMS

Mechanisms leading to breakdown, analyzed by fast electrical and optical measurements

PROEFSCHRIFT

Ter verkrijging van de graad van doctor aan de Technische Universiteit Delft op gezag van de Rector Magnificus, prof. ir. K.F. Wakker, in het openbaar te verdedigen ten overstaan van een commissie door het College van Dekanen daartoe aangewezen, op maandag 15 november 1993, te 14.00 uur.

Door

Petrus Henricus Franciscus Morshuis

elektrotechnisch ingenieur

geboren te 's-Gravenhage

Delft University Press / 1993

Dit proefschrift is goedgekeurd door de promotor
prof. dr. ir. F.H. Kreuger

Cover design by the author
CIP-data Koninklijke Bibliotheek, The Hague
ISBN 90-6275-931-9/CIP

Printed in the Netherlands

Aan Lidewij

Contents

Summary

The discharge mechanism in voids and its evolution is important for the degradation of an insulation material under electrical stress. This thesis describes the evolution of the discharge mechanism in voids bounded by a dielectric. Time-resolved detection and optical registration were used in parallel to find a relation between discharge parameters and the stage of degradation. Especially the relation between the duration of the discharge activity and changes in the discharge mechanism were studied.

In Chapter 1 an introduction is given to discharge mechanisms in voids and to discharge detection methods.

In Chapter 2 the experimental methods used in this study are described. It makes use of the fact that information on the discharge mechanism is present in the pulse shape of the discharge current. With a *time-resolved* detection system of 1 GHz bandwidth this information was extracted from the discharge signal. Optical registration of the discharge image provided a spatial image of the discharge at the moment of detection.

Chapter 3 presents the test results on dielectric bounded voids. It was found that the discharge mechanism evolves as a function of the duration of discharge activity. Three consecutive stages could be distinguished up to the start of significant degradation of the dielectric. Each stage could be recognized by its own set of characteristic electrical and optical parameters. These stages comprise: the *streamer-like* mechanism, the *Townsend-like* mechanism and the *pitting* mechanism.

Chapter 4 discusses the discharge stages presented in Chapter 3. Different theories have been developed explaining the occurrence of the different discharge mechanisms and the transitions between them. Experiments were performed to test these theories.

Chapter 5 presents the results of numerical calculations of the discharge

current. A model of the discharge process has been developed to describe the effect of several parameters on the shape of the discharge current.

Chapter 6 shows that the knowledge of the three stages can be used for diagnostic purposes, i.e. the degree in which a dielectric is deteriorated by discharges can be determined. The moving median of the pulse width is introduced as a diagnostic tool. Further, the possibilities of time-resolved measurements on full-size high voltage components is discussed.

Chapter 1
Introduction

1.1 General

Much effort has gone into understanding and predicting electrical breakdown since the start of the electrical era at the end of the nineteenth century. Despite all the energy spent, parts of this subject are still not well understood. Especially degradation and breakdown of solid insulating materials is of constant interest.

Synthetic materials have been used as insulating materials for some decades because of their excellent dielectric properties. Since in the 1930s the techniques of polymerization were developed, modern manufacturing processes like the casting of epoxy resin and the extrusion of polyethylene have resulted in products with good insulating properties. Especially polyethylene has been used because of its low dielectric losses and high breakdown strength of test specimens. Furthermore polyethylene can easily be shaped, it is relatively inexpensive and harmless to the environment. It would nevertheless be a mistake to regard polyethylene as an ideal insulating medium. The maximum allowable field strength in practice (up to 15 kV/mm) is far below the intrinsic breakdown strength of 800 kV/mm. The reason for this discrepancy is the enormous effect of microscopic defects in the insulating medium on the life of the insulator. The ultimate goal of avoiding all inclusions and voids during the manufacturing process of insulating constructions is far from being reached. Especially voids are difficult to avoid in polymeric materials. These voids may for instance result from the curing process of crosslinked polyethylene cables and are characterized by a diameter of a few microns. They might also occur as delaminations between two dielectrics or between a dielectric and a semi-conductor due to bad adhesion. The gas in these voids has a lower permittivity than the surrounding dielectric. This results in an enhanced electric field in the void which in turn will break down long before the breakdown strength of the dielectric is reached. This *partial* breakdown or *partial discharge* has been the object of many a study since the 1920s [24].

After it had been recognized that partial discharges form a serious threat to

the life of the insulation, different measurement techniques have been developed to detect the small electric signal that is induced in the leads of a sample under test when a partial discharge occurs.

1.2 Partial discharges in voids, a literature survey

Both the mechanism [47,53,44,23,6,66] and the deleterious effect [83,55,26,91] of partial discharges have been the object of numerous studies. In describing the mechanism the theory of breakdown in a gas between metal electrodes is often used. The fact that in this particular case one has to deal with a *partial* discharge makes the mechanism, however, more complicated. This results from the fact that the discharge is limited by the dielectric boundaries and from the fact that the characteristics of the (dielectric) boundaries are time dependent.
In the following a concise outline will be given of partial discharges in voids, their mechanism and the degradation which is caused by them.

1.2.1 Discharge mechanism

The first condition for a discharge to develop is the availability of a free electron in the void, preferably near the cathode. In this case the electron can initiate an electron avalanche travelling towards the anode. Given the presence of an initiatory electron it has been found that there exists a minimum value for the breakdown voltage: the ignition voltage. This value depends on the dimensions and the contents of the void, and the temperature and the pressure in the void. Usually the height of the void and the pressure are taken as parameters.
The emission of initiatory electrons from the cathode is a stochastic process [14] and therefore a time lag
τ_s occurs after the ignition voltage U_i has been reached before an avalanche starts, see Figure 1.1. The electric field in the void is too low for field emission, therefore the production of initiatory electrons will result from cosmic radiation and background radiation [14,66]. The contribution from each kind of radiation is estimated to be about 2×10^{-5} electrons $s^{-1}\cdot cm^{-3}\cdot Pa^{-1}$, resulting in a total amount of about 4×10^{-5} electrons $s^{-1}\cdot cm^{-3}\cdot Pa^{-1}$. Using these data it can be inferred that the electron production rate in a void of 1 mm^3 at ambient conditions (1000 hPa) is about 4×10^{-3} electrons per second.
This results in a statistical time lag of about 10 minutes!

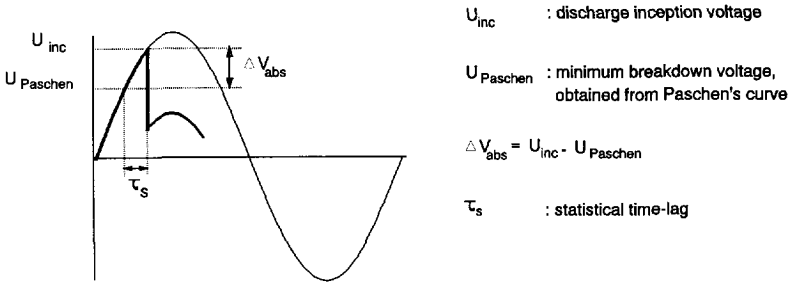

Figure 1.1 Relation between the statistical time-lag τ_s and the overvoltage ΔV_{abs}.

The probability *P(t)* of an avalanche starting in time t is given by [23]:

$$P(t) = 1-\exp\left[-\frac{t}{\tau_s}\right] \tag{1.1}$$

The presence of even small amounts of water vapor reduces the statistical time lag significantly due to the electrons detached from water molecules [56]. In practice τ_s can therefore considered to be in the order of milliseconds [24,56]. These values are several orders of magnitude larger than the formation time of an electron avalanche. Therefore considerable overvoltages[1] can be expected as is illustrated in Figure 1.1. The overvoltage is a major parameter determining the development of the discharge. Devins [23] has made an extensive study on the effect of the overvoltage on the discharge mechanism. A DC voltage was applied to an air gap between a dielectric and an electrode. The overvoltage was produced by superimposing the signal of a pulse generator on the DC voltage. Two different discharge mechanisms were introduced and named "Townsend-like" and "streamer-like".
In literature different physical mechanisms of discharges are described giving rise to a sometimes confusing nomenclature. An overview of the most commonly used nomenclature is shown in Table 1.1. In the discussion of the different discharge types some attention is given to the overlap of these terms.

[1] Here the absolute overvoltage ΔV_{abs} is meant, as opposed to the relative overvoltage ΔV used later in this thesis.

	Discharge nomenclature	Origin	In this study
	spark type	classic breakdown theory [?]	
I	streamer-like type	Devins [23]	streamer-like type
	fast developing type	Luczynski [53]	
	Townsend-like type	Devins [23]	
II	pseudo-glow type	Bartnikas [5]	Townsend-like type
	slowly developing type	Luczynski [53]	
	glow type	classic breakdown theory [?]	
II[a]	pulseless type	König [48]	Townsend-like type
	swarming micro partial discharge	Tanaka [83]	
III	corona-like type	Morshuis [61]	
	pitting type	Morshuis [64]	Pitting type

Table 1.1 Overview of the nomenclature of discharge mechanisms. During prolonged discharge activity the mechanism evolves from stage I to stage IV.

Streamer-like and Townsend-like discharges

The Townsend model of a discharge is that of a self-sustaining avalanche with successors initiated at the cathode. On the other hand the streamer breakdown model is based on the initiation of successive avalanches started in the gas by high energetic photons originating from the ionization in the high local space charge field.
Of major importance is the fact that there are two opposing forces determining the character of the discharge in a gap between dielectrics:

- the ionization process in the gap enhancing the field by the positive ion space charge
- the displacement current in the gap due to the current flowing in the external circuit, reducing the electric field in the gap

Figure 1.2 shows the total field in the void for different overvoltages. The

effect of the overvoltage can be clearly recognized in the fast build up of the space charge field for the larger values of the overvoltage ΔV_{abs}.

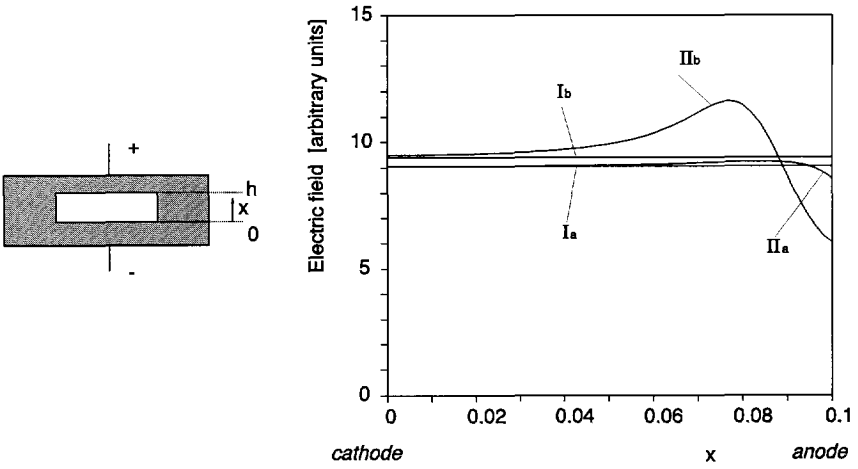

Figure 1.2 Total field in the gap consisting of Laplace field (I) and space charge field (II). a) $\Delta V = 1\%$ b) $\Delta V = 5\%$

With lower overvoltages the positive ion space charge field is outweighed by the reduction of the electric field due to the displacement current. This results in a decrease of the size of the consecutive avalanches. It was shown [23] that for a certain, critical value ΔV_{cr} of the overvoltage an increasing size of subsequent avalanches was obtained. For this overvoltage a critical space charge density is obtained. The value of the overvoltage to obtain this space charge density can be calculated. Below this *critical* overvoltage the Townsend-like mechanism is operative, above ΔV_{cr} the streamer-like mechanism is operative. It was found that the critical value of the overvoltage increased with decreasing gap, increasing thickness d and permittivity of the dielectric ε_r and increasing ignition voltage $U_{Paschen}$ of the air gap h.
For the discharge magnitude of Townsend-like discharges Devins found that it was linearly related to the overvoltage but independent of the gap height. The magnitude of streamer-like discharges however increases with increasing gap height and is rather insensitive to the overvoltage.

Glow, pseudo-glow and swarming micro partial discharge

Referring again to Table 1.1 two different names are given to a discharge mechanism that occurs after many hours of discharge activity. Often, after

prolonged discharge activity the discharges seem to disappear. Authors [73,67] have contributed this phenomenon to the gradual short circuiting of the void by conductive deposits at the walls of the void. "Disappearance" of the discharge pulses can, however, also be caused by a change of the discharge *mechanism*, leading to discharges that become to small to be detected by the conventional discharge detector [6,83]. This phenomenon is sometimes called "glow discharge" [6] or "swarming micro partial discharge" [42,65]. For a glow discharge the gap breakdown voltage is equal to the remanent voltage after breakdown. For pseudo-glow discharges the gap breakdown voltage is only slightly above the remanent voltage. Both types are characterized by a diffuse glow in the gap and lead to a (semi-)continuous series of minute discharges extending over several milliseconds.
As was already stated at the beginning of this chapter, the nomenclature of discharge mechanisms depends mainly on the author and is to some extent overlapping. In Table 1.1 the different discharge types are grouped together as was considered realistic. Three discharge types are left: the fast developing streamer-like discharge, the slowly developing Townsend-like discharge and the pitting discharge to be described later in this thesis. The glow and pseudo-glow discharges are grouped together because here the glow type is considered as the extreme case of the pseudo-glow or Townsend-like discharge (over-voltage $\Delta V \rightarrow 0$). In a recent discussion between Danikas and Bartnikas/Novak in [18] the latter elaborated on the discharge terminology as they defined it. They classified both streamer-like and Townsend-like discharges as "spark" discharges. Furthermore, they believe both discharge mechanisms to be governed by the Townsend mechanism.[2]

[2] This paper was published in the last stage of the preparation of this thesis, so no detailed discussion was possible.

1.2.2 Degradation caused by discharges

Streamer-like discharges are by some authors believed to be more damaging due to their large magnitude when compared to Townsend-like discharges [24,72]. Other authors believe the Townsend-like or glow discharge to be the most deleterious [21,83,45]. The author of this thesis, however, believes that the most extensive degradation takes place when a third discharge type, named "pitting discharge" is active [64], in a stage following the streamer-like and Townsend-like stages.
The deleterious effect of the discharge activity is revealed in a number of ways:

- by the chemical reactions between oxygen and ozone and polymer radicals at the surface of the void
- by the bombardment of the surface of the void by high energy ions resulting in the formation of polymer radicals
- by the deterioration of the void surface caused by UV radiation

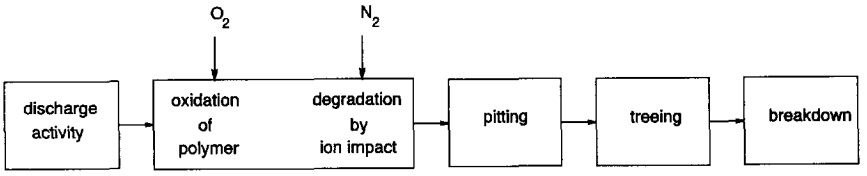

Figure 1.3 Simplified schematic diagram of the processes leading to breakdown.

According to Tanaka [83] discharges in nitrogen cause pits at the circumference of the void. These pits are considered to be the result of a continuous bombardment by streamer-like discharges in a small area of the void surface. If oxygen is present, highly oxidative products are created in the discharge process: O, O_3 and O_2^-. Due to the chemical reactions in the gas phase, hydrogen, carbon monoxide, methane and carbon dioxide are produced [91,83]. Reactions can take place between these products and polymer radicals. Gamez-Garcia et al. [27,26] have shown that, as a result of these chemical reactions, acids are produced. These acids are of a conductive nature and it is assumed that they reduce the voltage across the void and extinguish the discharge [27,67]. Voids which are initially filled with air are supposed to be oxidized uniformly within a layer thickness of some μm [15]. When all the oxygen is consumed it is assumed that the bombardment by nitrogen ions

causes pitting and subsequently tree initiation [83], as can be seen in Figure 1.3.

1.3 Discharge detection and evaluation

The discharge reveals itself in a number of ways [50]. It is accompanied by

- a charge displacement that causes a current in the leads to the object,
- radiation emitted by excited particles falling back to a lower energy state,
- ultra-sonic sound,
- heat generated by particle impact,
- chemical reactions.

Of these five the first two characteristics were used extensively in the study described in this thesis. A short chronological survey will be given of the methods which were developed to detect the optical and electrical signals.

1.3.1 Electrical detection and evaluation

In order to detect the electric pulse generated by the discharge different kinds of apparatus have been developed in the past. They can be divided in four main groups:

- tan δ measurement
- classic broad band detection
- ultra-wide band or time-resolved detection
- integrating bridge detection

tan δ measurement
Historically seen, since the development of the Schering bridge [75] it became possible to detect the presence of discharges, making use of their power dissipation (tan δ). This method however is not sensitive and other systems were developed which make use of the availability of oscilloscopes [29].

Classic detection
Some 50 years ago [2] first the RCL pulse detectors were introduced, later on followed by the RC pulse detectors which were known as broad band detectors. With the detectors which are nowadays commonly used a high

sensitivity and a good time resolution are obtained. The circuit shown in Figure 1.4a is the basic circuit for classic discharge detection.

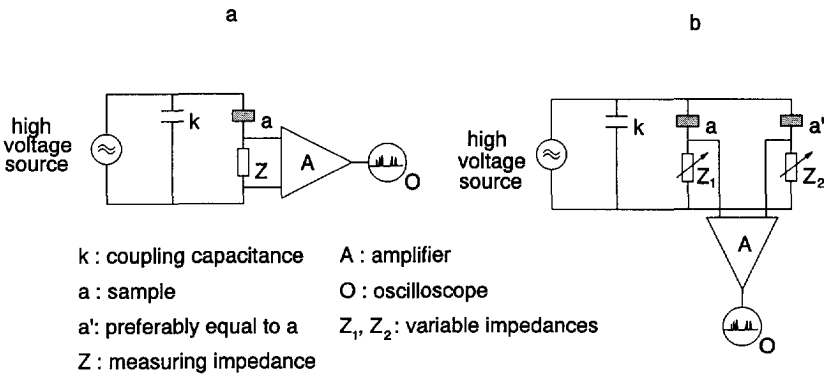

Figure 1.4 Classic detection system
a. straight detection
b. balanced detection

In order to suppress external disturbances the circuit can be balanced as shown in Figure 1.4b. Using this kind of system information is obtained on the discharge magnitude and the phase position relative to the 50/60 Hz voltage cycle. With the use of computer systems and other advanced electronic instrumentation it became possible to store and statistically process the data of the discharge process.

In 1969 Bartnikas [4] and in 1976 Kärkkainen [44] introduced the multichannel analyzer for obtaining discharge pulse height distributions. In 1978 Tanaka and Okamoto [84] developed a system capable of providing the three main pulse distributions: pulse height, pulse time interval and pulse phase distribution. They suggested the use of statistical moments like skewness and kurtosis to characterize these distributions. In the 1990s discharge analyzers were built which make use of the phase distribution of the discharge pulse height and of the discharge intensity [34,25,38].

In 1991 Gulski [34] extended the idea of Tanaka and built a discharge analyzer describing the discharge phase distributions with a set of 15 parameters (phase-resolved analysis). Based on the idea that different discharge sources are represented by a characteristic set of values of these 15 parameters (a so-called finger print), he introduced the recognition rate. The finger prints of a large number of different discharge sources were stored in a data base and used for the recognition of unknown discharge sources.

Time-resolved detection

The above described detection and evaluation methods make use of a relatively small bandwidth (up to 500 kHz) and record the discharge magnitude and the phase position. But for the study of the discharge *mechanism* these methods are not well suited. However, when the pulse shape of the discharge current is recorded with sufficiently high bandwidth of approximately 1 GHz, information on the discharge mechanism can be obtained.
Raether [71] was one of the first, in the 1950s and 1960s, to use an ultra-wide band or *time-resolved*[3] system for the study of the discharge process on a hun-

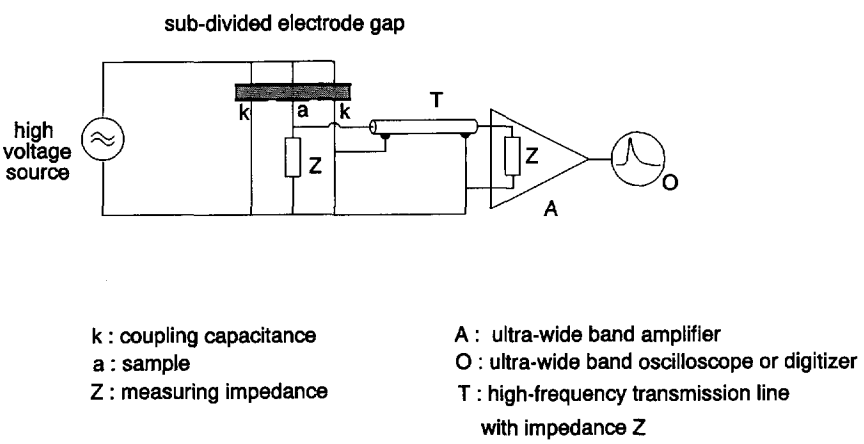

Figure 1.5 Basic diagram of a set-up for time-resolved detection.

dred nano second scale. Figure 1.5 shows the basic diagram of a time-resolved measuring set-up. With the introduction of fast digitizers and digitizing oscilloscopes in the last decade time-resolved measurements gained in importance for the study of the discharge mechanisms. The physics of the development of avalanches in gases was studied [89,88] but also the pulse characteristics of the discharge signal as related to the deterioration of the dielectric were examined [60,59,39,21].

[3] *time-resolved* as opposed to *phase-resolved.*

1.3.2. Optical detection and evaluation

In order to obtain permanent images of the light emitted by discharges photographic film was used first. Studies [43,69,57] were performed on the Lichtenberg figures [52] created by surface discharges.
This method, however, was only able to register the light in the visible spectrum for relatively high intensity discharges and the sensitivity could be obtained only by accumulating the light for a long period (minutes to hours). Mason [54], however, obtained some good results using this method for discharges in artificial cavities.
Later, due to the development of the photomultiplier, discharges with a much lower intensity could be registered. To obtain an enhanced sensitivity in the ultra violet region special photo cathodes were used. Furthermore, the temporal development of the light emitted by the discharge could be studied because of the short rise times (typically ≈ 1 ns) of photomultipliers in pulsed applications. Another method to register fast developing events is the Schlieren photography [76]. In this case the lens is kept open and a very sensitive photographic film is transported behind the lens at a very high speed. In the last decades image converters [30] and image intensifiers [63,61,39] were used more and more in combination with a video camera. The combination of a double image intensifier with a video camera was used in the underlying research and will be discussed in chapter 2.

1.4 Object of the present study

In the present research project the discharge mechanism in voids was studied making use of the information present in the time-resolved discharge parameters and the light emitted in the discharge process, see Figure 1.6. Especially the relation between the duration of the discharge activity and changes in the discharge mechanism were studied with a focus on the degradation of the dielectric.
One of the goals was to determine whether the occurrence of different types of discharge mechanisms is determined in a pure stochastic way or whether there is an evolution of the mechanism determined by a set of specific parameters. There are many indications that the discharge process is not time-invariant. Good examples are the reduction of the field in a dielectric bounded void due to the deposition of conductive discharge by-products and the evolution of the discharge regime. Especially the effects of these by-products on the discharge mechanism are regarded as important objects for further

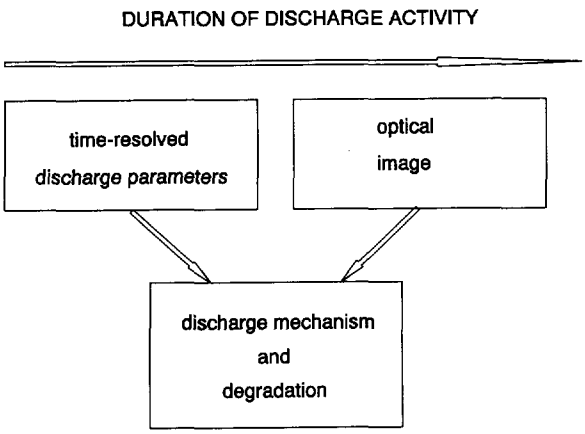

Figure 1.6 Study of the discharge mechanism and degradation process using time-resolved detection of discharge pulses and optical analysis of the discharge image.

study.
Another important goal was to find an explanation for the transitions between the different discharge mechanisms. Except for the academic interest, it is also of practical importance to know the causes for a specific discharge mechanism.

Chapter 2
Experimental methods

In this Chapter the following topics related to the experiments will be discussed:

- Samples containing voids
- The time-resolved detection technique
- The optical detection technique

2.1 Samples

All samples consisted of artificially introduced voids in solid insulating materials. The main dielectric material used was low density polyethylene (LDPE) with different contents of stabilizers and anti-oxidants (see Table 2.1). The basic material consisted of blown sheets of different thickness. The sheets were transparent, a requirement to obtain access to the void for the optical system. Other dielectric materials like polycarbonate (PC), polyester and polypropylene (PP) were used in a limited number of experiments. In these cases the basic material consisted of rolled or blown sheets of different thickness.
For all materials the samples were constructed with the "sandwich" method, creating disc-shaped voids, see Figure 2.1.
Special attention was paid to avoid sharp edges that might induce unwanted discharges at the circumference of the void. Before assembly, the sheets were inspected for irregularities and cleaned with cotton wool drenched in alcohol.
A minor amount of samples was produced with a method shown in Figure 2.2. This method was developed to create spherical and elliptical voids with less interfaces between sheets. The base material consisted of low density polyethylene granules. Each sample was produced in a two-step process. First, two polyethylene discs were pressure-moulded with a stamp in the shape of a half sphere or half an ellipsoid. The process temperature was 150 °C and the

Material	Additives	Density [g/cm^3]	DC volume resistivity [Ω·cm]	Relative dielectric constant (50 Hz)
LDPE	none	0.922	$>10^{16}$	2.2
LDPE	anti-oxidant	0.922	$>10^{16}$	2.2
LLDPE	anti-oxidants	0.918	$>10^{16}$	2.2
LDPE packaging material	?	?	$>10^{16}$	2.2
PP	anti-oxidant	0.90	$>10^{16}$	
PC	?	1.28	$8x10^{16}$	3.0
Polyester	?	?	$>10^{16}$	3.5

Table 2.1 Material parameters of the insulating materials.

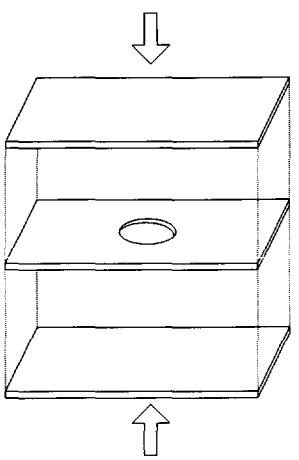

Figure 2.1 Sandwich method for the preparation of disc-shaped voids.

pressure was 40 kN/m^2. Subsequently, the two discs were pressed together with a pressure of 35 kN/m^2 to avoid the enclosure of unwanted air pockets. In this case spherical and elliptical voids were obtained, with only one in-

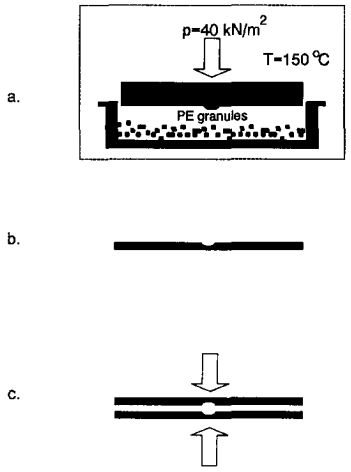

Figure 2.2 Method used to create spherical and elliptical voids in polyethylene.

terface between the two sheets.

2.3 Time-resolved detection

Several techniques can be applied to detect and measure partial discharges. Classic detection makes use of the quantity q, the apparent charge or the discharge magnitude. These methods however yield but little information on the discharge *process*. Measurement of $i(t)$, the apparent discharge current, is more promising, see Figure 2.3. With a preservation of the pulse shape of $i(t)$ a direct correlation with the charge carrier movement in the void is obtained when the parameters of the test circuit are known.
To examine the dynamics of the discharge process, a measuring system was developed for the registration of discharge pulses.
In order to relate the shape of the discharge pulses to the physics of the discharge process a *time-resolved* detection system was built. Such a system has a number of characteristics. The bandwidth of the system must be larger than the highest frequency component of the discharge signal. Also, the discharge return path should be as short as possible to minimize travelling wave problems and it should be of low inductance to prevent oscillations.
To accomplish all this a compact, subdivided electrode arrangement was used,

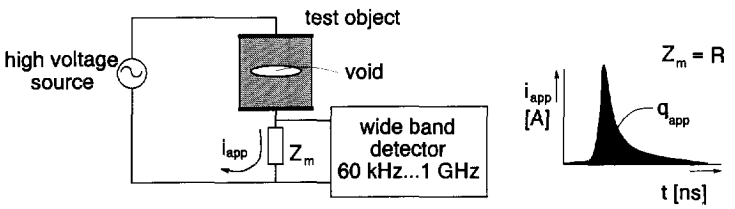

Figure 2.3 Measurement of the shape of the discharge current.

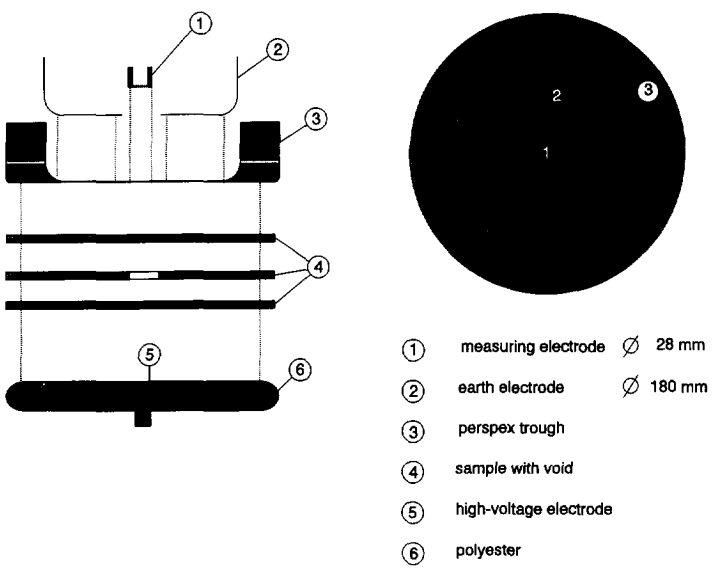

Figure 2.4 Experimental electrode set-up for time-resolved measurements.

as shown in Figure 2.4.

Electrode arrangement

A grounded guard electrode, coaxial with the measuring electrode, in combination with the high voltage electrode forms the coupling capacitor. In

order to obtain a small stray capacitance to earth, the diameter of the measuring electrode has to be chosen as small as possible. On the other hand, it should be large enough to prevent charge to be induced in the co-axial guard electrode. With the use of the Ramo-Schockley theorem [77], see Appendix A, an optimal relation between the diameter of the measuring electrode D_m, the diameter of the void D and the separation between high voltage electrode and measuring electrode d_{tot} can be obtained, see (2.1).

$$d_{tot} \leq 0.25 \cdot (D_m - D) \tag{2.1}$$

In the electrode arrangement used in this study the diameter of the measuring electrode was 28 mm, the largest void diameter used was 10 mm and the electrode separation was 4 mm. Thus, condition (2.1) is fulfilled.

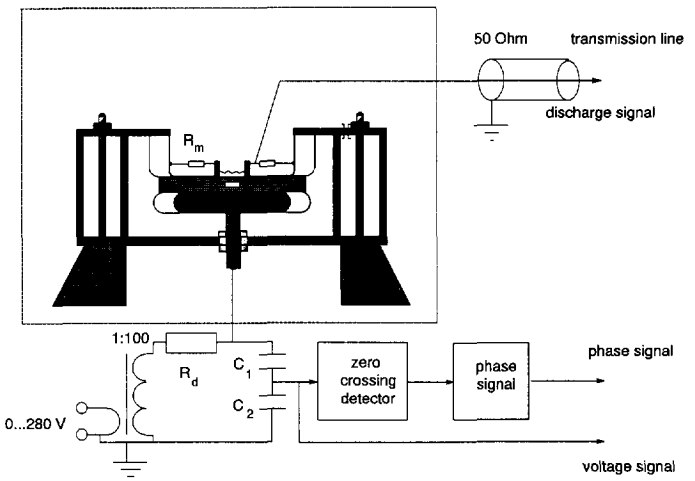

Figure 2.5 High voltage test set-up.

Discharge path

To uncouple the transient discharge current from the secondary winding of the high voltage transformer, a 1 MΩ resistor R_d was placed between the transformer and the test cell (Figure 2.5). In this way a short discharge path with a length of approximately 4 cm is obtained, smaller than a quarter of the shortest wavelength ($\lambda \approx 20$ cm) present in the discharge signal. Travelling wave problems are thus avoided [51]. R_d also limits the current in the high-voltage circuit in case of a breakdown.

The time constant of the measuring circuit

In order to maintain the original shape of the discharge signal, the time constant τ_c of the measuring circuit must be as small as possible, preferably much smaller than the time constant τ_d of the discharge itself. The value of τ_d is mainly defined by the speed of development of either the avalanche processes (Townsend-like discharges) or the process of streamer formation (streamerlike discharges). In the former case the values of τ_d are in the range between 2 ns and several hundreds of ns for voids between 40 μm and 1 mm height [63]. In the latter case values of τ_d are much smaller, typically some hundreds of picoseconds [64,90].

For the calculation of the time constant τ_c, the circuit was regarded as a system of capacitors and resistors. This is a simplification, because the void with space charge due to the discharge process cannot physically be regarded as a capacitance. The ins and outs of this subject have thoroughly been discussed by Pedersen and his co-workers [16].

For a first order calculation of τ_c the above assumed equivalent circuit is useful. Figure 2.6 shows the capacitance equivalent of the measuring circuit.

The time constant τ_c can now be calculated as follows:

$$\tau_c = R_m \cdot \left\{ C_s + \frac{1}{\frac{1}{C_v} + \frac{1}{C_d} + \frac{1}{C_c}} \right\} \tag{2.2}$$

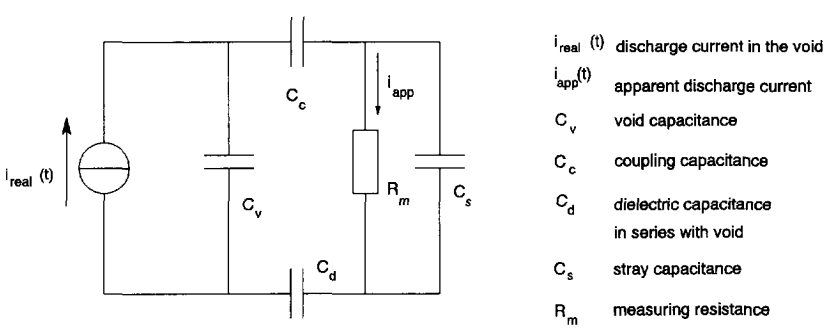

Figure 2.6 Capacitive equivalent of the measurement circuit.

The self inductance of the discharge path is negligible because of the compact electrode arrangement. Table 2.2 shows the calculated value of τ_c for the

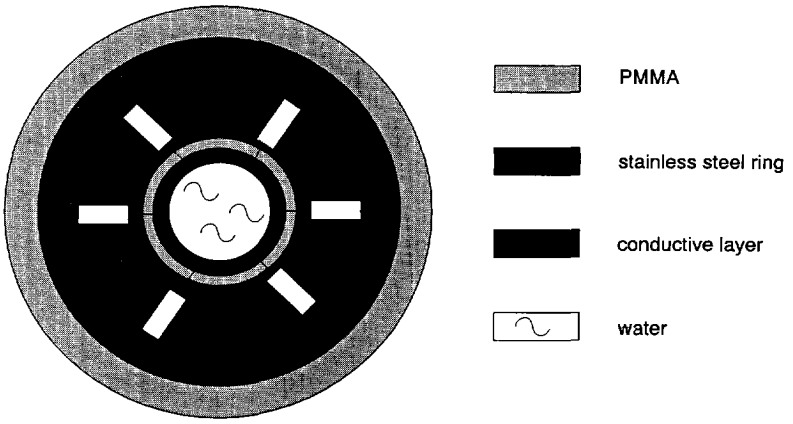

Figure 2.7 Top view of measuring electrode with a measuring impedance consisting of six resistors of 300 Ω each.

samples where the geometry of the samples has some effect on the circuit parameters. It can be concluded that the calculated value of τ_c of about 200 ps is well acceptable for measuring transients with the above mentioned time constant τ_d of some hundreds of pico seconds.

Measuring impedance

Unless stated otherwise, in all experiments a measuring resistor R_m of 50 Ω was used. In order to minimize the inductance in the discharge path, six low inductance resistors of 300 Ω each were radially connected as is shown in Figure 2.7.

Apparent versus real discharge current

The *apparent* value of the discharge transient is measured, instead of the desired *real* value in the void (see Figure 2.6). The apparent value is related to the value of the discharge transient in the test circuit. In order to obtain a high sensitivity the apparent value should not be much smaller than the real value. The method for calculating the real value of the charge displacement in the void is discussed in Appendix A. Table 2.2 shows the relation between the apparent and real values of the charge displacement. It can be deduced that from a void height of 0.4 mm onwards a satisfactory sensitivity is obtained. For smaller voids the sensitivity is rather low because of the dielectric in series with the sample.

h [mm]	D [mm]	τ_c [ns]	i_{app}/i_{real}
0.05	1	0.18	0.035
0.1	3.2	0.18	0.068
0.1	10	0.18	0.068
0.4	3.2	0.18	0.225
0.4	10	0.18	0.225
1.0	3.2	0.17	0.421
1.0	10	0.17	0.421

Table 2.2 Calculated values of τ_c and i_{app}/i_{real} for different sample geometries. *h:* void height, *D:* void diameter

Transmission and detection of the discharge signal

The transient voltage across R_m is transmitted by a 50 Ω transmission line to a scan converter or to a digitizing oscilloscope. The transmission line is terminated with 50 Ω, so that half the discharge current is measured and the resulting resistance is reduced to 25 Ω.

The device most frequently used was a 400 Msamples/second digitizing oscilloscope (HP 54502A) with a single shot analogue bandwidth of 100 MHz. Although sufficient for distinguishing the pulses from the three different discharge mechanisms, the results obtained with streamerlike pulses should be interpreted with care. The rise time τ_d of the streamerlike pulses is typically smaller than 1 ns, whereas the rise time[1] of this oscilloscope is 3.5 ns. For this reason some tests were repeated with a scan converter and two oscilloscopes[2] of resp. 1.5 GHz and 1 GHz single shot bandwidth.

[1] Rise time figures are calculated from: $\tau_r = 0.35/\text{Bandwidth}$.

[2] By courtesy of Hewlett Packard (HP54720D) and Tektronix (DSA 602A and SCD1000)

2.3 Automized registration of time-resolved discharge parameters

During the ageing tests with prolonged voltage application an automatic measurement procedure was used. This procedure was such that all the important discharge parameters were measured.
To accomplish this, the digitizing oscilloscope was controlled by a personal computer taking care of the following tasks:

a control of the settings of the oscilloscope, like full scale sensitivity and trigger level.
b control of the measurement of the discharge pulse parameters by the oscilloscope.
c data transport
data storage
on-line data representation.
d on-line interface between oscilloscope and operator

a Due to the dynamic range of the discharge pulse magnitude (maximum: 400 mA, minimum: $\leq$ 40 μA) the full scale sensitivity and trigger level of the oscilloscope had to be changed cyclically. After a pre-defined time interval the sensitivity and trigger level are respectively lowered and raised one step. Having arrived at the last step the sensitivity and trigger level are set to their maximum, respectively minimum values. In this way the oscilloscope has the properties of a multi channel analyzer. Table 2.3 shows the sensitivity and trigger levels used in the above procedure.
b When the oscilloscope is triggered by a discharge pulse, the following pulse parameters are measured:
- pulse height
- rise time between the 10% and the 90% level
- pulse width between the 50% levels
- pulse width between the 20% levels.

Further, the discharge ignition phase angle is measured. The measurement of the pulse parameters by the oscilloscope is a relatively slow process and takes about 1 second, resulting in a pulse registration rate of about 1 registration per second.
The pulse width between the 20% pulse height levels was measured to account for pulses with a shape as in Figure 2.8.
To detect both the peak at the beginning of the pulse and the width of the plateau thereafter, the pulse width at 20% of the maximum of the pulse was

cycle #	full scale sensitivity [mA]	trigger level [mA]
1	0.02 - 0.64	0.02
2	0.2 - 1.6	0.2
3	0.4 - 3.2	0.4
4	2 - 16	2
5	10 - 80	10
6	50 - 400	50

Table 2.3 Settings of the oscilloscope for the different cycles.

measured as well.

c After the measurement the values of the pulse parameters are stored in the memory of the computer for later evaluation. At the same time these data are used for on-line representation of the discharge process. Figure 2.9 shows an example of data representation on the screen of the

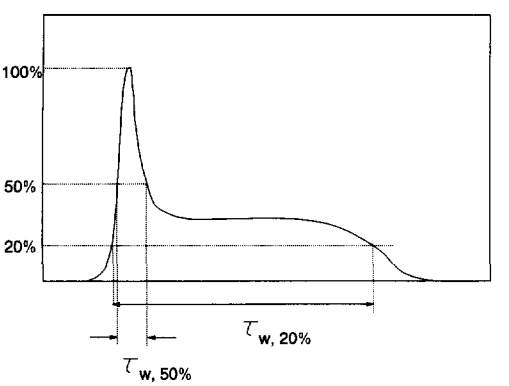

Figure 2.8 The pulse width between the 20% levels of the pulse height ($\tau_{w,\,20\%}$) for pulses with a peak and a plateau.

monitor. Phase distributions of both discharge pulse height and discharge

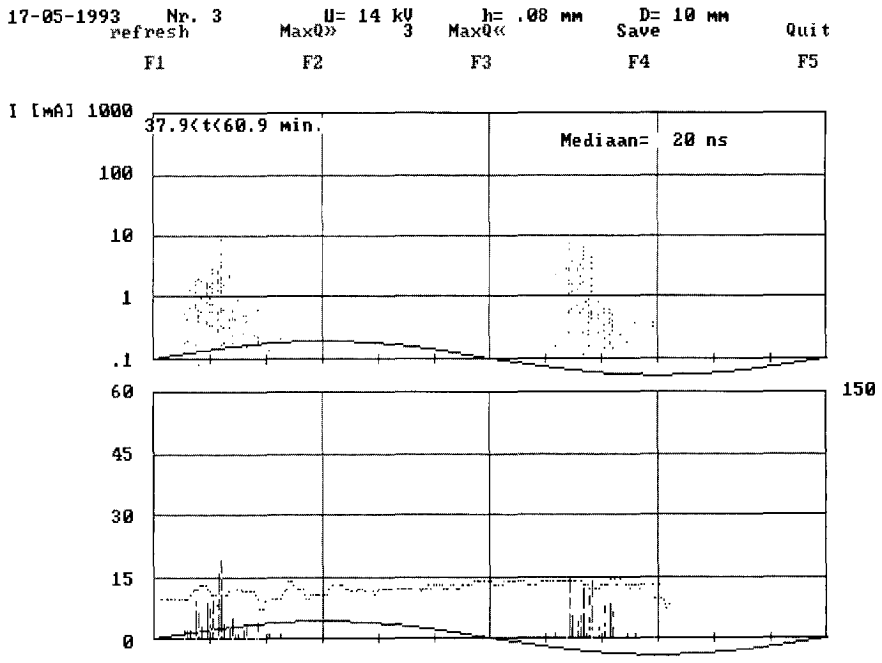

Figure 2.9 Example of on-line data representation on the monitor.

intensity are shown. Additionally, discharge pulses belonging to different discharge mechanisms are represented in different colors. This is performed after measurement of the pulse width which is compared with the expected pulse width of a Townsend-like discharge.

d During a test the operator can change the settings of the equipment. For instance, when the amplitude of the discharge pulses decreases with time, the number of steps in the process of cyclical change of sensitivity and trigger level can be decreased.

2.4 Optical detection

To obtain information on the spatial distribution of the discharge in the void, additional measurement facilities are necessary. Optical analysis of the light emitted by the discharges enables tracing of the exact location of a discharge and therefore the area where deterioration of the dielectric may take place. In

order to correlate the discharge image with the electrical discharge pulse, the optical system has to be gated. In this way the optical and electrical system can operate synchronously.
For the optical study of the discharge events a video camera with a two stage image intensifier was used. The first stage consisted of a second generation multi-channel plate with variable gain. A first generation image intensifier was used in the second stage. In this way an overall sensitivity of 10^{-5} lux was obtained. The photocathode was treated for an enhanced sensitivity in the blue part of the spectrum and the near ultra-violet (an S20 photocathode was used).
Further, the photocathode could be gated in order to make photographs with exposure times ranging down to 200 ns. The video frames were digitized by

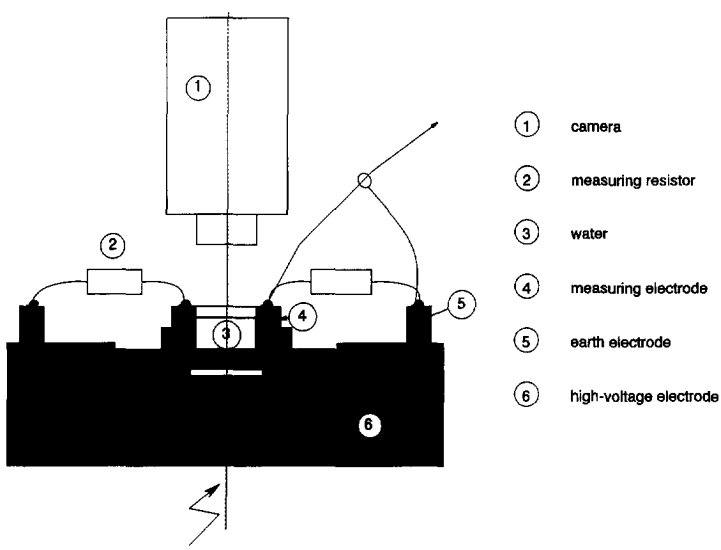

Figure 2.10 Construction of the measuring electrode in order to obtain optical access to the void.

a frame grabber and further processed with image processing software TIM developed by Delft University of Technology [?].
In order to obtain optical access to the void special requirements were imposed on the electrode system. A common solution for the problem of getting optical access is to evaporate a very thin and transparent gold layer on

top of the sample. In the present case, however no good compromise could be obtained between the required conductivity and the required transparentness.
Another solution was found. The measuring electrode was made transparent by using the conductive properties of water with dissolved NaCl (see Figure 2.10). Although the water, the perspex discs and the polyethylene sheets absorb a large part of the UV radiation of the discharges in the void, the sensitivity of the camera was sufficient to register the radiation in the visible region of the spectrum. Most of the radiation originates from the nitrogen 2nd positive $C^3\Pi_u$ - $B^3\Pi_g$ groups with wave lengths between 270 nm and 550 nm and a maximum at 337 nm [85,33]. A Schneider f0.95 lens was used to obtain the high sensitivity of 10^{-5} lux. The total light amplification of the system could be varied within a wide range to account for the different luminosities of the different discharge types. Figure 2.11 shows a block diagram of the optical system. As can be seen in Figure 2.10 the camera faces the void surface perpendicularly and the radial extension of a discharge is registered. The spatial resolution of the system was limited by the camera resolution: 350 lines per mm. With the used viewing angle this resulted in a resolution of 0.07 mm in the void.

2.5 Synchronization of optical and time-resolved detection

In order to compare the optical image of a single discharge with the electrical transient produced by that discharge, the optical and electrical system were synchronized.

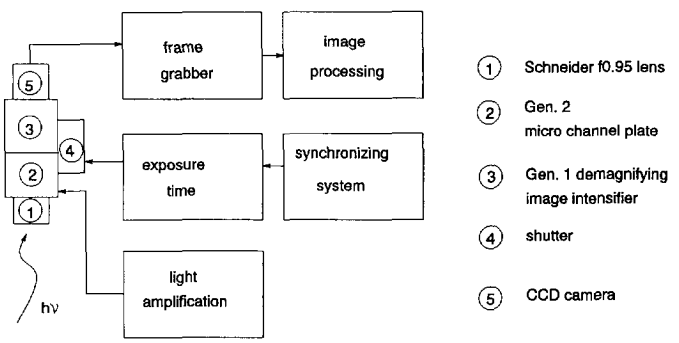

Figure 2.11 Block diagram of the optical system

The basic idea is simple. A framegrabber and an oscilloscope operate in a master-slave configuration. The framegrabber control unit supplies an output pulse that arms[3] the oscilloscope and opens the shutter of the camera. If the oscilloscope is triggered by a discharge it sends a trigger output pulse to a control unit that disarms the oscilloscope and closes the shutter of the camera within 100 ns.
Discharge pulses can be captured at different preset phase angles of the test voltage. Figure 2.12 shows a diagram illustrating the operation of the synchronic measurements.

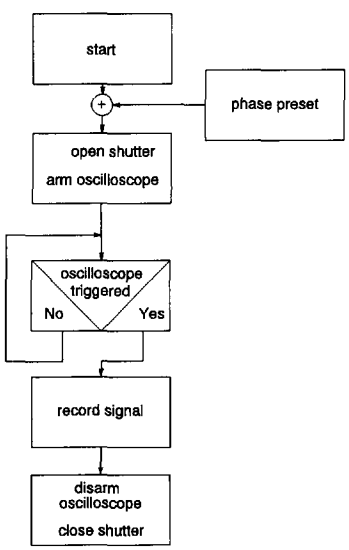

Figure 2.12 Operation of the synchronic opto-electrical measurements.

[3] i.e. the oscilloscope starts waiting for a trigger.

The time resolution of the system is limited by the minimum exposure time of the camera, approximately 200 ns. Discharges igniting within this time interval are integrated by the camera in one frame.
The optical system supplies spatial resolution as well. In chapter 3 it is shown that in some instances multiple discharges ignite within a very short time interval of a few nanoseconds. Because of the spatial resolution of the optical system it became clear that more than one discharge event was present. The electrical system was proved to be too slow in this case and recorded a single pulse as a result of superposition of several pulses.

Chapter 3
Evolution of the discharge mechanism

In this chapter the results are presented of discharge measurements on samples with artificially created voids during prolonged electrical stress.
The experimental set-up as described in Chapter 2 was used for the opto-electrical studies of the discharge process. Voids of different geometry were tested, flat and square, with a void height ranging from 30 μm to 2 mm and a void diameter between 1 mm and 20 mm. For an overview of void dimensions see Table 3.1.

	height [mm]								
diameter [mm]	0.03	0.05	0.1	0.2	0.4	1.0	1.8	2.0	3.7
1.0				■			■		
3.2	■	■	■	■					
5.0	■	■	■	■	■	■			
10			■	■	■	■	■	■	■
20			■	■			■	■	■

Table 3.1 Overview of void dimensions used in the experiments.

Unless stated otherwise, the samples described in this chapter were made of low density polyethylene. A small number of experiments was performed with other dielectrics: polypropylene, polyester and polycarbonate.
Monitoring of both the discharge image and the pulse shape of the discharge current provided information on the momentary state of the discharge process. A number of optical and electrical parameters were recorded to serve as indicators for the process of dielectric degradation at the surface of the void. Each experiment started with a virgin sample, i.e. a void in a dielectric without a history of electrical stress. Unless stated otherwise, the test voltage was chosen to be 25% to 50% above the discharge inception voltage. The

calculated inception voltage proved to be close to the measured inception voltage. The Paschen curve [17] was used to determine the void breakdown voltage and hence the inception voltage.

3.1 Evolution of the discharge mechanism in three stages

The main result of these experiments is the classification of the discharge process in three stages. These stages are successive in time and they are found for all sample geometries, i.e. for flat and square voids of different heights, as well as for different dielectric materials.

Stage I - Virgin sample

This first stage is characterized by discharges with a steep

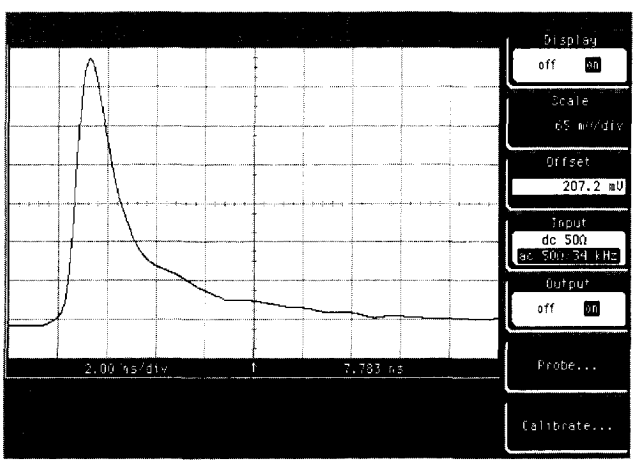

Figure 3.1 Typical current pulse shape of a streamer-like discharge, $D = 10$ mm, $h = 0.1$ mm.

front (some hundreds of picoseconds) and a short duration (approximately one nanosecond). These discharges are called "streamer-like". Figure 3.1 shows a typical example of the pulse shape of such a discharge. The magnitude of a single discharge is approximately constant for a given void height. The discharges ignite in groups with a very short time period between consecutive discharges (nanoseconds, or even a fraction of a nanosecond). Optical images

show that the area affected by a single discharge is *restricted to a small part of the void surface*, see Figure 3.8. This area is approximately constant. In one voltage cycle the void surface is successively discharged by a large number of single discharges.

Stage II - during 1 hr to 50 hrs. of discharge activity

After 10 to 60 minutes at an average fieldstrength in the sample of 5 kV/mm, the discharge mechanism changes. The formation of the discharge is now a "slow" process and the discharges are called "Townsend-like". This can be

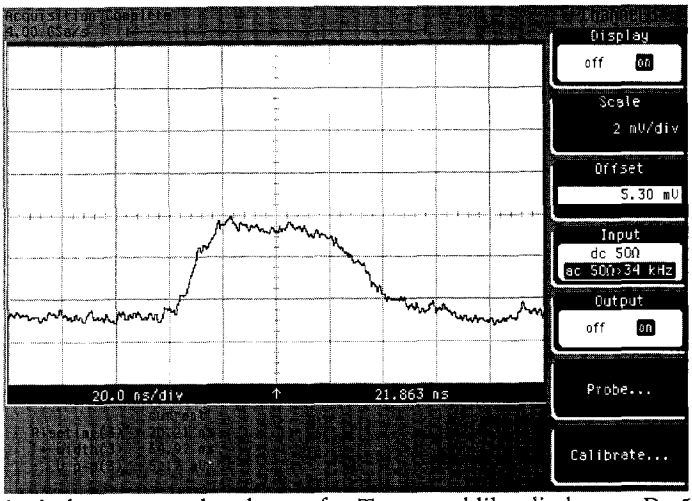

Figure 3.2 Typical current pulse shape of a Townsend-like discharge, D=5 mm, h=0.1 mm.

recognized in the front and the
total length of the pulse shown in Figure 3.2. The rise time can be as long as several tens of nanoseconds. The duration of the discharge is proportional to the height of the void and can last several hundreds of nanoseconds. Contrary to the streamer-like discharges of stage I, the magnitude of the single Townsend-like discharges is widely scattered.
Optical images show that a single discharge covers a greater part of the void surface and sometimes the complete void surface. Optically seen the discharge process is a *diffuse* process.
In the course of this second stage crystals of oxalic acid are formed. These crystals tend to grow with the ongoing discharge activity and they lead to the

third stage.

Stage III - after more than 50 hrs. of discharge activity

After several tens of hours (at a fieldstrength of about 5 kV/mm) the discharge magnitude decreases. Pulse shape analysis shows the existence of a

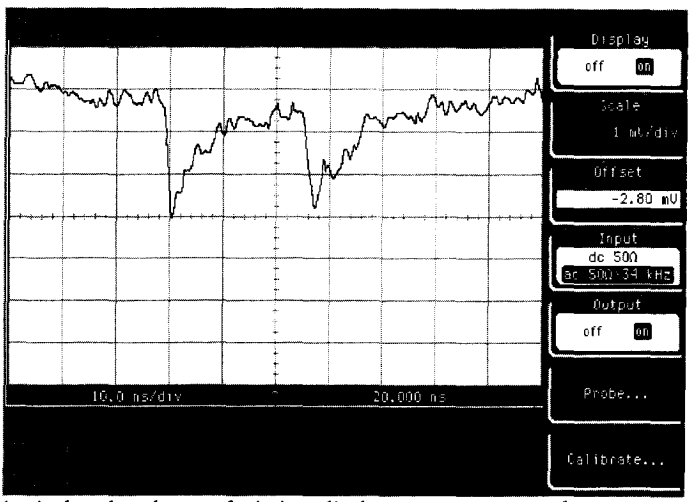

Figure 3.3 Typical pulse shape of pitting discharges, D=5 mm, h=0.1 mm.

third type of discharge, characterized by a small pulse height and a high repetition rate, up to several discharges per microsecond. The rise time of this discharge is comparable with that of streamer-like pulses. The decay time however is considerably longer, typically 10 to 15 ns. Figure 3.3 shows a typical example of a series of such discharge pulses. Optical images and examination of the void surface with an optical microscope show that these discharges ignite at locations where clusters of crystals are present. Due to the fact that these discharges were found to cause a severe pitting of the dielectric these discharges were named "pitting". As the shape of the pulses is similar to that of corona discharges it is sometimes called "corona-like" as well [?].

In the following paragraphs the observation of these three types of discharges is described in detail. For each type the characteristics are discussed on the basis of:

- electrical pulse shape analysis,

- optical discharge image analysis,
- microscopical and chemical analysis of the surface of the void.

3.2 Streamer-like discharges

3.2.1 Pulse shape

The shape of a discharge pulse is characterized by a number of parameters. The following pulse parameters were measured:

- pulse amplitude $\hat{\imath}$ (in μA or mA)
- pulse rise time t_r (in ps or ns)
- pulse width t_w (in ns)
- pulse decay time t_d (in ns)

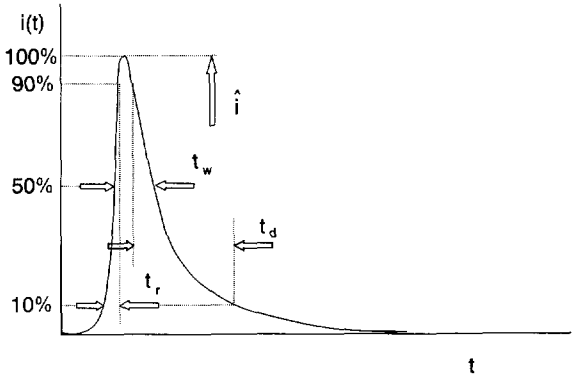

Figure 3.4 Definition of the discharge pulse parameters in stage I.

The definition of these parameters is illustrated in Figure 3.4.
Streamer-like discharges are characterized both by their pulse shape and their optical appearance. If the void geometry is changed, the general characteristics are not affected.

Rise time
The pulse rise time t_r is extremely small for all void geometries tested (see Figure 3.5). There is a relation between the rise time and the height of the void. However, the rise time is well below the transit time required by

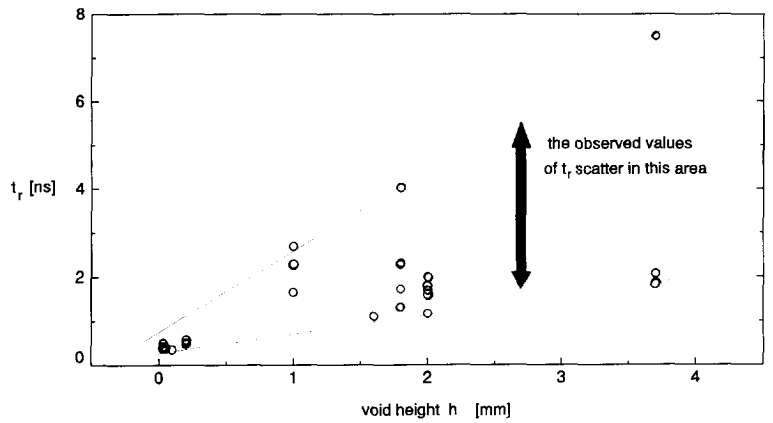

Figure 3.5 Pulse rise times measured for voids with a height ranging from 30 μm to 3.7 mm.

electrons to cross the void. This fact led to the adoption of a streamer-like mechanism: the rapid growth of the discharge current can be explained by a streamer process [23,53]. Photo-ionization in the gas is the main ionization process and results in a fast development of the discharge. Ultra high bandwidth systems are needed to measure these rise times correctly[4] [?]. The scatter in the magnitude of t_r may well result from the different initial rates of growth of the discharge channel. Further, superposition of pulses also leads to a scatter in the measured values of t_r. This topic will be further discussed in Chapter 4.

Decay time

The pulse decay time t_d is also clearly affected by the height of the void as can be inferred from Figure 3.6. It is assumed that the decay time is either the result of a *slowly* decreasing electron current due to detachment of electrons from electronegative atoms in the final stage of the discharge development [?], or the result of surface discharges at the base of the discharge channel [44]. There is some evidence [Kärkaïnen] that larger decay times originate from the

[4] The ongoing development of digitizers and oscilloscopes of over 1 GHz single shot bandwidth will undoubtedly lead to the observation of still shorter rise times.

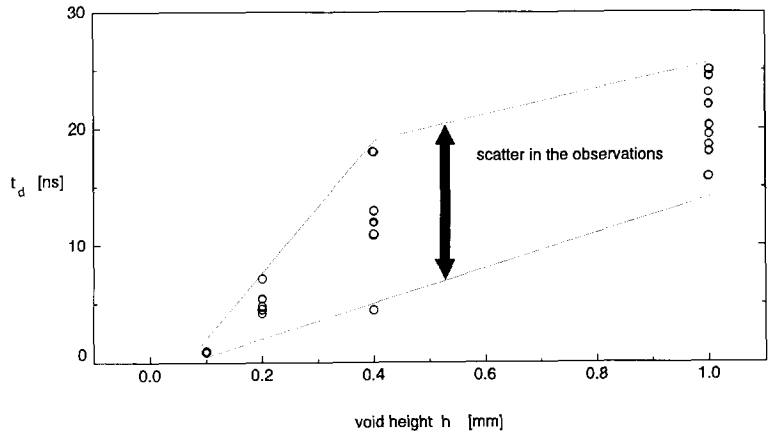

Figure 3.6 Pulse decay times measured for voids with a height ranging from 30 μm to 1 mm. For clarity the specific values of h are shown in the diagram.

larger extension of the surface discharges.

Pulse width

The pulse width t_w increases also with the void height. This is mainly caused by the increased decay time.

Pulse amplitude

The pulse amplitude $\hat{\imath}$ in stage I is large compared with the other types of discharges, and has a typical value between 10 and 100 mA. Figure 3.7 shows the amplitude distribution of single streamer-like discharges for different values of the height of the void h. The pulse height is proportional to the height of the void, see Figure 3.7.

The diameter of the void may have a considerable effect on the *measured* amplitude of the discharge current. Figure 3.8 shows the results of a series of measurements on a 20 mm diameter, 1 mm high void. The time-resolved discharge signal and discharge image are shown. Both observations were made at the same time. It can clearly be seen that discharges, although separated in space, ignite in groups with a very short time interval between

successive discharges (several nanoseconds). In a number of cases the individual discharges are no longer dissolved in the oscillograms. The resolution of the

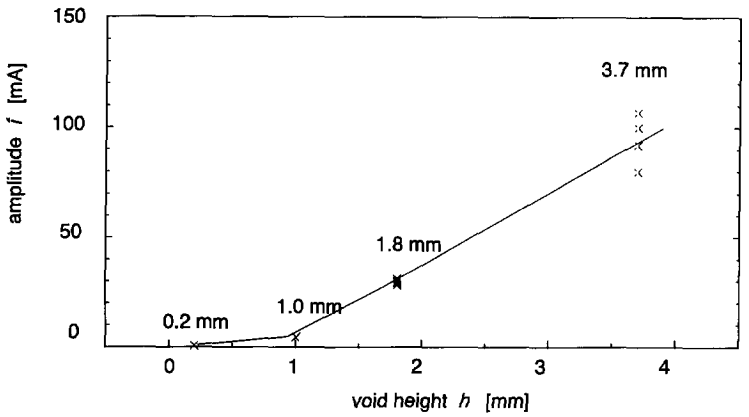

Figure 3.7 Discharge pulse amplitude as a function of the void height. For clarity the exact values of h are shown in the diagram.

measurement system is no longer sufficient to discriminate between consecutive discharges and superposition of pulses will occur. A situation in which single pulses can only marginally be discriminated is shown in Figure 3.9. In addition, this figure illustrates the small scatter of the pulse amplitude of single discharges. The larger the D/h ratio, the larger the effect of the superposition will be.

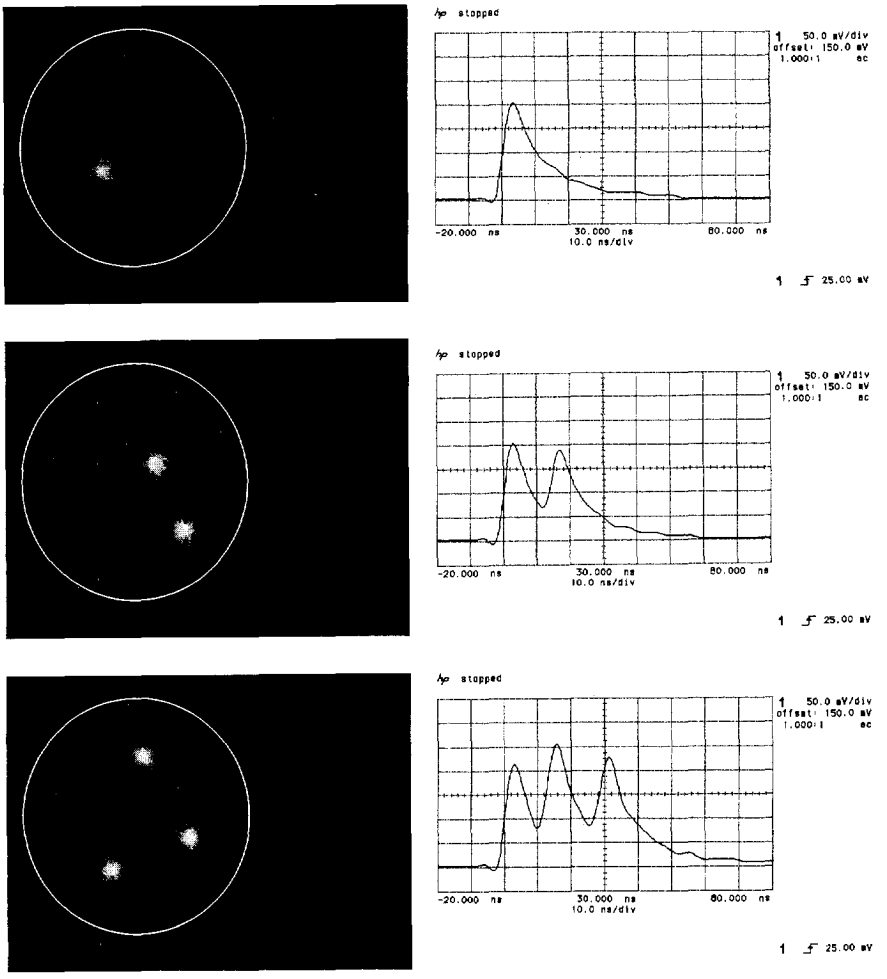

Figure 3.8 Synchronic captured optical and electrical discharge signals of groups of discharges. $D=10$ mm, $h=0.8$ mm.

3.2.2 Discharge image

As described earlier, optical observation provides a means to identify single discharges as a result of their spatial distribution over the void surface. Figure 3.10 shows the optical images of *single* discharges for different void geometries. A discharge site is represented by a circular area of high light intensity. The rule of thumb that the diameter of the discharge is

Figure 3.9 Superposition of consecutive discharges for voids with a large D/h ratio, $D=20$ mm, $h=1$ mm.

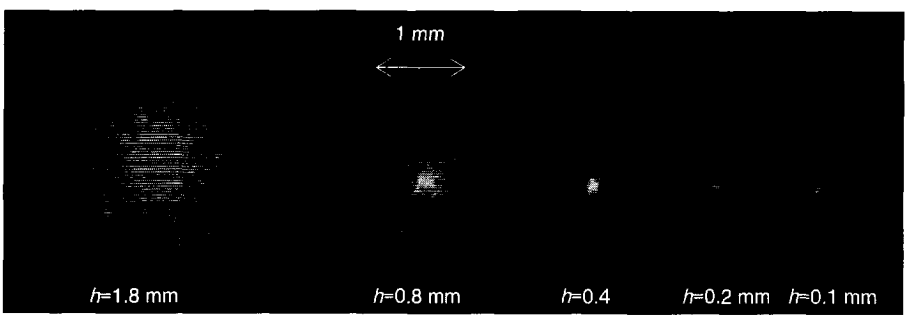

Figure 3.10 Optical images of single discharges for different values of the void height h. The diameter of the void is 10 mm.

approximately equal to the void height, introduced by Mason [54], is supported by the results shown in Figure 3.10. The resolution of the video camera is not sufficient to show small details, however, when contact photographs of the discharge are made, characteristic Lichtenberg figures appear, see Figure 3.11.

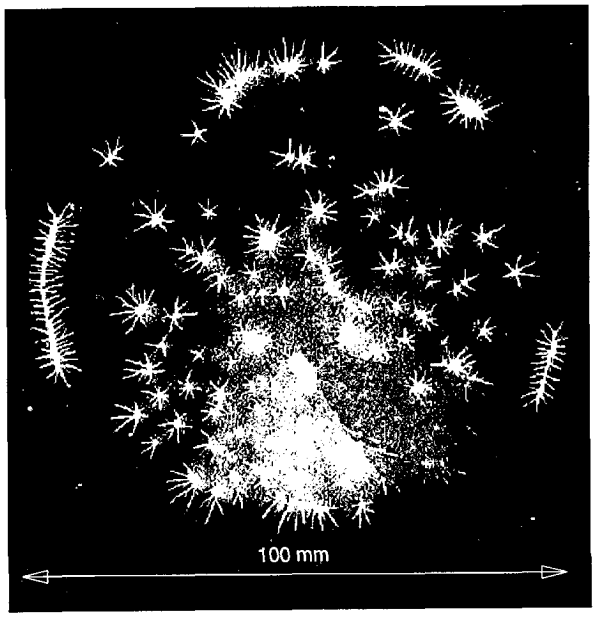

Figure 3.11 Contact photograph of the surface discharges at the base of streamer-like discharge channel (Lichtenberg figures), $h = 1$ mm, $D = 100$ mm. The photo was made at the beginning of stage I.

3.2.3 Analysis of the void surface

In the course of the discharge process, discharge by-products can be seen to accumulate at the surface of the void. A large part of the void surface is covered by a layer of very small droplets, see ?. Most of these by-products are of an acid nature, infrared analysis showed the existence of COOH groups. The deposition of a layer of droplets leads to the next stage, as described in the following section.

3.3 Townsend-like discharges

3.3.1 Pulse shape

The same pulse parameters were determined as in the case of streamer-like discharges, but because of the specific shape of the Townsend-like pulses an extra parameter was introduced, the pulse width at 20% of the pulse amplitude

$t_{w,20\%}$ (see Chapter 2, section 2.6, Figure 2.10). Like the other types of discharges, these Townsend-like pulses can also completely be characterized by their pulse shape and their optical image.
The Townsend-like discharge type is very sensitive to the geometry of the void. The most characteristic features are the rise time t_r and the pulse width t_w.

Rise time
Rise times of several tens of nanoseconds are measured. This is much longer than the electron transit time. This is an indication that the discharge is governed by a Townsend process and consists of a number of generations of avalanches. Figure 3.12 shows an example of a long rise time for a void with a height of 1 mm and a diameter of 20 mm. The measured rise time (131 ns) is much longer than the electron transit time which is approximately 5 ns for this void height. The rise time shows a large scatter, as can be seen in

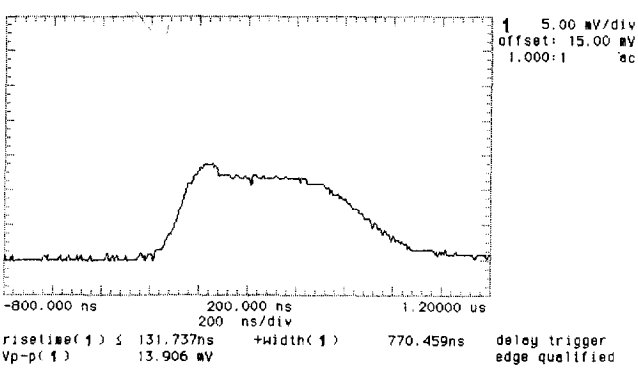

Figure 3.12 Example of a Townsend-like discharge pulse with a long rise time t_r, D=20 mm, h= 1 mm.

Figure 3.13a and Figure 3.13b. This scatter can be explained by the ignition at different overvoltages and will be discussed in Chapter 5.

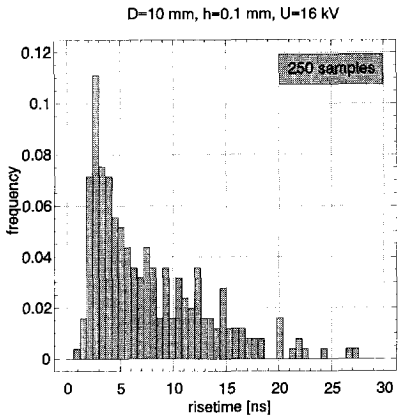

Figure 3.13a Rise time histogram h=0.1 mm, D=10 mm.

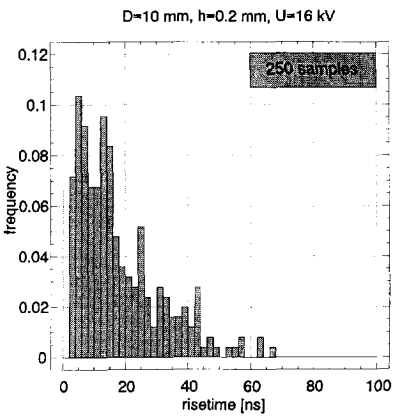

Figure 3.13b Rise time histogram h=0.2 mm, D=10 mm.

Pulse width

The pulse width is unambiguously determined by the height of the void, see also Luczynski [53]. Figure 3.14b and Figure 3.14c show pulse width histograms for voids with a height of 50 μm, 0.1 mm, 0.2 mm and 0.4 mm. If it is assumed that all positive ions

- are produced in front of the anode and
- move as a sheet of charge towards the cathode with a drift velocity W_i

then the following relation can be obtained:

$$t_w \approx \frac{h}{W_i} = \frac{h}{\mu_i E}$$

with W_i the ion drift velocity, μ_i the ion mobility and E the electric field in the void. Figure 3.15 shows the measured values of t_w as well as the discharge pulse width calculated for a wide range of void heights with μ_i=2.6 $cm^2V^{-1}s$ [3]. The magnitude of E was calculated taking the breakdown voltage from the Paschen curve: $E = V_{Paschen}/h$. It can be seen that the measured values do well agree with the calculated values. Hence, there exists an unambiguous relation between t_w and the height of the void.

In the Townsend-like process the majority of electrons and positive ions is created at the anode side of the void. While the positive ions drift to the cathode side they contribute to the discharge current. Because the ions have a more or

less constant[5] velocity their contribution to the discharge current will be constant until the ions have crossed the void. Apart from the typical pulse shape as shown in Figure 3.2 other shapes were encountered as well. Figure 3.16 shows an example of a Townsend-like pulse with a pronounced peak. A correlation was found between the shape of the discharge pulse, the lateral extension and the luminosity of the discharge.

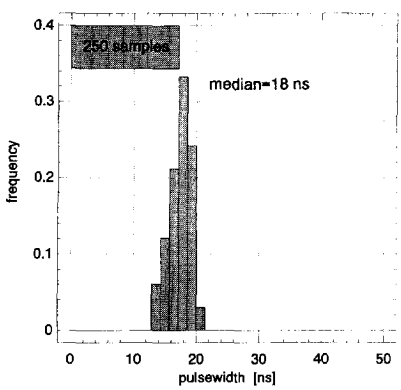

Figure 3.14a Pulse width histogram for $h=50$ μm.

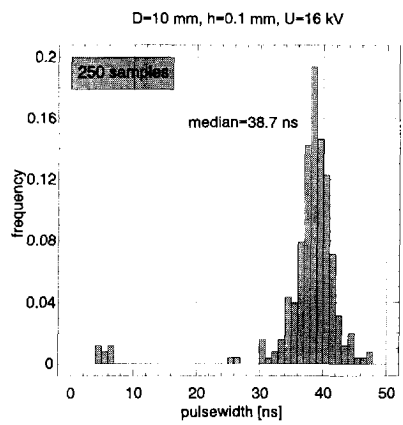

Figure 3.14b Pulse width histogram for $h=0.1$ mm.

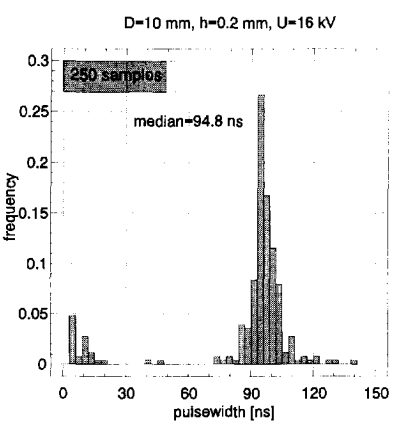

Figure 3.14c Pulse width histogram for $h=0.2$ mm.

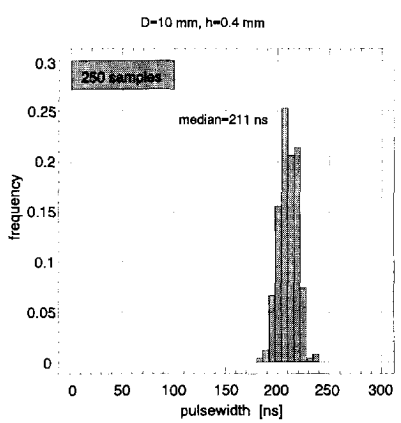

Figure 3.14d Pulse width histogram for $h=0.4$ mm.

[5] This drift velocity is constant only by approximation, it is subject to minor changes due to the changing (space charge) field in the void.

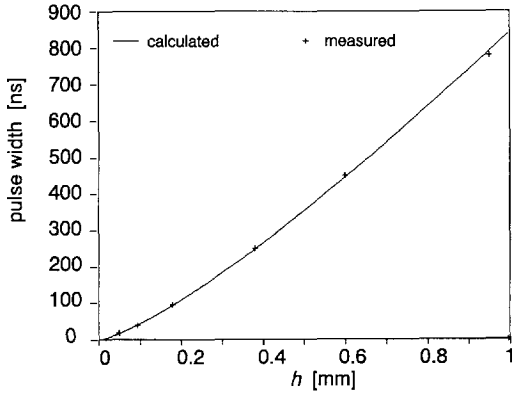

Figure 3.15 Relation between the pulse width of a Townsend-like discharge and the void height.

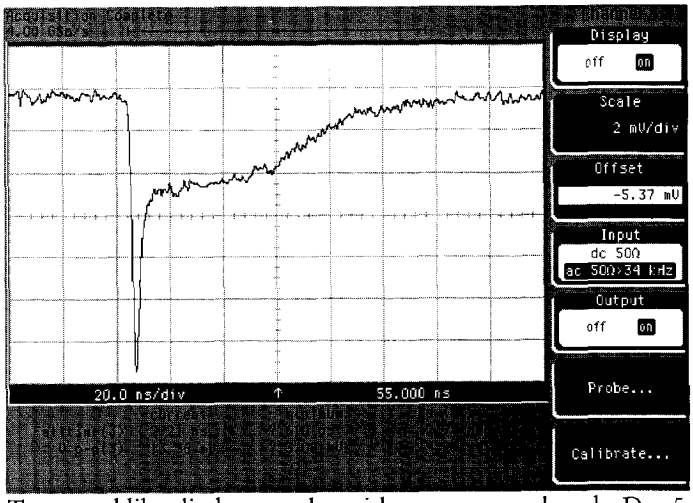

Figure 3.16 Townsend-like discharge pulse with a pronounced peak. D= 5 mm, h= 0.1 mm.

A long rise time, i.e. a slowly developing series of avalanches, is also characterized by a relatively large lateral extension. Discharges with an over-

shoot behave differently. Optically they are characterized by a diffuse pattern with a luminous center. The lateral extension is relatively small, see Figure 3.17.

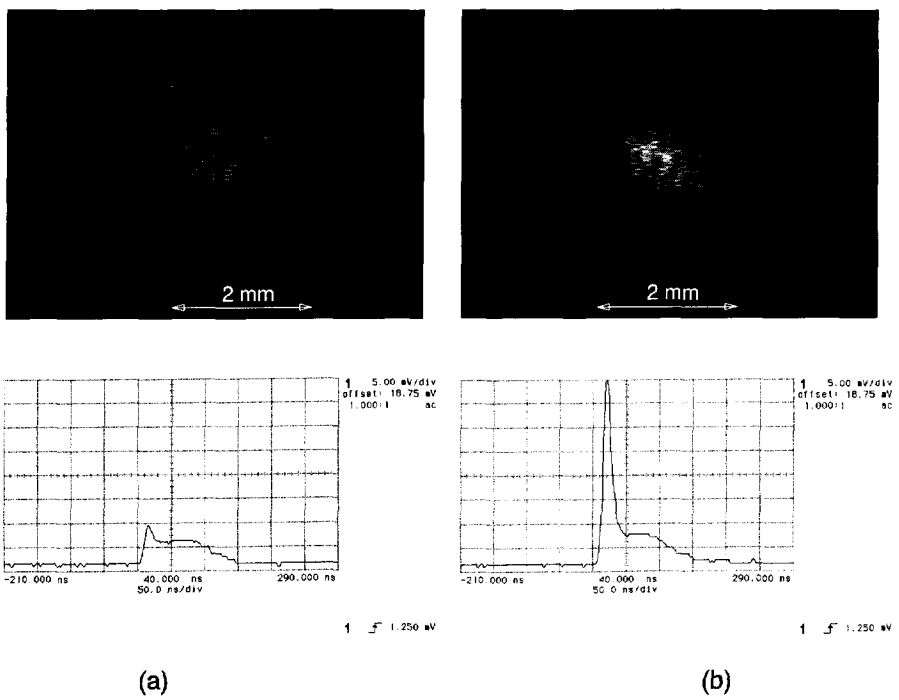

Figure 3.17 Optical image and pulse shape of Townsend-like discharges without (a) and with (b) overshoot.

Pulse amplitude

The amplitude of the Townsend-like current pulses shows a large dynamic range, starting with pulses below the detection threshold of the electrical system. Figure 3.18 shows an amplitude histogram of Townsend-like discharges for a 10 mm diameter, 0.1 mm high void obtained from the results of 250 amplitude measurements. Optical images of the discharges show that the pulse amplitude is closely related to the discharged area, see **3.2.2.** Further, the amplitude depends highly on the value of the overvoltage, as will be shown in Chapter 5.

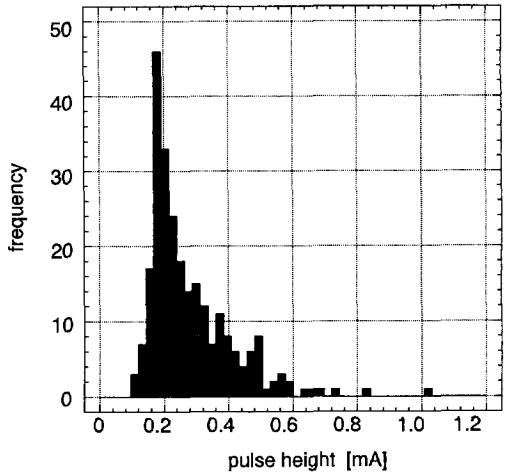

Figure 3.18 Amplitude histogram of Townsend-like current pulses, $h = 0.1$ mm, $D = 10$ mm. Total number of pulses is 250.

3.3.2 Discharge image

The discharge image of the Townsend-like discharge is completely different from that of the streamer-like type. The discharge covers a large part of the surface of the void and is optically *diffuse*. Figure 3.17 shows optical images of Townsend-like discharges with the corresponding discharge pulses for different void geometries. It can clearly be seen that for voids with a larger diameter the area covered by a Townsend-like discharge increases. Further it

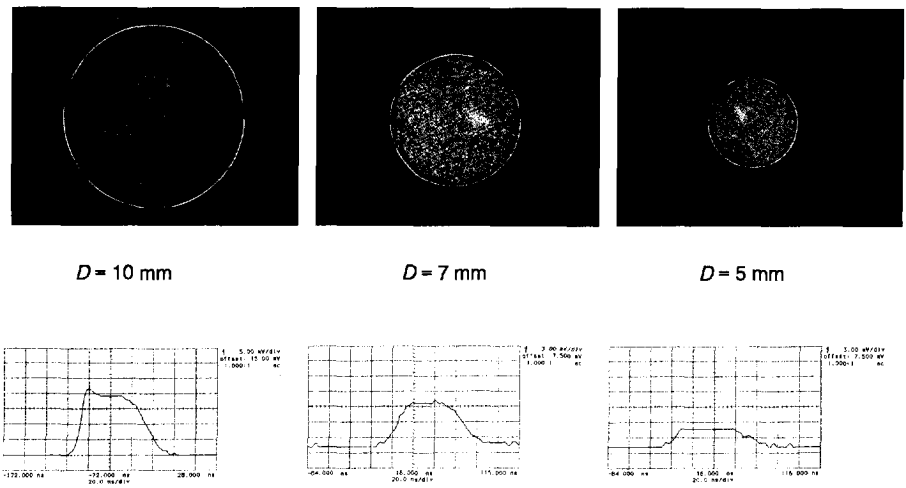

Figure 3.19 Optical images of Townsend-like discharges obtained for different void geometries.

is shown that the pulse amplitude is related to the discharged area.

3.3.3 Analysis of the void surface

In the course of this Townsend-like discharge process the appearance of the void surface changes. Area's with whitish gel are found, as well as crystals and powder (see Figure 3.20). The crystals were determined by infra red spectroscopy to consist of COOH groups. This result is consistent with the findings of Gámez-García [27] who determined the crystals as oxalic acid (HOOC-COOH). The whitish gel was defined as an acid substance (formic, acetic and benzoic acid). The acid deposition was found to be of a conductive nature. Surface resistivity measurements were performed with the set-up described in Chapter 2. For a number of samples the surface resistivity was measured at specific times during the discharge ageing process. It was discovered that during the deposition of the discharge by-products a sharp decrease occurred in the surface resistivity (see Figure 4.16). The effects of this conductive layer on the physics of the discharge process are discussed in Chapter 4.

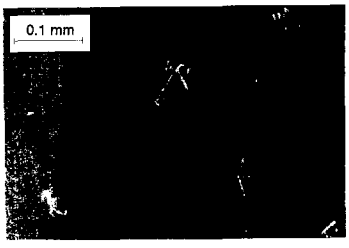

A

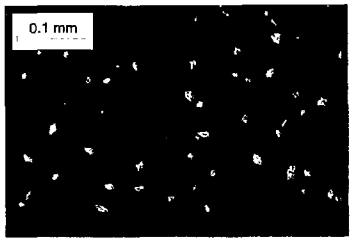

B

Figure 3.20 Photographs of the void surface after 50 hrs of discharge activity, A and B are details.

3.4 Pitting discharges

3.4.1 Pulse shape

Because of their effect on the void surface the type of discharge occurring in stage III was named pitting. The same pulse parameters as in the case of streamer-like discharges were studied. The most characteristic features are the rise

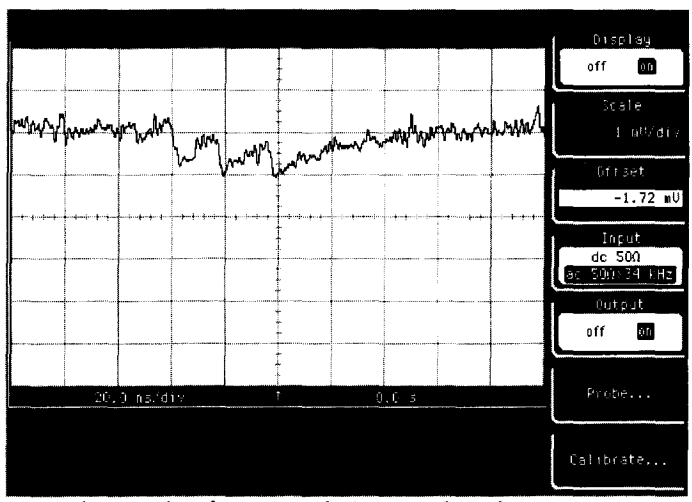

Figure 3.21 Typical example of a series of pitting pulses, h=0.1 mm, D=10 mm.

time t_r and the amplitude $\hat{\imath}$. In addition, the discharge repetition rate N_{rep} is found to be rather high: in the order of several tens per microsecond. Figure 3.21 shows a typical example of a series of pitting pulses. Pulses within one series tend to have the same amplitude $\hat{\imath}$. They show a distinct tail, decay times between 10 and 15 nanoseconds were registered for a 0.1 mm high void.

Rise time
The rise time is comparable to the rise time of streamer-like discharges.

Pulse amplitude
The pulse amplitude shows little scatter as can be seen in Figure 3.22. The amplitude $\hat{\imath}$ is relatively small, in the order of 200 μA (for streamer-like discharges this was some tens of mA and for Townsend-like discharges some

hundreds of μA).

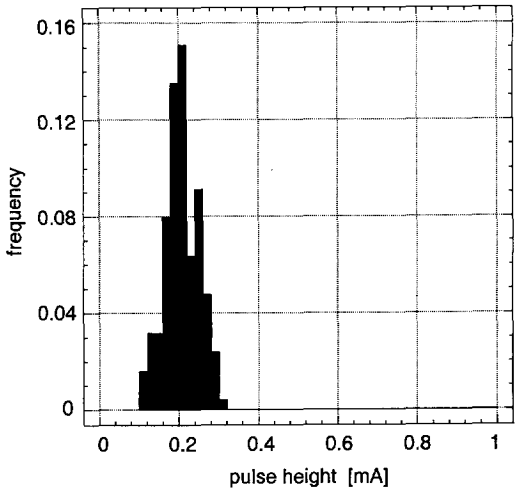

Figure 3.22 Pulse amplitude histogram of pitting discharges, h=0.2 mm, D=10 mm.

3.4.2 Discharge image

Optical analysis shows that pitting discharges are very localized events. The above mentioned high repetition rate follows from varying the exposure time: Images obtained with an exposure time of 20 ms are seen in Figure 3.23. These images show bright spots due to the accumulation of the light of a large number of consecutive discharges. If smaller exposure times are used the brightness of the spots decreases due to the smaller number of discharges observed.

Figure 3.23 Optical image of pitting discharges, $h = 0.1$ mm, $D = 10$ mm. Exposure time 20 ms. The image is built of a large number of consecutive discharges.

3.4.3 Analysis of the void surface

A close observation of the void surface, as illustrated in Figure 3.24, shows that the surface is covered with clusters of crystals at the top of which pitting discharges ignite. The crystals have different shapes, but all have sharp edges with a radius of curvature smaller than a micrometer. The clusters act as field intensifications and thus as most likely positions for discharge ignition. Figure 3.25 gives an example of a cluster of crystals after 100 hrs of discharge activity.

After prolonged discharge activity the clusters are eroded in the central area. Further, the dielectric surface below the eroded central area is deteriorated. Pits with a diameter of several tens of micrometers and a depth of about 10 micrometer are shown on the photograph in Figure 3.23, Figure 3.26. In contrast to the classic opinion [83], these pits were not only found at the edges of the void, but also in the central area. The occurrence of pits at the edges has been explained in literature to be caused by the decreasing field in the center of the void: It could be concluded from field calculations that the conductive layer increases the field at the edges of the void.

The field at the crystal tips, however, is far larger: several times the mean value in the void. The discharge activity can therefore be maintained in the center of the void as well.

The growth of the pits in this stage is considered to be of the utmost impor-

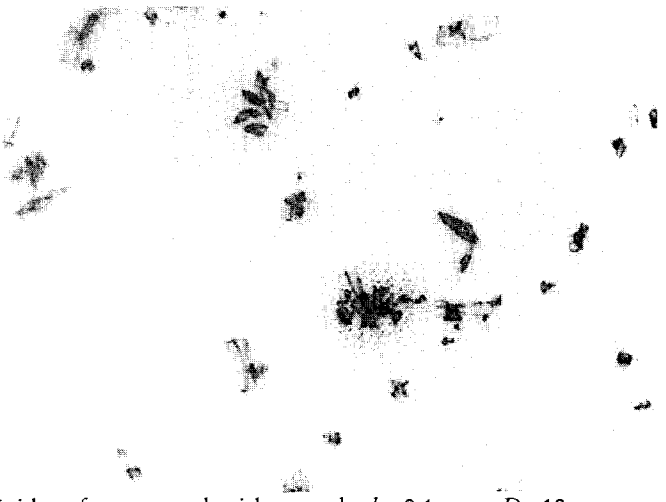

Figure 3.24 Void surface covered with crystals. $h=0.1$ mm, $D=10$ mm.

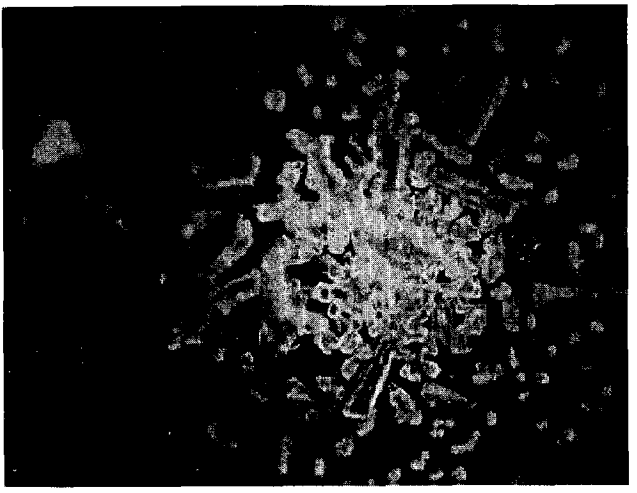

Figure 3.25 Cluster of crystals after 100 hrs of discharge activity. $h=0.1$ mm, $D=10$ mm.

tance because they lead to significant deterioration of the dielectric.

3.5 Transition between stages I and II

Several parameters affect the transition between the stages. The most important parameters are: the test voltage, the relative humidity in the void, the shape of the void and the thickness of the dielectric. In the following the effect of these parameters will be described. Because the transition between the

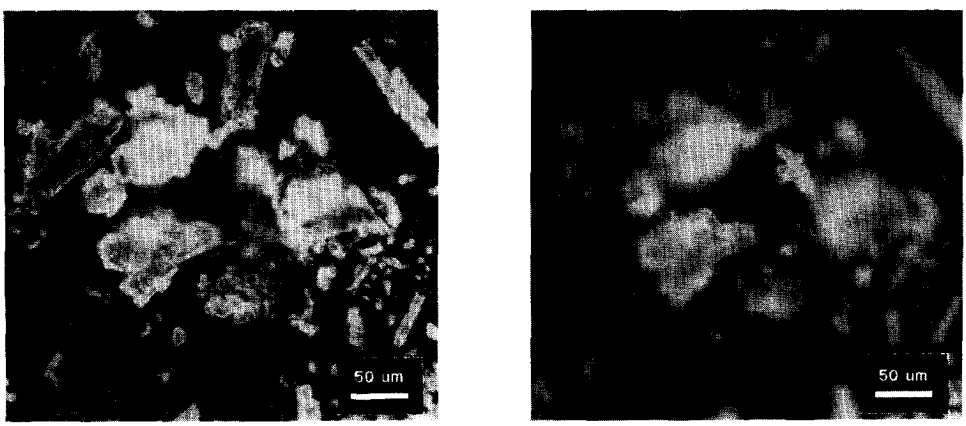

Figure 3.26 Crater or pit, as a result of the interaction of pitting discharges with the void surface. Photographs I and II are focussed on the void surface, resp. the crater surface.

stages is a continuous process the transition time T_{trans}

$$T_{transit} = T \mid m \geq \frac{T_{w,streamer-like} + T_{w,townsend-like}}{2} \tag{3.4}$$

was defined as the instant in time that the number of Townsend-like pulses equals the number of the streamer-like pulses in a set of 50 consecutive discharges. In practice the median m was measured of the pulse width for 50 subsequent discharges. For each new discharge pulse m was calculated again by discarding the "oldest" discharge in the series of 50. In this way, similar to moving average, a *moving median* was obtained, see also Figure 3.27, Figure 6.7. The moment of transition occurred when m reaches a value halfway between the mean pulse width of streamer-like and Townsend-like discharges, see equation (3.4).

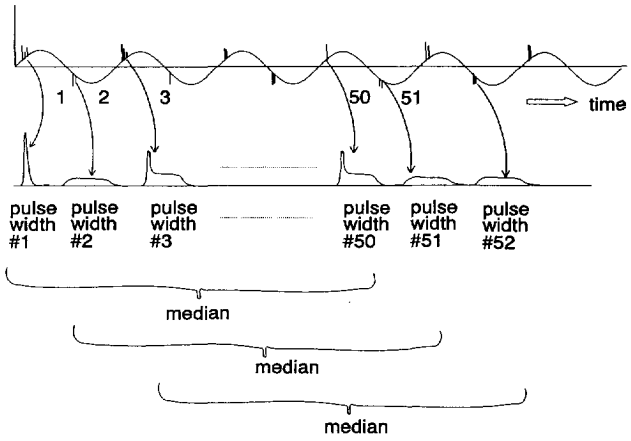

Figure 3.27 Calculation of the *moving median*, which serves as an indicator for the transition time.

3.5.1 Effect of the test voltage

For voltages just above the inception voltage ($1...1.2 \times U_{inc}$) no transition from streamer-like to Townsend-like takes place. Instead, after several hours the discharges extinguish or exhibit a very erratic behavior. For higher voltages a transition does occur and the higher the voltage the faster the transition takes place. Figure 3.28 shows the behavior of the *moving median* for several values of the test voltage. Figure 3.29 shows $T_{transition}$ as a function of U/U_{inc}

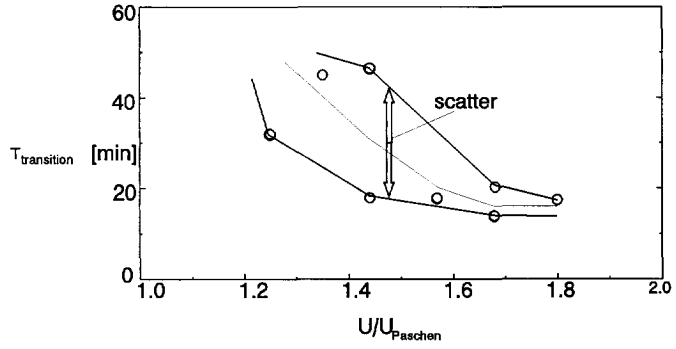

Figure 3.29 $T_{transition}$ as a function of U/U_{inc}. h=0.2 mm, D=10 mm.

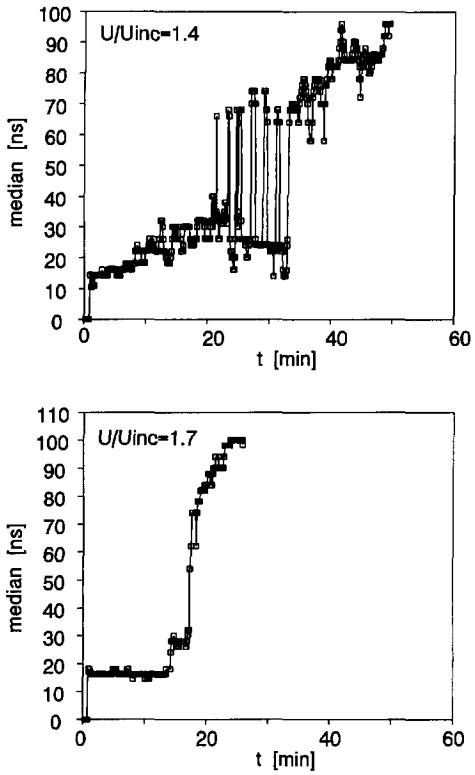

Figure 3.28 Behavior of the *moving median* as a function of the test voltage.

for a void with $h=0.2$ mm and $D=10$ mm. Because an increase of the test voltage leads to a larger discharge intensity, the growth of a layer of discharge by-products increases as well. If this layer is responsible for the change of the discharge mechanism, the decrease of $T_{transition}$ with increasing discharge intensity is explained. This topic will be discussed in more detail in Chapter 4. For voltages above 1.75 times U_{inc}, $T_{transition}$ seems to decrease no longer.

3.5.2 Effect of the shape of the void on the transition

It was found that the transition between stage I and stage II takes place faster for flatter voids. For equal values of U/U_{inc}, voids with a smaller value of D/h

result in larger values of $T_{transition}$. Figure 3.30 shows the values of $T_{transition}$ for a range of D/h values from 15 to 100.

Voids with small *D/h* ratio's

One has to be careful when drawing conclusions from the data of voids with small *D/h* ratio's. The diameter of these voids was relatively small, below 3 mm. Because the amplitude $\hat{\imath}$ of Townsend-like discharges decreases quadratically with decreasing D ($\hat{\imath} \propto$ void area) an increasing number of discharges is not detected. However, the optical system was still able to register Townsend-like discharges and showed that for voids with smaller *D/h* the process of transition takes more time.

Voids with large *D/h* ratio's

For voids with a very large *D/h* ratio (100) sometimes Townsend-like discharges were registered at the start of a test at $U/U_{inc} \geq 1.5$. The reason for this abnormal behavior is not yet clear, though the reason might be the large

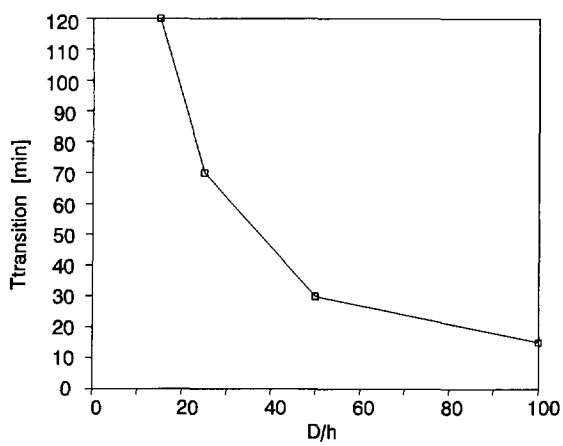

Figure 3.30 Values of $T_{transition}$ for a range of *D/h* values from 15 to 100.

amount of initiatory electrons as this amount is proportional to the void area. This observation might be in agreement with the results of Luczynski [53]. Occasionally he observed "series of slowly developing discharges...during the initial period lasting some few minutes".

3.6 Summary

The evolution of the discharge mechanism in dielectric bounded voids is characterized by three distinctly different consecutive stages. Figure 3.31 shows for each stage the characteristic pulse shape, discharge image and the appearance of the dielectric.
The test voltage has a significant effect on the transition time between the stages: Higher voltages lead to shorter transition times.
It was found that in flat voids the transition occurs faster than in "square" voids.

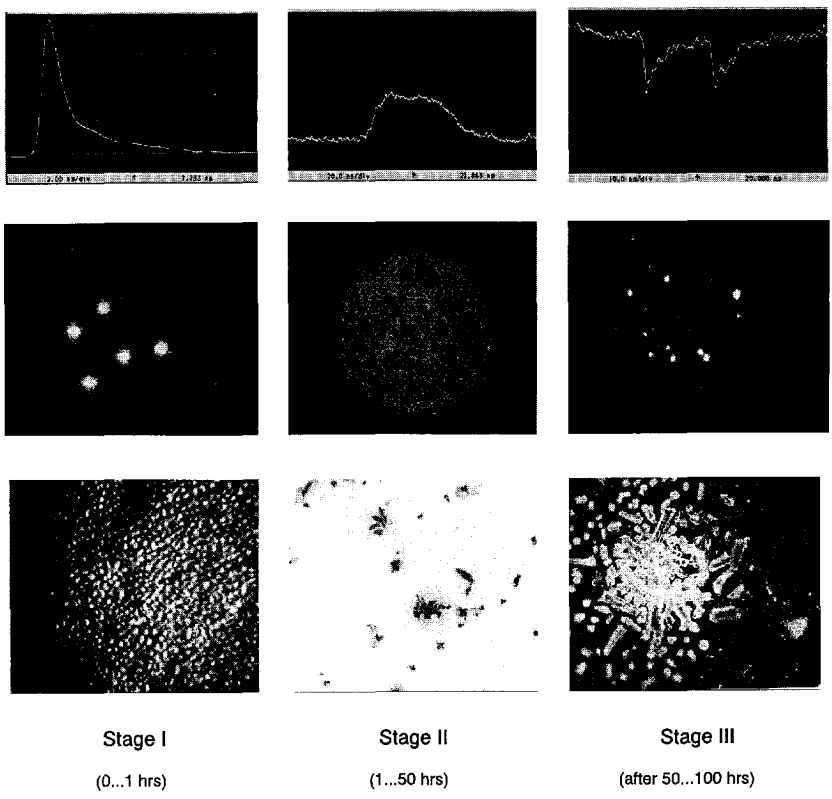

Figure 3.31 Evolution of the discharge mechanism, described by *pulse shape, optical image* and *effect on the dielectric.*

Chapter 4
Discharge mechanisms

In this chapter an analysis is given of the three different discharge mechanisms in a void and of the transitions which take place between the mechanisms. This chapter starts in section **4.1** with a short description of the breakdown process between *metal* electrodes because of the similarities with the discharge mechanism in dielectric bounded voids. In section **4.2** some parameters are introduced that have an effect on the transition between the streamer-like and the Townsend-like mechanism between *dielectric* electrodes. These parameters are discussed in sections **4.3**...**4.6** on the basis of experimental data. The chapter ends with section **4.7** where a model is presented explaining the occurrence of pitting discharges.

4.1 The discharge mechanism between metal electrodes

The following ionization processes will be considered: avalanches, Townsend discharges and streamer discharges. The latter two processes are self-sustained and lead to breakdown.

4.1.1 Avalanches

For the development of a single electron avalanche two conditions have to be fulfilled:

- an initiatory electron has to be available located at a suitable position in the electrode gap
- the mean value of the effective ionization factor shall be $\alpha_{eff} > 0$. In air this is true for field strengths above 2.44 kV/mm at 1 bar [8].
  ($\alpha_{eff} = \alpha - \eta$, where α is the ionization coefficient [cm^{-1}] and η the attachment coefficient [cm^{-1}])

Initiatory electrons are supplied by cosmic or background radiation or by charge deposited at the surface of the electrodes as a result of earlier discharges [66]. In the case of clean metal electrodes without any insulating oxidation layer, the background radiation is important only.
Single avalanches occur at voltages below the ignition voltage of a self-

sustained discharge, generally these avalanches escape detection because of their small magnitude.

4.1.2. Self-sustained discharge

For an avalanche to develop into a self-sustained discharge it is essential that
- an initiatory electron is available at a suitable position in the electrode gap, preferably near the cathode.
- the electric field exceeds a threshold value to fulfill the condition $\alpha_{eff} > 0$
- sufficient secondary electron production exists due to feedback either in the gas or at the cathode.

The initiatory electron has to be available close to the cathode to obtain the maximum length of the ionization path to the anode. This results in the maximum number of ionizations N_i.

$$N_i = \int_0^h \alpha N_e(x)\, dx \tag{4.1}$$

with

$$N_e(x) = \exp[(\alpha-\eta)x] \tag{4.2}$$

so that

$$N_i = \frac{\alpha}{\alpha-\eta}\cdot\left(\exp[(\alpha-\eta)h]-1\right) \tag{4.3}$$

with α Townsend's first ionization coefficient, h the gap separation, η the electron attachment coefficient, N_e the number of electrons, N_i the number of positive ions and x the distance travelled by the electrons in the gap.

If an initiatory electron is present when the electric field exceeds the threshold value a discharge ignites. The production of initiatory electrons is a stochastic process and the probability $P(dt)$ for the occurrence of an initiatory electron during a time interval dt is given as [23]:

$$P(dt) = 1-\exp[-f_e\, dt] \tag{4.4}$$

with f_e the production rate of initiatory electrons. f_e is the product of the radiative absorption by matter C_{rad}, the radiative flux density Φ_{rad}, the gas density ρ and the volume V close to the anode where an initiatory electron can start a self-sustained discharge:

$$f_e = C_{rad} \cdot \phi_{rad} \cdot \rho \cdot V \tag{4.5}$$

In the case of natural background radiation C_{rad} Φ_{rad} was estimated by Niemeyer [66] to be of the order 2.10^6 $kg^{-1}s^{-1}$.
The probability for an electron to be produced after a time dt is given by Zuber [94] as:

$$P(t > dt) = \exp[-dt\, f_e] \tag{4.6}$$

or

$$P(t > dt) = \exp\left[-\frac{dt}{\tau_s}\right] \tag{4.7}$$

with τ_s the average statistical time lag.
Therefore, on the average an initiatory electron is present after a certain time-lag τ_s. During τ_s the electric field in the electrode gap rises above the threshold field and the discharge ignites at an overvoltage.

Townsend mechanism

In the process of ionization, atoms are excited and send θN_i photons in all directions, see Figure 4.1.

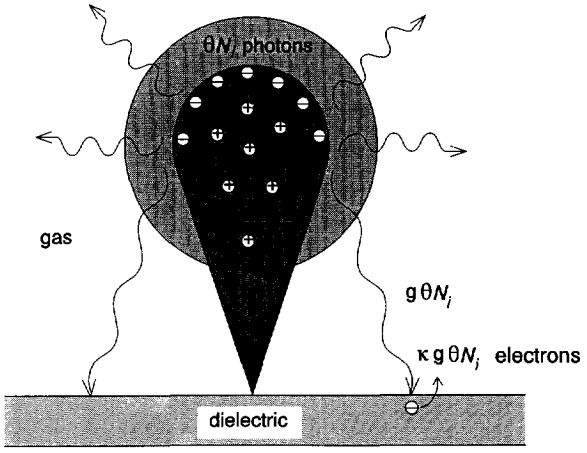

Figure 4.1 Diagram showing the secondary ionization process due to photons.

A number of $g\theta N_i$ photons arrive at the cathode and liberate $\kappa g\theta N_i = \gamma_{ph} N_i$ secondary initiatory electrons, with g a geometry factor, θ the average number of photons produced by one electron moving 1 cm in the direction of the

field and κ the number of electrons released from the cathode per incident photon. The N_i positive ions will liberate $\gamma_i N_i$ new initiatory electrons. The total amount of new initiatory electrons is

$$N_{e0} = \gamma_i N_i + \gamma_{ph} N_i = \gamma N_i \tag{4.8}$$

where γ represents the combined feedback by photons and ions.

During the transit time of the first N_{e0} initiatory electrons
N_c new initiatory electrons are produced at the cathode:

$$N_c = \left[\gamma \frac{\alpha}{\alpha-\eta}\left[\exp[(\alpha-\eta)h]-1\right]\right] \cdot N_{e0} \tag{4.9}$$

If an initiatory electron has at least one successor due to secondary ionization the discharge becomes self-sustained.

$$\frac{N_c}{N_{e0}} = \mu \geq 1 \tag{4.10}$$

with μ the number of new initiatory electrons produced per avalanche.
In Figure 4.2 an example is shown of a discharge with μ slightly more than 1. The local peaks at the front of the pulse represent the moments where a new avalanche has crossed the void.
Combining (4.8), (4.9) and (4.10) the criterion for a Townsend breakdown is obtained when:

$$\exp[(\alpha-\eta)h] \geq \frac{\alpha-\eta}{\alpha\gamma}+1 \tag{4.11}$$

or when

$$\mu \geq \frac{\alpha-\eta}{\alpha} \qquad \text{with } \mu = \gamma\exp[(\alpha-\eta)h] \tag{4.12}$$

or with $\alpha \gg \eta$

$$\mu \geq 1$$

Streamer mechanism

If the discharge develops as a result of an overvoltage, i.e. if the value of α is large, the effect of space charge can no longer be neglected. The space charge in the front of the avalanche induces a space charge field. It is commonly accepted that if the space charge field approaches the Laplace field, the ionization is strongly enhanced and a streamer breakdown starts to take place:

the emission of UV radiation is strongly enhanced and photo ionization takes place in the gas.

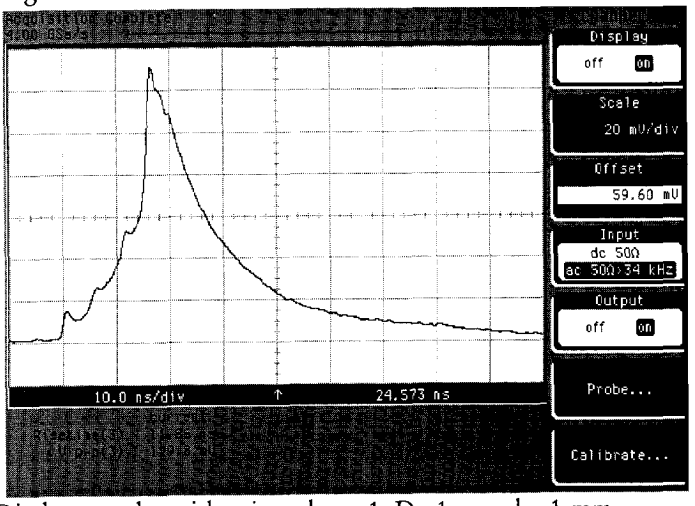

Figure 4.2 Discharge pulse with μ just above 1. D=1 mm, h=1 mm.

The space charge field E_{space} in the front of the avalanche can be approximated by [71]:

$$E_{space} = e^2 \frac{\exp[(\alpha-\eta)x]}{16\pi\varepsilon_0 kTx} E_0 \tag{4.14}$$

with E_{space} the space charge field in kV/mm, E_0 the Laplace field in kV/mm, x the length of the avalanche, e the elementary charge in C, T the absolute temperature in K and k the Boltzmann constant in J K^{-1}.
The avalanche grows to a critical length x_{cr} if $E_{space} \approx E_0$.
Consequently the following condition has to be fulfilled:

$$N_{cr} = \exp[(\alpha-\eta)x_{cr}] = \frac{16\pi\varepsilon_0 kTx_{cr}}{e^2} \tag{4.15}$$

This criterion is first fulfilled at $x_{cr} = h$. The breakdown values of gaps between metal electrodes follow an empirical relation [17].
Calculating the breakdown value using this relation, the corresponding ionization factor α_{eff} (= α - η) follows from the empirical relation [8]:

$$\alpha_{eff} = pk\left[\frac{E}{p} - \left[\frac{E}{p}\right]_0\right]^2 \text{ cm}^{-1} \tag{4.16}$$

with k= 0.22 cm bar kV^{-2}, and $(E/p)_0$ = 24.4 kV cm^{-1} bar^{-1}.

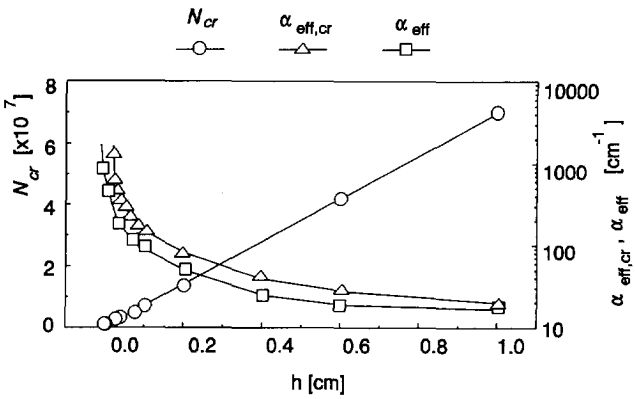

Figure 4.3 N_{cr}, α_{eff} and $\alpha_{eff,cr}$ as a function of the gap length h.

Figure 4.3 shows N_{cr}, α_{eff} and $\alpha_{eff,cr}$ as a function of h (= x_{cr}). Here $\alpha_{eff,cr}$ is the minimum ionization factor needed to obtain N_{cr} at x_{cr}. α_{eff} is the value of the effective ionization coefficient obtained from (4.16). For values of h greater than 6 mm α is very close to $\alpha_{eff,cr}$, and a streamer breakdown mechanism is likely to occur.
Which one of the criteria, (4.12) or (4.15), will be fulfilled depends on the gas (α, η, θ) and the cathode material (γ, κ).

The Townsend breakdown mechanism will be operative if

$$\frac{\alpha-\eta}{\alpha}\frac{1}{\gamma} < N_{cr}-1 \quad , \Rightarrow \gamma > \frac{\alpha-\eta}{\alpha}\frac{1}{N_{cr}-1} \tag{4.17}$$

It is clear that the streamer criterion ($N_{cr} \approx 10^8$) is fulfilled for very small values of γ only. The overvoltages which are necessary for obtaining N_{cr} charge carriers for gap distances between 0.5 mm and 10 mm are calculated and shown in Figure 4.4.
The overvoltage ΔV is defined as the extra voltage needed to obtain N_{cr}, divided by the breakdown voltage $U_{Paschen}$ given by the Paschen curve, times 100%:

$$\Delta V = \frac{U}{U_{Paschen}} \cdot 100\%$$

From Figure 4.4 it can be inferred that for small gap distances h relatively large values of ΔV are required. This illustrates the tendency towards the streamer breakdown mechanism for large gaps between metal electrodes. An implication of the above is that a streamer can take place in small gaps only if γ is very small (« 10^{-4}) or if ΔV is large.
Pfaue [70] performed an experiment with a copper cathode in ether. Ether in

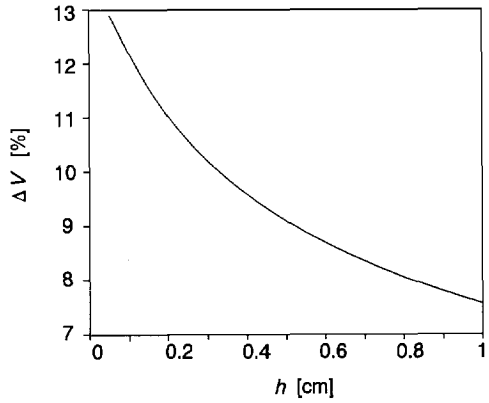

Figure 4.4 Overvoltages needed to obtain a streamer breakdown for gap distances between 0.5 mm and 5 mm.

combination with a copper cathode has a very low γ_{ph}-value so that a streamer mechanism takes place easily. By covering the cathode with CuI (copper iodide) the work function of the cathode was significantly lowered. This resulted in a high γ_{ph}-value and a Townsend breakdown took place, with a long series of avalanches as shown in Figure 4.5.
Figure 4.6 shows a plot of α as a function of γ for h = 0.1 mm if Townsends' breakdown criterion is fulfilled. It can be seen that the streamer criterion is fulfilled (αh = 16...18) for very small values of γ only
($\gamma \leq 10^{-7}$). This holds true for the situation that no overvoltages are applied. The transition from a Townsend breakdown mechanism to a streamer breakdown mechanism can be obtained by applying an overvoltage sufficiently high so that

$$\frac{\alpha}{\alpha-\eta}\frac{1}{\gamma} + 1 > N_{cr} \tag{4.19}$$

with N_{cr} in the range 10^6...10^8.

In general it can be said that for gases with electro-negative properties like humid air and SF_6 a lower overvoltage (3.5%...4.3%) is required than for gases with $\eta \approx 0$ such as N_2 and Ar (18%...21%) [46] . In this case α-η or α_{eff} decreases, thus the α required to fulfill condition (4.19) decreases. Because α increases quadratically with the overvoltage a lower overvoltage is needed.

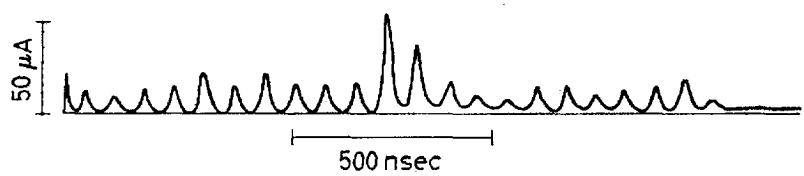

Figure 4.5 Extreme example of a Townsend discharge. Shown is the current of a number of generations of avalanches in ether due to the liberation of secondary electrons from the cathode by photons. (p=368 Torr, h=0.6 mm) [Pfaue].

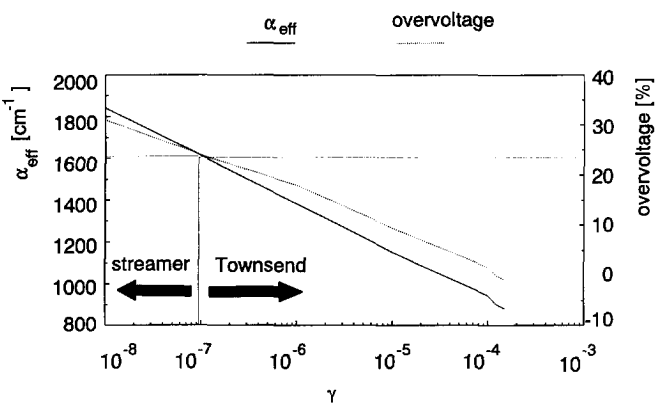

Figure 4.6 γ as a function of α

4.2 Discharge mechanism in a void between dielectrics

The discharge theory for dielectric bounded voids has a number of characteristics in common with the theory for electrode bounded gaps as described above. Generally, it is found that discharge ignition voltages are about equal

for both situations. Therefore the Paschen curve is widely used for calculating breakdown voltages of dielectric bounded voids, with an error in the order of 5..10%. The most striking difference is obviously the self-limiting effect of the discharge between the dielectric planes.
The discharge mechanism prevailing for a particular gas-dielectric combination is imposed by the same set of parameters α, η, γ. It is obvious that α and η, being properties of the gas, are unaffected by the dielectric electrodes. The coefficient γ however is largely affected by the cathode material. In literature [93,81] hardly any information can be found on the value of γ of dielectrics. Most researchers use the values of γ known for metal electrodes. In the underlying study the effect of different values of γ on the discharge mechanism was examined. Therefore a test set-up was built to measure γ in an indirect way.
Further, the ionization coefficient α is affected by overvoltages that are likely to be present in the case of small voids. These overvoltages occur due to the statistical time-lag τ_s.

In the following the discharge mechanisms and in particular the transitions between the stages are studied using the above mentioned parameters.

4.2.1 Transition between discharge mechanisms

In stage I discharge pulses were observed with a short rise time and short pulse width. The rise times are considered to be too short for a breakdown process with several generations of avalanches, such as the Townsend breakdown process. Therefore it is supposed [23,53,63,21] that a mechanism similar to the streamer breakdown is operative, where photons acting at light velocity provide secondary ionization in the gas. This means that the streamer criterion is fulfilled before the Townsend criterion is reached, (4.19).

In this study a direct connection was found between the deposition of a conducting layer and the occurrence of the Townsend-like mechanism: in a simple experiment part of the layer was removed. It was optically observed that a streamer-like type was active at this particular part and a Townsend-like type was prevailing at those parts where the layer was still present. Replacing the side walls of the void with a virgin material had no effect on the discharge mechanism. Refilling the void with fresh gas had a minor effect. Therefore it can be concluded that it is the layer of by-products that governs the discharge mechanism.
In order to study the cause of this effect the following parameters, all

properties of the layer, were examined for their possible relation to the discharge mechanism:

- the availability of shallow electron traps in the layer
- the value of γ of the layer
- the enhanced conductivity

The first two parameters deal with the availability of free electrons for the initiation and the feedback of the discharge process. The conductivity affects the distribution of potential initiatory electrons across the surface of the void.

4.3 The availability of shallow electron traps

If τ_s is large, significant overvoltages occur, leading to a large value of α. Devins [23] used overvoltages to obtain discharges with the properties of a streamer (streamer-like discharges). He showed the occurrence of Townsend-like discharges at low overvoltages in a void between a glass plate and a metal electrode, with a transition to streamer-like discharges at a specific overvoltage.

The value of the τ_s is affected by properties of the gas, the dielectric and the amount of cosmic and background radiation, see Figure 4.7.
The properties of the dielectric are important because of the liberation of trapped electrons from the dielectric surface. The number of *detrapped* electrons per second has its effect on the time-lag as well. But also, the always present background radiation is a source of initiatory electron production.

Before a discharge ignites, an initiatory electron has to be available to start the ionization process. These initiatory electrons are produced by:

1 photo-ionization in the gas by natural cosmic and radioactive radiation (background radiation)
2 liberation of electrons deposited by earlier discharges and trapped at the surface of the dielectric

According to Niemeyer [66] the average rate at which photoelectrons are produced by background radiation is:

$$\begin{aligned} \dot{N}_{erad} &= C_{rad} \cdot \Phi_{rad} \cdot \rho \cdot \pi r^2 (h - l_{\min}) \\ (C_{rad} \cdot \Phi_{rad})_{nat} &\approx 2 \cdot 10^6 \ \mathrm{kg^{-1} s^{-1}} \end{aligned} \qquad (4.20)$$

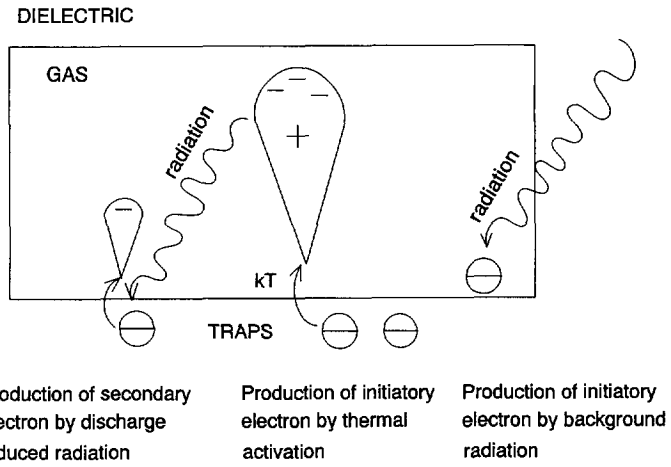

Figure 4.7 Sources of initiatory electron production affecting the statistical time-lag τ_s and the production of secondary electrons.

with C_{rad} a constant describing the radiative absorption by matter, Φ_{rad} the radiative flux density, ρ the gas density, r the radius of the discharged area, h the height of the void and l_{min} the minimum length for an initiatory electron to travel to obtain a self-sustained discharge. If the voltage across the void is equal to the minimum breakdown voltage, l_{min} is equal to the height h of the void. In the case that an overvoltage is present l_{min} is smaller than h. This means that, for a given overvoltage the expression $\pi r^2(h-l_{min})$ represents that part of the void where electrons are suitaby placed to initiate breakdown. For a void with a height of 0.1 mm and a radius of 5 mm we get:

$$\pi r^2(h-l_{\min}) < \pi r^2 h = 7.9\times10^{-9} \quad \mathrm{m}^3 \tag{4.21}$$

Thus the production rate of photoelectrons is:

$$\dot{N}_{erad} < 2\cdot10^{6}\cdot7.9\cdot10^{-9} = 1.6\cdot10^{-2}\ \mathrm{s}^{-1} \tag{4.22}$$

Trap density

Degradation of the dielectric by so called *hot* electrons with energies above

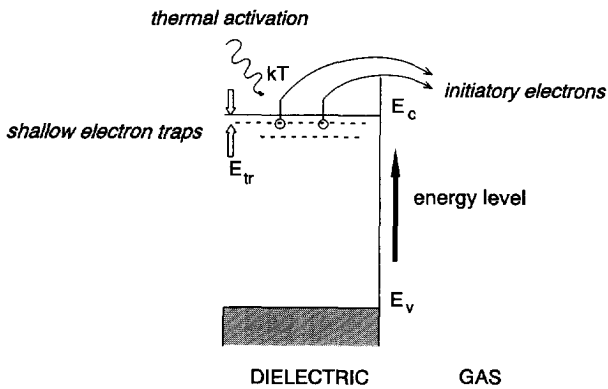

Figure 4.8 Electron traps at the surface of the dielectric due to discharge induced degradation.

$\approx$4 eV produces electron traps in the surface layer of the dielectric [12] (see Figure 4.8). These traps decrease the mobility of electrons in the dielectric and form a reservoir of potential initiatory electrons.
Before the void is discharged for the first time the number of traps is limited and a small portion of the surface traps is filled. The liberation of electrons from the surface traps comes into effect when the discharge process has been started by background radiation. While the discharge process is active new traps and also deeper traps are formed in the dielectric surface layer. Cartier [12] found a rapid increase of the trap density from 10^{12} to 10^{16} cm^{-3} due to radiation induced degradation of the dielectric.

Modelling

An existing model [66] is used to estimate the emission rate of electrons from the void surface. In the following this model is described and used to describe the influence of the condition of the void surface on the emission rate.
A discharge deposits a charge q at the void surface. The corresponding $N_e = q/e$ (e: elementary charge $=1.6\times10^{-19}$ C) electrons trapped at the surface of the void are available as initiatory electrons after the reversal of the electric field in the void. N_e decreases with time t because part of the charge is lost due to:

- a surface conductivity of the side walls leading to a charge flow to the opposite void surface

- diffusion of electrons to deeper traps, or deeper into the dielectric from where they can no longer be liberated

The first cause of electron loss can be important for small spherical voids where the walls form a considerable part of the total void surface. Prolonged discharge activity in such a void leads to an increase of the surface conductivity. This loss of electrons can be considerable, even to the effect that the discharge process stops because of a lack of initiatory electrons. In the literature [83,40,45,73] this behavior is often mentioned.

The second cause is applicable for all shapes of voids and is accounted for as follows [66]: the electrons trapped at the surface are supposed to have an average life time τ_{tr}. The number of electrons remaining in the surface traps after a time t is a negative exponential function of t:

$$N_e^I = N_e \cdot \exp(-t/\tau_{tr}) \tag{4.23}$$

These remaining electrons can be detrapped, i.e. become available as an initiatory electron, by phonon- or thermal activation [41]. The number of thermal activations per second ν_0, the characteristic phonon frequency is of the order of $10^{12}...10^{13}$ s^{-1} (this is the infra-red area of the spectrum, $\lambda \approx 30$ μm). The depth of the surface traps of hexatriacontane n-$C_{36}H_{74}$ was measured by Cartier et al. [13]. For thin sheets a minimum trap depth of 0.65...1.3 eV was measured. Because n-$C_{36}H_{74}$ is similar to polyethylene these data are used here. Taking into account the losses due to diffusion to deeper traps the rate of initiatory electron production is:

$$\dot{N}_{einit} = \frac{q}{e} \cdot \exp\left[-\frac{t}{\tau_{tr}}\right] \cdot \nu_0 \cdot \exp\left[-\frac{E_{tr}}{kT}\right] \tag{4.24}$$

with k the Boltzmann constant.

The value of τ_{tr} was considered by [66] to be in the order of a few milliseconds.

To obtain an impression of the order of magnitude of the electron production rate two examples are given.

In the first example a virgin insulating material is considered. Due to amorphos regions, additives and impurities in the polymer shallow traps are present, but in limited amounts. Therefore a large number of electrons diffuses deeper into the dielectric from where they can no longer be extracted. To take this into account, an average trap depth $E_{tr} = 1.6 \times 10^{-19}$ J (1 eV) was used in this example.

In the second example a thin layer of discharge by-products is present at the interface between dielectric and gas.

While the dielectric surface is degraded traps are filled and more traps are pro-

duced, leading to an increase of the conductivity. When all traps are filled there is an equilibrium between the trapping and detrapping processes. Boeck [10] has found a gradual increase of the conductivity of the *bulk* of dielectrics subjected to prolonged discharge activity. He attributed this increase to the subsequent filling of shallow and deep traps in the dielectric. After the discharge activity was stopped he observed an exponential decrease of the conductivity which he explained by detrapping processes.

The above theory is accepted as plausible. In this thesis, however, the (de)trapping processes in the layer of discharge by-products are considered. As was stated earlier, when this layer is removed the discharge mechanism changes.
The polymer surface is supposed to be degraded by hot electrons to a depth of 2 to 5 nm for energies below 20 eV [13]. It is known that this layer has a large number of -shallow- traps. The by-products consist of broken polymer chains, cross-linked polymer chains and oxidation products, species that are known [58,80,82] to have a large number of traps. In this case a large number of traps is available at the surface of the dielectric. The surface layer can be considered as an *electron reservoir*. To account for this a smaller average trap depth is used than in the first example: $E_{tr} = 1.0\times10^{-19}$ J (0.65 eV).

In both examples the other parameters have the following values: $\tau_{tr} = 1\times10^{-3}$ s, $\nu_0 = 1\times10^{12}$ s^{-1}, $T = 293$ K, $k = 1.38\times10^{-23}$ J K^{-1}.

A void is considered with a diameter of 10 mm and a height of 0.1 mm. Further it is assumed that a discharge has deposited an amount of charge of $q = 100\times10^{-12}$ C at the upper surface of the void (see Figure 4.9). All charges are supposed to be located in shallow surface traps from where they can be extracted to serve as initiatory electrons. The resistivity of the void surface is considered to be large and to have no effect on the process. Now we can calculate the production rate of initiatory electrons:

$$\dot{N}_{einit} = 6.3\times10^{18}\cdot\exp\left[-\frac{t}{1\times10^{-3}}\right]\cdot\exp\left[-\frac{E_{tr}}{1.38\times10^{-23}\cdot293}\right] \qquad (4.25)$$

For example 1 this leads to

$$\dot{N}_{einit} = 4.1\times10^{3}\cdot\exp\left[-\frac{t}{1\times10^{-3}}\right]\ \text{s}^{-1} \qquad (4.26)$$

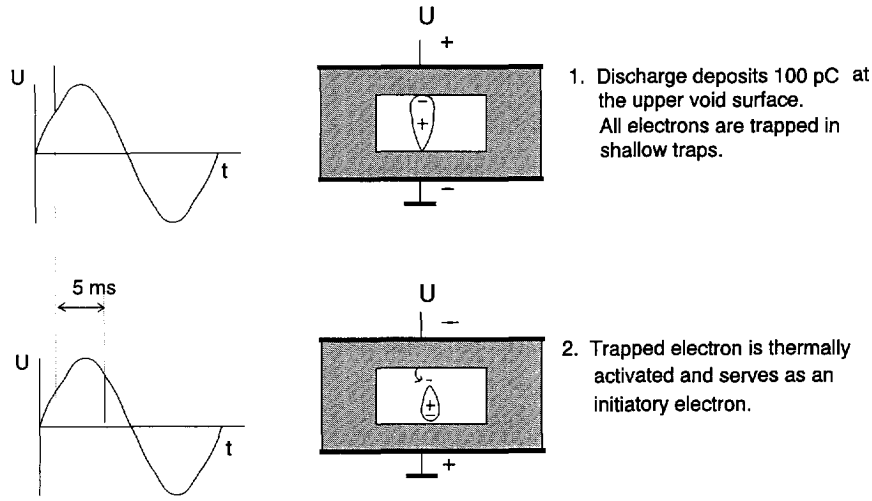

Figure 4.9 Schematic of the production of initiatory electrons.

and for example 2 to

$$\dot{N}_{einit} = 1.1\times10^{10}\cdot\exp\left[-\frac{t}{1\times10^{-3}}\right] \quad s^{-1} \tag{4.27}$$

Let us now consider the first discharge after field reversal, for example 5 ms after the last discharge of 100×10^{-12} C. The trapped electrons at the upper side of the void can now act as initiatory electrons. The electron production rate is:

$$\dot{N}_{einit} \approx 30 \ s^{-1} \tag{4.28}$$

for the first example, and

$$\dot{N}_{einit} \approx 8\times10^{7} \ s^{-1} \tag{4.29}$$

for the second example.
These production rates lead to an average time-lag of

$$\tau_{ave} = 0.5\cdot\frac{1}{\dot{N}_{einit}} \tag{4.30}$$

i.e. for the virgin void of the first example τ_{ave} = 15 ms
and for the aged void of the second example τ_{ave} = 5 ns.

It is evident that the overvoltages to be expected for aged voids are very small indeed, time lags in the order of microseconds to nanoseconds lead to overvoltages in the order of tenths of percents.
These examples are given to be illustrate the enormous effect of the average surface trap depth on the electron production rate and thereby on the expected overvoltage at which a discharge ignites. They do not pretend to present the exact values of τ_{ave}.

4.4 The value of γ

The aim of the study described in this section was to look for a difference between the value of γ of virgin and of aged dielectrics.
Saeki and Gosho [74,32] have made comparative tests on a number of dielectrics as well as on metals to compare the number of photo-electrons liberated by the radiation of an ultra-violet source. The results indicated a significant difference up to 2 orders of magnitude between insulating materials and metals. Yumoto et al. [93] irradiated different dielectrics (PE, PETP, PP and PS) with a deuterium lamp emitting a continuous spectrum from 160 nm to the visible light region. It was found that these dielectrics emitted about 500 times less electrons than gold. Tom et al. [86] measured the photo-current of epoxy surfaces using radiation of different wave lengths, 30...345 nm. Reference measurements on stainless steel showed a yield twice that of the epoxy surfaces for wave lengths between 160 and 250 nm. Takahashi et al. [81] tried to calculate the value of γ in a set-up with two spherical electrodes covered with a dielectric layer. They mentioned values of γ with the same order of magnitude as for metals.
In the underlying study it was considered to be important to study the effect of the ageing processes in the void on γ. In order to obtain information on the magnitude of γ of polyethylene in its virgin state and in an aged state, covered with a layer of discharge by-products, a test set-up was developed similar to the one used by Saeki [74]. The test conditions however were better controlled. Figure 4.10 shows the experimental test set-up.
The test sample consisted of a disc with a 6 cm diameter and a thickness between 0.1 and 1 mm. One side of the sample was glued on the lower messing electrode with conductive paint. The other side of the sample faced the upper electrode with an air gap of 15 mm in between. The upper electrode was subdivided and consisted of a central measuring electrode and a coaxial electrode at earth potential. The measuring electrode consisted of a metal grid

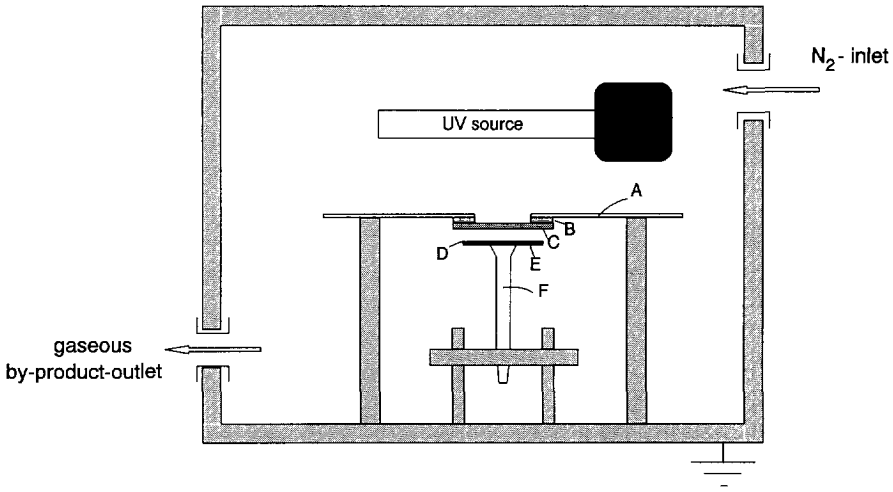

A messing electrode, connected to ground
B PVS spacer
C copper grid, measuring electrode connected via pA meter to ground
D sample
E copper support for sample
F messing contact, connected to -1000 V voltage source

Figure 4.10 Set-up for measurement of the photo current or γ.

of 20 wires per cm, allowing illumination of the sample by an ultra violet source situated above the electrode. The UV source emitted UV-radiation with a peak at 254 nm ($\equiv$ 4.9 eV) and a smaller peak at 185 nm ($\approx$ 6.7 eV), see Figure 4.11. Photo-electrons liberated from the sample surface were directed to the measuring electrode by applying a small electric field of 67 V/mm between upper and lower electrode. The lower electrode was operated at -1 kV. The measuring electrode was connected to ground via a picoampère meter (Keithly 617). This meter measured the photo-electron current. The entire test arrangement was placed in a light-tight box that could be flushed with dry air or with nitrogen. The gas in the test set-up was refreshed constantly because of the production of ozone by the radiation. Without flushing the test set-up electron attachment to ozone molecules was considerable, leading to a decrease of the measured current.
A quantification of the light intensity at the sample surface was made using

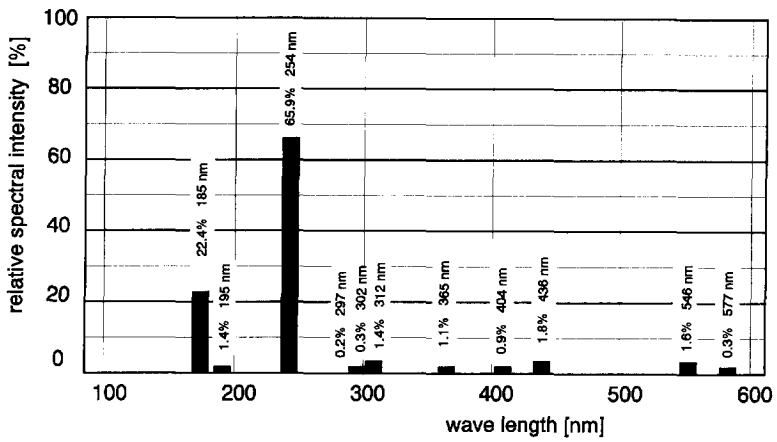

Figure 4.11 Spectral emission by the UV source [ ].

an UV sensor. The order of magnitude of the intensity was 100 $\mu W/cm^2$.

4.4.1 Test procedure

First the sample was placed in the test set-up and the UV source was switched on together with the ventilation system. This was done in order to get an equilibrium in the gas, a constant production of ozone against a constant refreshing of the gas. After 20 minutes the voltage source was switched on and with a delay of 15 seconds the current measured by the picoampère meter was registered by a single shot digitizing oscilloscope.

The value of the photo current was measured for a number of different dielectric sheets, before and after subjection to discharges in the time-resolved discharge set-up. Samples in which Townsend-like discharges occurred as well as samples in which streamer-like discharges occurred were measured.

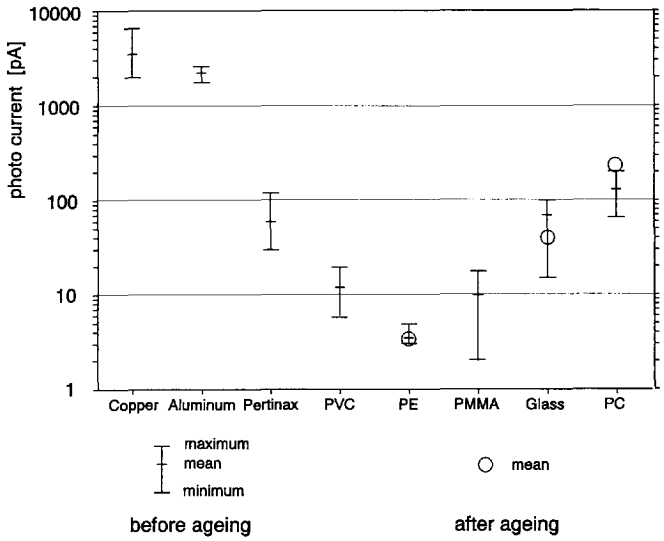

Figure 4.12 Photo-current measured for Cu, Al, Pertinax, PVC, PE, PMMA, glass and PC.

4.4.2 Test results

Figure 4.12 shows the test results for a number of different samples. The main conclusion is that the photo current of polyethylene and other dielectrics is very small, *several orders of magnitude smaller* than that of conductors like copper or aluminum.
It was further found that in most cases the value of the photo current for aged samples was either equal to or smaller than that of non-aged samples (see Figure 4.12). For both aged and non-aged polyethylene sheets the photo current was below the detection sensitivity of the picoampere meter.
Consequently, the results do not seem to support the hypothesis that Townsend-like discharges are caused by an increasing value of γ_{ph}, or at least the γ_{ph} measured in a *steady state* as has been done here. It is in this respect probable that the electrons in the shallow *surface* traps, have already diffused deeper into the dielectric before both the DC voltage and the UV irradiation are applied. In that case they can no longer be liberated.
In the actual case of a sample being subjected to discharges the traps are constantly (re-)filled within milliseconds and the trapped electrons can serve as a source of secondary electrons.
A further reason for this negative result could befully that in the first 15

seconds of irradiation all surface traps are emptied. The very small conductivity of the dielectric inhibits the refilling of the traps. Therefore, small currents are measured in the static set-up of Figure 4.10, especially for polyethylene due to its very low conductivity. Indeed, when the bulk resistivity of the different dielectrics is plotted against the measured photo current a clear trend is shown, see Figure 4.13.

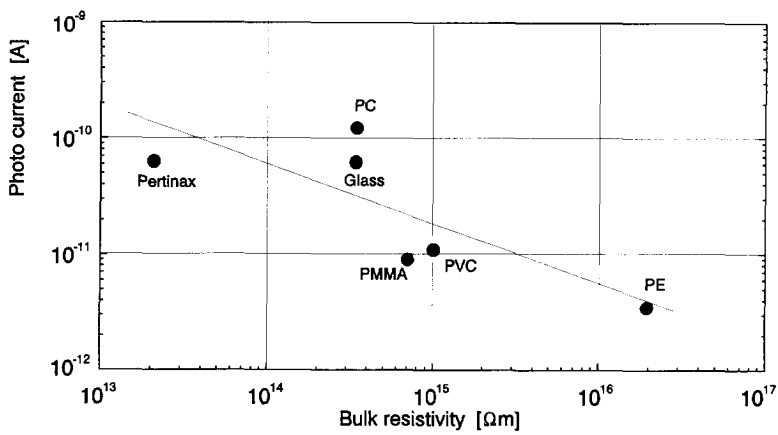

Figure 4.13 Photo current due to the radiation of different dielectrics, plotted against the bulk resistivity of the dielectric.

In the case of the polycarbonate samples no transition to Townsend-like discharges occurred. Here the value of the photo current of polycarbonate decreased after subjection to discharges. The reason for this behavior is not clear. A possible explanation could be a relative decrease of the number of shallow traps at the dielectric surface as compared to the number of deep traps, contrary to the other materials.

4.5 The resistivity of the void surface

4.5.1 Test procedure

The surface resistivity was measured as a function of the duration of discharge activity. Every 5 minutes the discharge set-up was opened and the resistivity of the sample surface was measured.
Figure 4.14 shows the test set-up used for resistivity measurements. The probe consisted of two co-axial electrodes with a guard in between these electrodes.

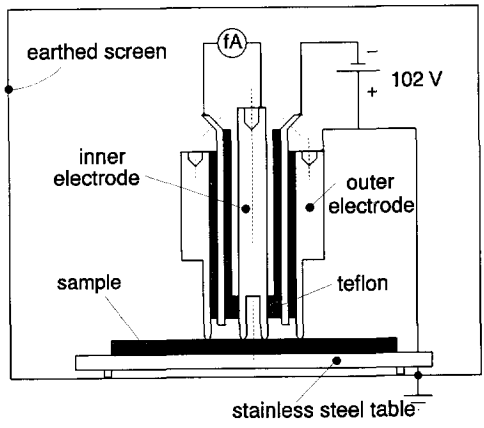

Figure 4.14 Test set-up for surface resistivity measurements.

The dielectric sample was placed on an earthed stainless steel table and the probe was placed on top of the sample. A DC voltage of
102 V was applied between both electrodes of the probe and the surface current was measured by a picoampère meter (Keithley 617). Current flowing through the bulk of the sample was directed to the earthed table, see Figure 4.15. To avoid the effect of condensation of water vapor all measurements were performed with a relative humidity less than 40%. The contact between the probe tips and the surface is of major importance. Therefore some tests were performed applying the probe with different forces on the sample. A pressure of ≈ 20 N/m^2 ensured a good contact.
The value of the current was registered 10 minutes after voltage application at a time when the current was approximately constant. After the surface resistivity had been measured the sample was placed back in the discharge set-

up for further exposure to discharges. In contrast to Hudon et al [40] who measured the surface resistivity of a series of epoxy samples, each one after a different exposure time, this method has the advantage of obtaining the evolution of the surface resistivity for one and the same sample. A drawback is the fact that, opening the sample, the gas contents of the void are refreshed. The main effect is that the void is supplied with a fresh amount of oxygen.

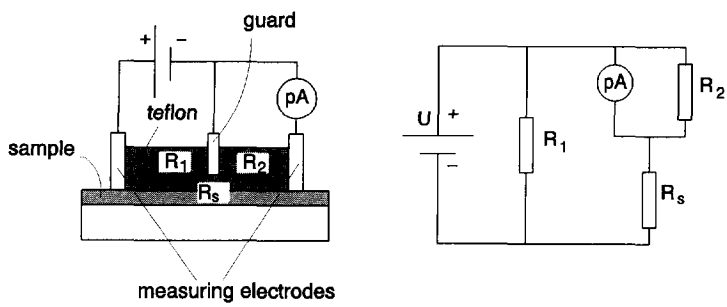

Figure 4.15 Schematic representation of the surface resistance measurement set-up. $R_2 \gg R_s$.

4.5.2 Test results

Figure 4.16 shows the results of surface resistivity measurements obtained for a polyethylene sheet exposed to discharges for a period of 1 hr. It can be seen that the largest decline of the conductivity occurs within the first 10 minutes of the discharge activity. This agrees with the fact that after 10 minutes the first discharges with the properties of a Townsend breakdown are observed. After several tens of minutes, when the resistivity reached a low and stable value, the large majority of streamer-like discharges is replaced by Townsend-like discharges. To illustrate this, Figure 4.17 shows the percentage of Townsend-like and streamer-like discharges as a function of the discharge exposure time.

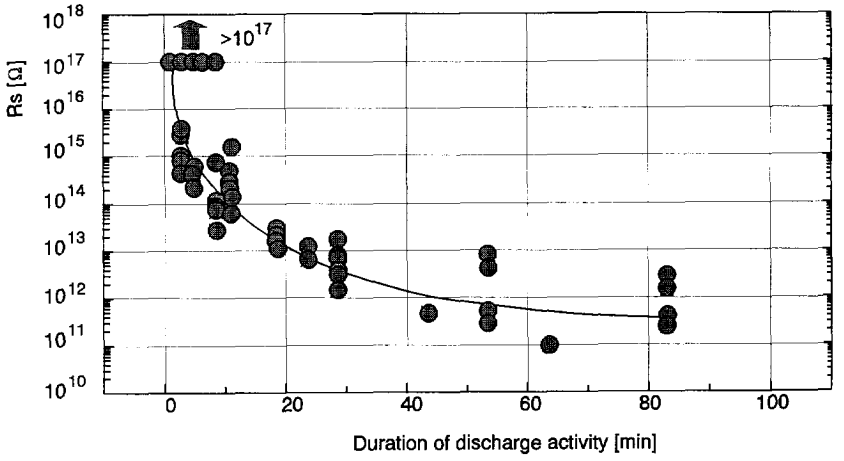

Figure 4.16 Surface resistivity of a polyethylene sheet with an exposure to discharges from 0 to 60 min.

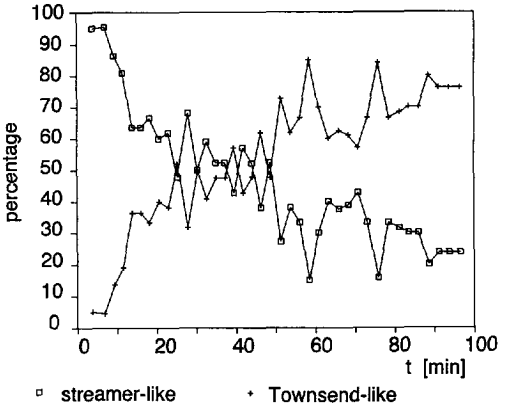

Figure 4.17 Percentage of Townsend-like and streamer-like discharges as a function of discharge exposure time.

4.6 Effect of the constituents of the gas in the void

As was shown in Chapter 3 different substances were deposited at the void surface: droplets, crystals and powder.

It was found by Gamez-Garcia et al [27] that the products deposited at the surface of the void mainly consist of acids. The particles and UV radiation in the discharge process break covalent bonds at the polymer surface, resulting in the formation of radicals:

$RH \rightarrow R\cdot + H$

These radicals react with oxygen and form new radicals:

$R\cdot + O_2 \rightarrow ROO\cdot \rightarrow ROOH$ (using H_2O or H from the polymer)
$ROOH \rightarrow -COOH \rightarrow (COOH)_2$

thus forming, amongst others, oxalic acid.
It was found that the formation of the oxalic acid crystals required the simultaneous presence of H_2O, CO_2 and CO. When absorbents of CO_2 and CO were introduced, droplet formation was found, whereas otherwise both crystals and droplets appeared. The oxidizing reactions of the discharge at the void surface will produce the CO and CO_2. The moisture in the void will provide the H_2O. Even in the case of an initial absence of H_2O, oxidation of the polymer will provide this essential constituent.

To verify the hypothesis that the formation of oxalic acid leads to
a) a Townsend-like mechanism
b) and later to an extensive degradation at the site of clusters of oxalic acid crystals, a number of tests were performed in which one of the constituents of the discharge by-products was either absent, or present in very limited amounts only.

4.6.1 Measurements in different gases

Void between PE electrodes filled with dry synthetic air, (79% N_2, 21% O_2)

Available: N_2 and O_2
(initially) not available: CO, CO_2 and H_2O

The transition time between the first and the second stage was measured for two types of polyethylene sheets at four samples per type. The results are

shown in Figure 4.17, transition times between 100 and 440 minutes were measured. For comparison: the transition times for voids filled with ambient air of 40% ±4% humidity fell in the range between 20 and 30 min. This proves that either the relative humidity or a constituent like CO_2 have a clear effect on the evolution of the discharge process. Initially no moisture was available for the production of oxalic acid crystals. Therefore the hydrogen constituent had to become available during the oxidation of the polymer.
After opening the samples filled with synthetic air, hardly any crystal formation was found. Instead, the void surface was covered with a very fine

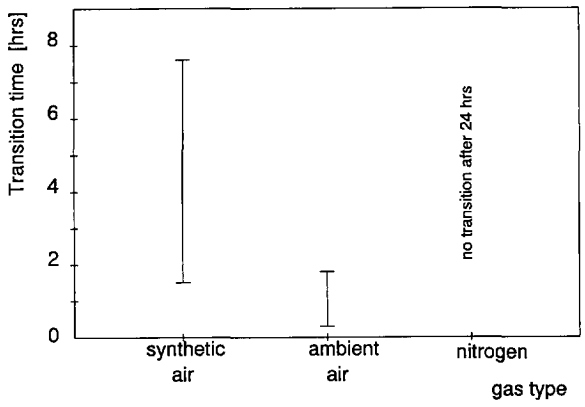

Figure 4.18 Transition times from streamer-like to Townsend-like mechanism for different gaseous void contents.

dust. In one of the samples one cluster of large crystals was found. At the center of this cluster a crater was visible. This indicates the importance of the elements forming the crystals: even if one of the constituents is available in limited amounts only, one group of crystals can lead to crater formation. If all constituents are available in large amounts more crystals are formed and the probability of crater formation is enhanced.

Void between PE electrodes filled with pure nitrogen

Available: N_2
(initially) not available: O_2, CO, CO_2 and H_2O

The absence of O_2 and moisture should inhibit the formation of oxidation products and thus oxalic acid. Therefore it was expected that

a) no transition to the Townsend-like mechanism would occur and
b) no crystals would be formed.

(Further, in the absence of oxygen the time-lag is expected to be small, resulting in low values of the overvoltage.) Even after 20 hrs of discharge activity no Townsend-like discharges were observed, see Figure 4.17. The discharge process during these 20 hrs was very stable, hardly any change of discharge magnitude or the minimum ignition phase were observed, see Figure 4.19.

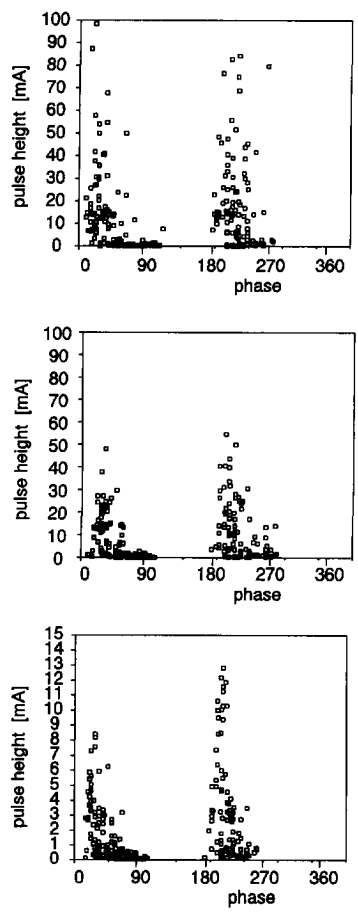

Figure 4.19 Evolution of the discharge pulse parameters during a 24 hr test in nitrogen. D = 10 mm, h = 0.2 mm.

The wide phase distribution that is observed in all discharge tests, was present even after 20 hrs, see Figure 4.19. This is an indication that discharges still ignited after a time-lag and this confines with the fact that they were of a streamer-like nature.
Considering the surface conductivity: After opening the sample the void surface was found to be covered homogeneously with small droplets (diameter $\approx 2\mu m$). This layer of droplets has a low surface resistivity, $\approx 10^{14}\ \Omega$. The absence of the constituents H and O apparently prevented the forming of a Townsend advancing layer.

4.6.2 Electron attachment

Some researchers [40, 83] claim that the disappearance of oxygen in the gas phase during the initial discharge activity is responsible for a change in the discharge mechanism. Part of the potential initiatory electrons are then attached to oxygen molecules, leading to an increase of the time-lag. Thus overvoltages occur resulting in a streamer-like process. Together with the oxidation of the dielectric surface the gas phase oxygen disappears, the time-lag decreases and the Townsend-like mechanism takes place.
This theory was checked by opening several samples and refilling them with ambient air after the transition to the Townsend-like mechanism had occurred. When the sample was closed and replaced in the test-cell the Townsend-like mechanism was still prevailing although a small number of streamer-like discharges were present during the first 10..20 seconds. A number of tests as described in section 4.6.1 were performed with pure nitrogen in the sample. The absence of an electro-negative gas in that case did not result in a Townsend-like mechanism. Therefore it is unlikely that the transition can be explained by oxygen consumption only.

4.6.3 Conclusions

The presence of a layer of oxidation products, due to ageing, proves to be a necessary condition for the transition from streamer-like to Townsend-like discharges. It is proposed that shallow traps in the layer of oxidation products at the dielectric surface are responsible for an enhanced availability of initiatory electrons. This leads to a reduction of the time-lag and thereby favors the Townsend-like mechanism. This hypothesis could be checked by measuring the trap depth as well as the number of traps for virgin dielectrics and dielectrics aged with different gases, which might be an interestic topic for further study.

The conductivity of the dielectric surface is *not* the reason for the transition, it is only the result of the acid nature of these by-products and of the trapped charge. Further, there is *no* relation between γ_{ph} in the static situation as described in section 4.4 and the discharge mechanism.
It was also found that the electro-negative properties of oxygen in the gas phase have no significant effect.

4.7 Pitting mechanism

The pitting mechanism that occurs after several tens of hours of discharge activity originates from the field concentrations at the tips of clusters of sharp crystals. Cluster formation was also recently reported by Dejean [21] and Foulon [?] who observed a concentration of discharge activity at the locations where "nodules" of discharge by-products were clustered.

The field at the tip of a (conductive) crystal was calculated with a finite element field calculation program. The surface of the void surrounding the crystal was assumed to be conductive. Surface resistivity measurements have pointed out that this assumption is allowed. The dimensions of the crystal were taken as follows: diameter 10 μm, height 20 μm. The height of the void h was 0.1 mm, the diameter D was 10 mm. The total thickness of the dielectric, with a permittivity ε_r=2.2, was 4.5 mm. Figure 4.20a shows the equi-potential lines in the vicinity of the crystal. The field enhancement of about 2 times is significant; it is shown in Figure 4.20b along the vertical axis of the crystal.
The following theory is formulated for explaining the pitting discharge type.

I. The field enhancement explains both the concentration of the discharge activity at the location of sharp crystals and the high discharge repetition rate. The electric field at the tip of the crystals reaches the breakdown value before other parts of the void. Further, due to the field enhancement more discharges can ignite per voltage phase as is shown in Figure 4.22.

II. The conductive nature of the void surface leads to a quick redistribution of the charges deposited at the surface by the discharges. Therefore the breakdown voltage of the void is reached much faster than in the case of a

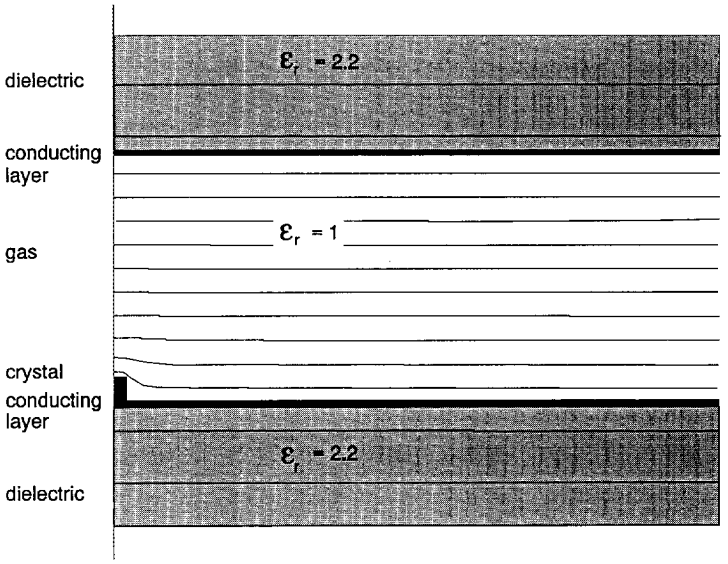

Figure 4.20a Equi-potential lines at the tip of a conductive crystal located at the (conductive) void surface.

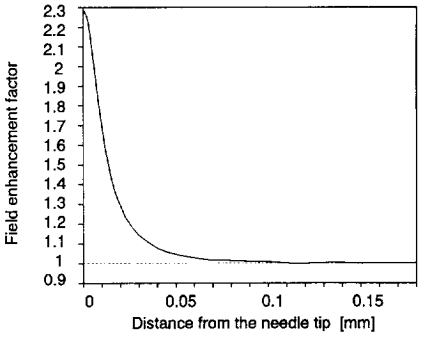

Figure 4.20b Field enhancement in the vicinity of the crystal tip.

(virgin) non-conductive surface. This is illustrated in Figure 4.21 where the results are shown of measurements on pitting discharges. This type of discharges was obtained after 40 hrs of discharge activity in a 10 mm diameter,

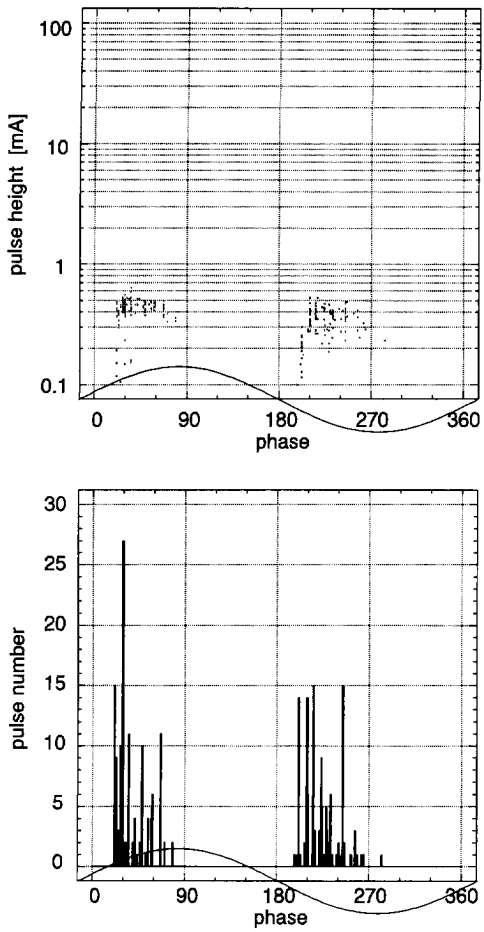

Figure 4.21 Pitting discharges, pulse height-phase and pulse number-phase distributions. D=10 mm, h=0.4 mm.

0.4 mm high void in polyethylene. Figure 4.21 shows both the pulse height distribution and the pulse number distribution as a function of the voltage phase. It can be seen that the discharges are grouped around specific phase angles. The phase distances between the groups are about equal.

As an example the discharge repetition rate is calculated using the following parameters:

test voltage (across the void) U=4.5 kV
ignition voltage U_i=3 kV
extinction voltage U_e=1 kV

The recurrence of discharge ignition can be represented as shown in Figure 4.22a. With a field enhancement factor of 2 the repetition rate increases, as can be seen in Figure 4.22b. The deposition of a conductive layer at the void surface leads to a rapid distribution of charges across the surface. This results in an accelerated re-ignition of the discharge, see Figure 4.22c. The result of these model calculations quite well explains the results of the above described experiment. Using this model it would be expected that the discharge repetition rate increases with a rise of the surface conductivity. This was not directly verified by experiments, but the fact that the repetition rate increases with time, like the surface conductivity, does support this hypothesis.

The localized attack of the insulating material by discharges with a high repetition rate is supposed to be the cause of the formation of pitts. The exact mechanism behind this degradation is still unknown. There is some evidence [28] that the continuous interaction of hot electrons with the dielectric leads to the creation of traps deeper in the dielectric. The electrons trapped in these charges lead to a concentration of the field favorable for the initiation of an electrical tree. The presence of highly reactive species might lead to an electrochemical degradation process. More research is needed to understand the exact mechanism, which might possibly lead in the direction of the chemics of the degradation process.

The recognition of the onset of pitting discharges is very important because the pitts will eventually lead to electrical treeing and subsequent breakdown of the dielectric.

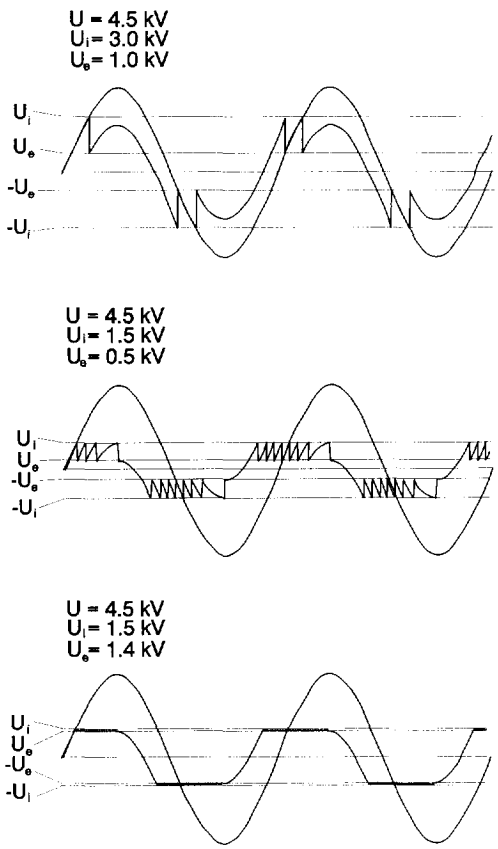

Figure 4.22 Recurrence of discharges. a) no field enhancement, b) with field enhancement, c) rapid redistribution of surface charge.

Chapter 5
Mathematical model of the discharge mechanism

In this Chapter the effect of the overvoltage and the secondary Townsend coefficient on the shape of the discharge pulse are studied using a mathematical model. The results are meant to be indicative.

5.1 Computer simulations of the growth of the discharge current

In order to calculate the temporal growth of the discharge current, both the continuity equations for electrons and ions and the Poisson equation have to be solved. Figure 5.1 illustrates the continuity equations.

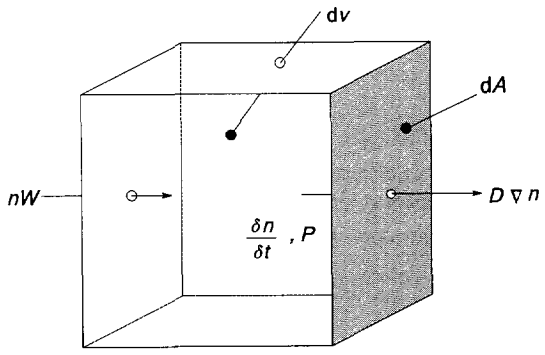

Figure 5.1 Illustration of the continuity equations.

The rate of particle density change in a volume element dv equals the net flux of particles diffusing through dA into dv, minus the net flux of particles drift-

ing through dA out of dv, plus the production of particles within dv:

$$\int\int\int \frac{\partial n}{\partial t} \cdot dv = \int\int D\nabla n \cdot dS - \int\int nW \cdot dS + P \tag{5.1}$$

with n particle number density [cm^{-3}], D diffusion coefficient [$cm^2\ s^{-1}$], W drift velocity [$cm\ s^{-1}$] and P particle production [s^{-1}]. P is the net particle production per second that is the result of ionization processes minus the loss of particles due to attachment and conversion processes.
The Poisson equation:

$$\nabla^2\psi = -\frac{\rho}{\varepsilon} \tag{5.2}$$

with ψ the space charge potential [V] and ρ the charge density [$C\ cm^{-3}$].
Here, it is assumed that the process is axis-symmetric, i.e. the lateral extension of the discharge is equal in all directions. In this case cylindrical coordinates can be used.
In a further approximation it is assumed that the discharge has a constant diameter much larger than the height of the void, the problem to be solved can be considered to be one-dimensional.
In this case the following set of equations are obtained:

$$\begin{aligned}
\frac{\partial n_e}{\partial t} &= -W_e\frac{\partial n_e}{\partial x} + D_e\frac{\partial^2 n_e}{\partial x^2} + (\alpha-\eta)W_e n_e \\
\frac{\partial n_i}{\partial t} &= W_i\frac{\partial n_i}{\partial x} + D_i\frac{\partial^2 n_i}{\partial x^2} + (\alpha-\eta)W_e n_e \\
\frac{\partial^2\psi}{\partial x^2} &= -\frac{e}{\varepsilon}(n_i - n_e)
\end{aligned} \tag{5.3}$$

with n_e the electron charge density [cm^{-3}], n_i the positive ion charge density [cm^{-3}], W_e the electron drift velocity [$cm\ s^{-1}$], W_i the ion drift velocity [$cm\ s^{-1}$], e the elementary charge and ϵ_0 the vacuum permittivity.
In a first approximation it is assumed that $W_i = \mu_i E$, with μ_i the ion mobility [$cm^2\ V^{-1}\ s^{-1}$] independent of E. The value used for μ_i is 2.6 $cm^2\ V^{-1}\ s^{-1}$, taken from [53]. W_e was approximated by [53]: $W_e = 8.81\times10^3\times E^{0.715}$. Further it is assumed that only direct ionization takes place, the ionization coefficient α being equal to:

$$\alpha \approx 2.2\times10^{-7}\cdot(E - 2.44\times10^4)^2 \tag{5.4}$$

with E the field strength in $V\ cm^{-1}$ and α in cm^{-1}.

Photo ionization at the cathode is taken as the major source for secondary initiatory electrons.
The boundary condition at the cathode is:

$$n_e(0,t) = n_{e0} + \gamma_{ph} \int_0^h \alpha n_e(x,t)\,dx \qquad (5.5)$$

with n_{e0} the initiatory electron density at $t = 0$, and γ_{ph} the second Townsend coefficient for photons.
In Appendix B the procedure for solving the continuity equations and obtaining the charge distribution in the void is described. The current flowing in the external circuit is calculated as well.
If the diameter of the discharge is small as compared to the height of the void

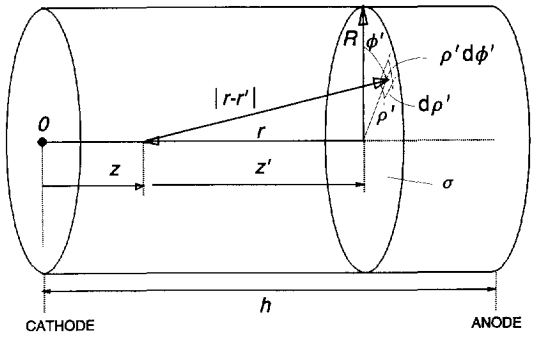

Figure 5.2 Diagram illustrating the cylindrical method for the calculation of the space charge field.

[56] the calculation of the space charge field using the one-dimensional Poisson equation introduces large errors. This is the case at the start of the development of the discharge when the radial expansion due to photo-ionization at the cathode is still small. Therefore the field is also calculated using the cylindrical method introduced by Davies et al [20] that takes into account the small diameter/height ratio.

Suppose that the cylinder shown in Figure 5.2 consists of a number of infinitely thin disks. Each disk has a radius R and carries a uniform surface charge density $\sigma(z')$. The distance $|\mathbf{r}\text{-}\mathbf{r}'|$ between the point $\mathbf{r}'$ at radius ρ and angle ϕ (in cylindrical coordinates) and the point $\mathbf{r}$ on the axis of the disk (the

z' axis) is given by

$$\begin{aligned}\Phi &= \frac{\sigma}{4\pi\varepsilon_0}\int_0^{2\pi}\int_0^{R}\frac{\rho' d\rho' d\phi'}{\sqrt{\rho'^2+z'^2}} \\ &= \frac{\sigma}{4\pi\varepsilon_0}2\pi\int_0^{R}\frac{\rho' d\rho'}{\sqrt{\rho'^2+z'^2}} \\ &= \frac{\sigma}{2\varepsilon_0}\left(\sqrt{R^2+z'^2}-|z'|\right)\end{aligned} \tag{5.6}$$

for both positive and negative z'.
The axial electric field E_z due the surface charge on a disk at a distance z' can be found by taking the gradient of Φ in the z' direction.

$$\begin{aligned}E_z &= -\frac{\partial\Phi}{\partial z'} = -\frac{\sigma}{2\varepsilon_0}\frac{d}{dz'}\left(\sqrt{R^2+z'^2}-|z'|\right) \\ &= -\frac{\sigma}{2\varepsilon_0}\left(\frac{z'}{\sqrt{R^2+z'^2}}\mp 1\right)\end{aligned} \tag{5.7}$$

The upper sign applies to positive z', the lower sign to negative z'. When the z axis is used we obtain $dE(z)$, the electric field due to a surface charge density at $(z+z')$

$$dE(z) = -\frac{\sigma(z+z')}{2\varepsilon_0}\left(\frac{z'}{\sqrt{R^2+z'^2}}\mp 1\right) \tag{5.8}$$

Using the principle of superposition the total electric field $E(z)$ is given by

$$E(z) = \int_{-z}^{h-z} -\frac{\sigma(z+z')}{2\varepsilon_0}\left(\frac{z'}{\sqrt{R^2+z'^2}}\mp 1\right)dz' \tag{5.9}$$

The electron avalanche has a radial expansion that is determined by the radial diffusion R of the electrons on their way to the anode.
According to Loeb the value of R (at which the charge density has decreased to e^{-1}) is

$$R = \sqrt{6Dt} = \sqrt{6\cdot\frac{2}{3}u_t\frac{x}{E}} \tag{5.10}$$

with D the diffusion coefficient, u_t the thermal energy of the electrons in the field E. Using the value of u_t = 1.7 V, as given by Raether [71], the following relation is obtained:

$$R = \sqrt{C\frac{x}{E}} \qquad (5.11)$$

with C = 6.8 V

With the use of the cylindrical method the field was calculated for the situation shown in Figure 5.3a where the front of an electron avalanche has crossed 50% of the void.
The height h of the void is 1 mm and the (Laplace) field E in the void is 4.7 kV/mm. The radius R of the avalanche at x = 0.5 mm can be calculated to be 24 μm using (5.11).
Figure 5.3b shows both the electron density distribution and the positive ion density distribution. Figure 5.3c shows the same field calculated with the one-dimensional Poisson equation. It is shown that the error is quite large when the one-dimensional Poisson equation is used. The result of the cylindrical method on the other hand is quite close to the exact three-dimensional solution [56].

5.1.1 Calculation of the discharge current between metal electrodes

The effect of different values of γ and ΔV on the development of the discharge was calculated using the one-dimensional continuity equations and the cylindrical method for the space charge field calculation.

For both the Townsend and the streamer breakdown mechanism the formation of space charge is of importance [71]. For the Townsend mechanism the cloud of positive space charge, produced by a succession of electron avalanches, accelerates the ionization process by an enlargement of α. In the case that the Townsend criterion is just fulfilled ($\mu = \gamma\exp[\alpha h]$ slightly larger than 1), the space charge field lifts the value of μ above 1 after a large number of avalanches, accelerating the current growth.
To illustrate this, an example is given of a Townsend discharge between metal electrodes, *not limited by a dielectric*, in series with the void.
Figure 5.4 shows the discharge current on a logarithmic scale in a 0.1 mm gap between electrodes with initially μ = 1. The diameter of the discharged area is taken as 10 mm, assuming a lateral spreading of the discharge because of the

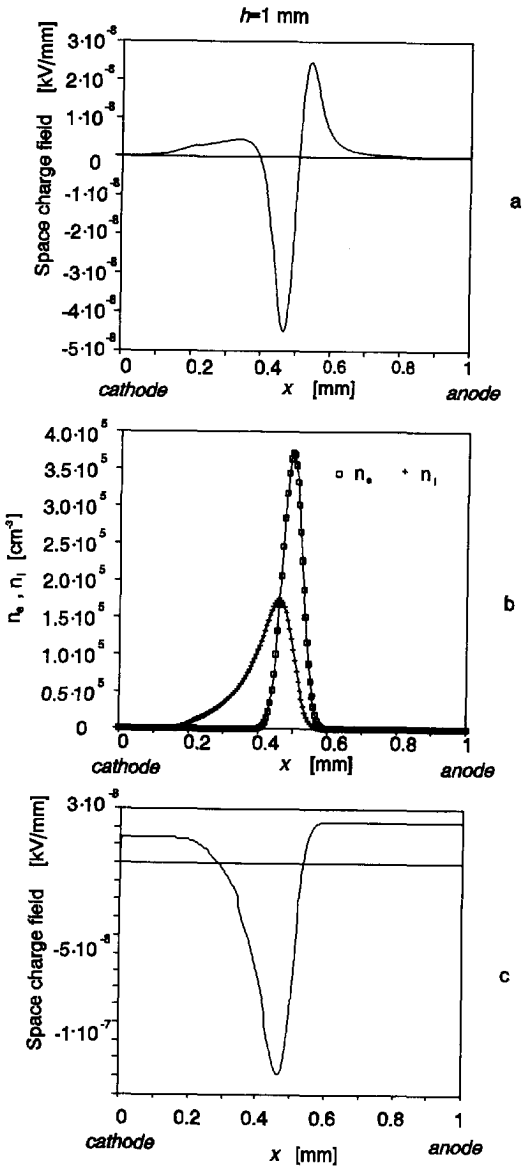

Figure 5.3 Test of the cylindrical method.

large number of generations of avalanches. The moment that the space charge field starts to have a significant effect on α, after about 40 avalanches is clearly

visible. At this point the current starts to rise very fast and is limited by the external circuit only, the Townsend mechanism is replaced by the streamer mechanism. With μ constant, the electron current should grow exponentially. In the first 10 ns this can be recognized in the behavior of the logarithm of the current that tends to go to a constant value when the oscillations damp out.

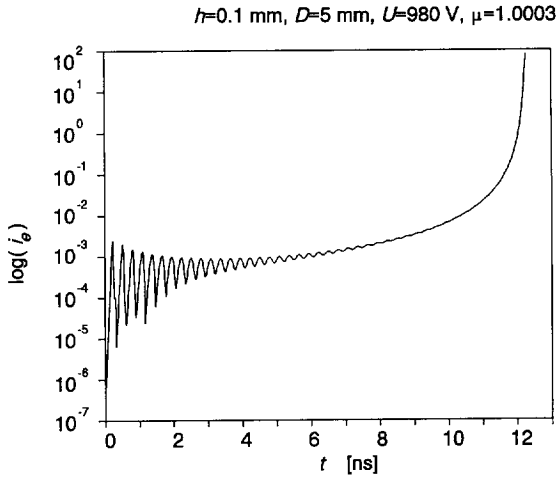

Figure 5.4 Current of a Townsend discharge with the effect of positive ion space charge.

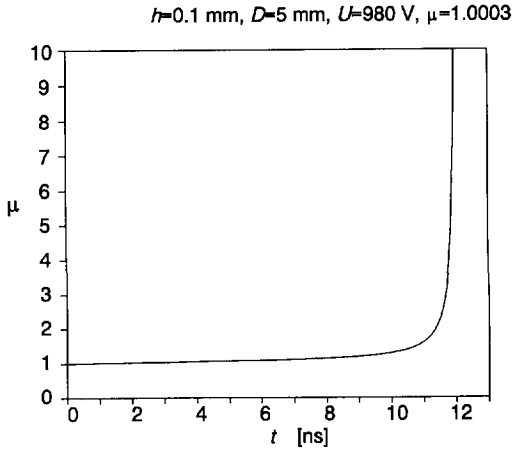

Figure 5.5 The value of μ as a function of time. When the space charge field comes into play the value of μ rises steeply.

When the space charge comes into play the value of μ rises steeply, see Figure 5.5.

In the *streamer* mechanism it is the effect of the *electron* space charge [71] of the first avalanche that leads to breakdown. To accomplish this effect a very high number of electrons ($10^7..10^8$) has to be present in the front of the avalanche. A space charge field results in photo ionization in the gas, leading to a very fast breakdown. The high number of electrons in the first avalanche can be obtained with electrode-gas combinations with a very low value of γ. For $\gamma < 10^{-7}$ α has to be large, and the critical number of electrons is reached to obtain $\mu=1$ for a self-sustained discharge. In this case no Townsend breakdown occurs.
For electrode-gas combinations with larger values of γ, α is relatively small, and the critical number of electrons for streamer breakdown is not reached with $\mu=1$. Only when overvoltages are applied and $\mu>1$ the critical number is obtained.
The overvoltage ΔV is in this case defined as the percentile overvoltage across the gap relative to the minimum breakdown voltage V_{min} for this particular gap calculated from the breakdown condition $\mu=1$:

$$\Delta V = \frac{V - V_{\min}}{V_{\min}} \times 100\% \qquad (5.12)$$

The calculations were made for a void with a height of 0.1 mm and a constant thickness of the dielectric in series with the void.

5.1.1 Calculation of the discharge current between dielectric electrodes

In this section the discharge current is calculated for three combinations of ΔV and γ:

- 1. large ΔV ($>10\%$) and small γ ($<10^{-7}$)
- 2. small ΔV (1%···10%) and large γ (10^{-5}···10^{-4})
- 3. very small ΔV ($<1\%$) and large γ (10^{-5}···10^{-4})

1. Large ΔV, small γ (streamer-like discharges)
If γ is very small, $\gamma < 10^{-7}$, a self sustained discharge will occur with large overvoltages only. For overvoltages above 10% the space charge field was

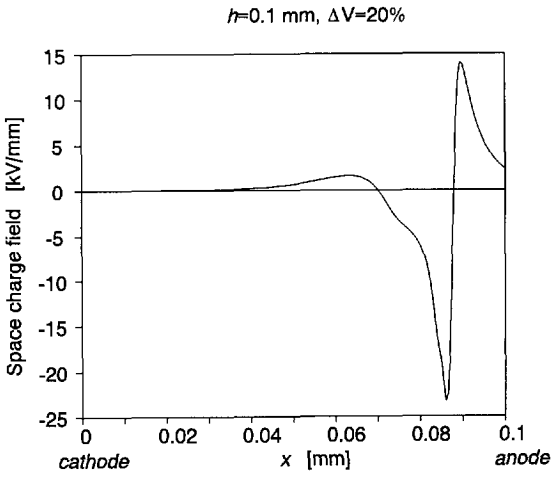

Figure 5.6 Space charge field in the void when the avalanche has crossed 90% of the void.

calculated to reach high values, approximating the Laplace field. Figure 5.6 shows the space charge field at the moment that the avalanche has crossed 90% of the void ($\gamma = 10^{-7}$ and $\Delta V = 20\%$). The discharge current, as shown in Figure 5.7 first rises exponentially but after 0.17 ns when the avalanche has crossed 90% of the void it rises over-exponentially due to the increase of α. The current was plotted on a logarithmic scale in order to see any deviation from the exponential behavior that would indicate a change of μ. Further calculation of the current was not possible. However, the extremely fast rise time of the current together with the high value of the space charge field of 14 kV/mm predict the onset of a streamer. A streamer velocity of about 10^8 cm/s [71] explains the very short rise times that are measured for streamer-like discharges in Chapter 3.

2. Small ΔV, large γ (streamer-like and Townsend-like discharges)

If the overvoltage is low, the critical number of electrons is not reached and the electron space charge field is not sufficiently high to obtain a streamer-like discharge. If $\mu \geq 1$, that is, if γ is sufficiently high, secondary avalanches are initiated in the circumference of the initial avalanche. The discharge spreads out over the void surface with a growing number of generations of avalanches as can be seen in the optical images of Townsend-like discharges in Chapter 3. It was assumed that the discharge radius grows with approximately 100 μm per avalanche generation. With this assumption, a void surface of 10 mm

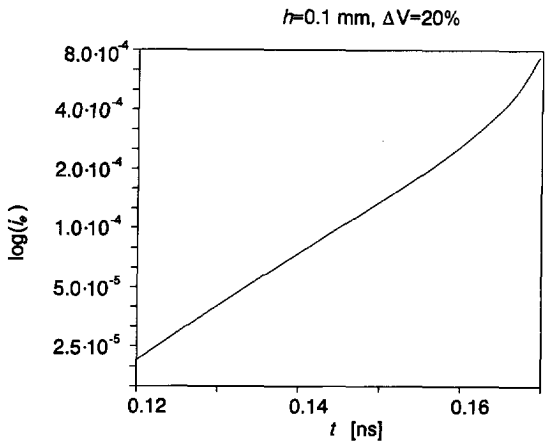

Figure 5.7 Development of the discharge current with a sharp rise when the space charge field comes into effect.

diameter is discharged within 50 generations, which is supported by the measurements of the discharge current synchronous with the light emitted by the discharge.

Because of the decreasing electric field in the void caused by the charge deposited at the void surface, the value of α decreases and the size of the succeeding avalanches S_a decreases until the ionization process stops.

$$S_a = \exp\left[\int_0^h \alpha(x)\,dx\right] \tag{5.13}$$

At this point the discharge current consists only of the current of positive ions.

Figure 5.8 shows both the electron and the ion current for $\gamma = 6.675 \times 10^{-6}$ and $\Delta V = 1\%$ ($\mu = 1.38$). It can be seen that the electron current starts to decrease after about 50 generations of avalanches. At this point μ drops below 1, see ?, and the discharge is no longer self-sustained and stops. After about 20 ns the electron current has decreased to zero. At this point the current of positive ions has a constant value. This lasts until the first ions reach the cathode after the ion transit time. The constancy of the ion current agrees with the plateau that is found in the Townsend-like pulses in Chapter 3.

The large number of avalanches in the Townsend-like discharge result in a growing number of relatively immobile positive ions in the void. These ions give rise to a significant space charge field if their number is sufficiently high.

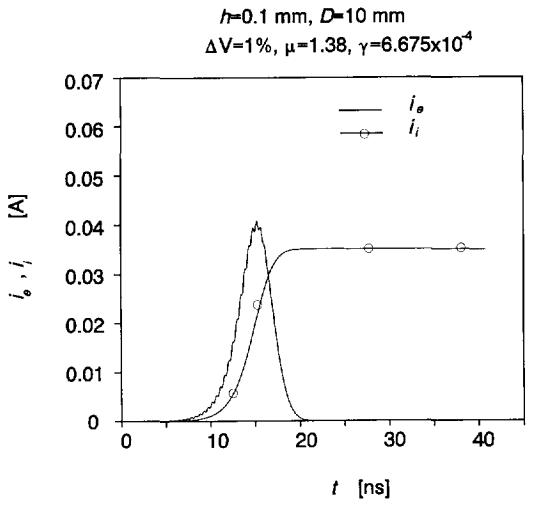

Figure 5.8 Electron and ion current for $\mu = 1.38$, $\gamma = 6.675 \times 10^{-4}$ and $\Delta V = 1\%$.

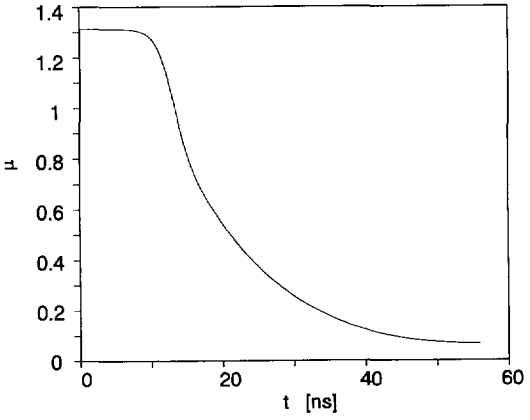

Figure 5.9 μ as a function of time, see the last Figure.

In the space charge enhanced field the ionization factor α grows rapidly, resulting in a very fast current growth. In this case the discharge process, initially starting with μ slightly larger than 1, is accelerated by the space charge enhanced ionization, leading to a value of $\mu \gg 1$. If the magnitude of

the space charge field approaches the magnitude of the Laplace field, even a transition to a streamer-like mechanism can occur. Whether the space charge induced acceleration takes place depends on the value of the total field, i.e. the space charge induced field superimposed on the Laplace field.
Figure 5.10 shows the discharge current at an overvoltage of 2.5%, a value of γ of 6.675×10^{-4} and an initial value of μ of 2.3. In this case the increase of the space charge field outnumbers the decrease of the Laplace field, resulting in a very fast current growth after 5 ns.

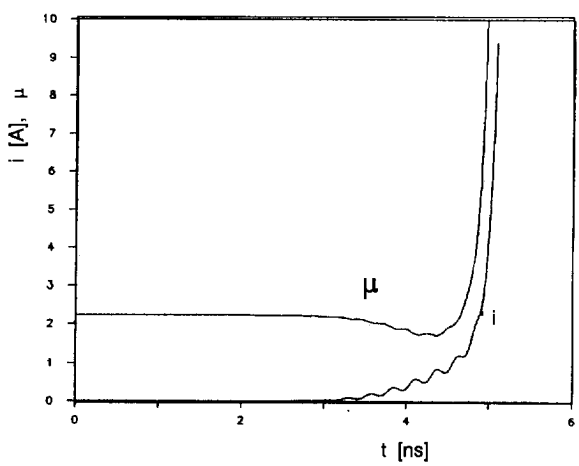

Figure 5.10 Transition to a streamer-like discharge when the increase of the space charge field is larger than the decrease of the Laplace field.

This behavior has indeed been found in practice, Figure 5.11 shows a discharge pulse of a 1 mm high, 1 mm diameter void with a distinct transition from the Townsend-like to the streamer-like mechanism. The peaks in the initial stage of the discharge represent the transit times of the succeeding generations of avalanches.

3. Very small ΔV, large γ (Townsend-like discharges)

For very small overvoltages the rate of increase of the space charge field is not large enough to result in a net increase of the avalanche size S_a. The discharge consists of an initially increasing avalanche size ($\mu > 1$) that breaks off when μ drops below 1 due to the charge collected at the void surface.
Figure 5.12 shows the discharge current calculated for values of ΔV of 0.5%, 1% and 1.5%. In all cases the value of γ was 6.675×10^{-4}. It can be seen that the peak of the electron component at the start of the discharge pulse becomes

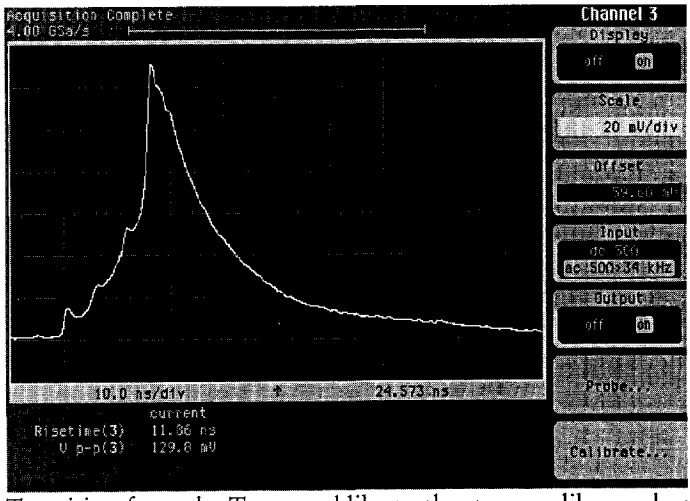

Figure 5.11 Transition from the Townsend-like to the streamer-like mechanism after the space charge field comes into effect.

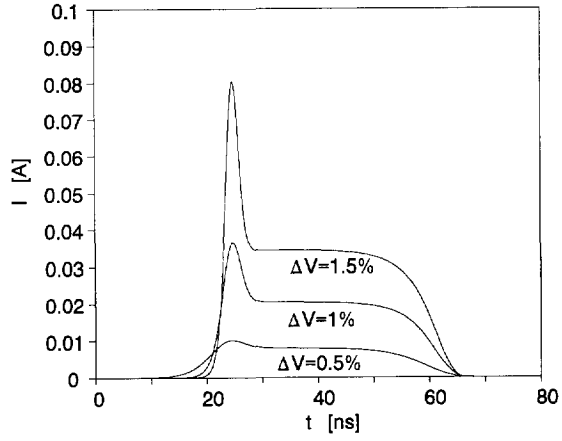

Figure 5.12 Townsend-like discharges for very small overvoltages.

more pronounced with higher overvoltages. This is the pulse shape that was measured for Townsend-like discharges in Chapter 3.

Figure 5.13 shows the voltage across the void as a function of time for different values of the overvoltage. It can be seen that the residual voltage V_{res}, the voltage when the discharge current is reduced to zero, is largely effected by the value of ΔV. For small values of ΔV V_{res} is very close to the ignition

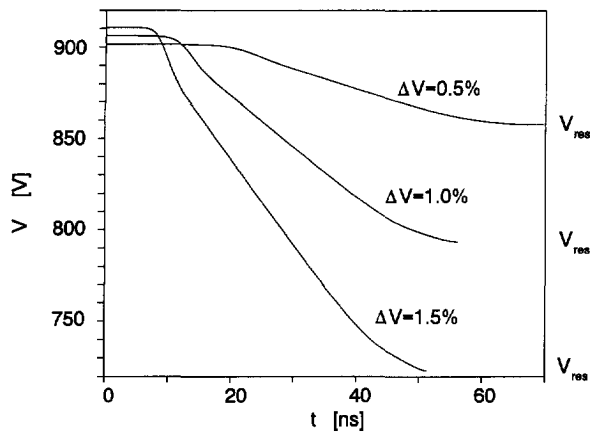

Figure 5.13 Decrease of the voltage in a 0.1 mm high, 10 mm diameter void for different overvoltages. Note the effect of the overvoltage on the residual voltage.

voltage V_i. For practical purposes this leads to the conclusion that the number of discharges per voltage cycle increases with decreasing overvoltage. At very low overvoltages a high discharge repetition rate might lead to a semi-continuous discharge current, see also Chapter 4, page ?.
If the conductivity of the walls of the void increases, surface currents can redistribute the surface charge deposited by the discharge. In the ultimate situation the drop of the voltage is reduced to zero, $V_{res}=V_i$, and the ionization process proceeds as long as the voltage across the void exceeds the minimum breakdown voltage ($\mu \geq 1$). This predicts the onset of a Townsend-like discharge with a very long duration (up to milli-seconds). In this study no such discharges were measured. However, the fact that their amplitude is very small, see Figure 5.12, may lead to the assumption that they escape from being detected. The optical method should however detect such discharges, but in all cases in this study where a glow was detected an electrical signal of moderate duration was detected.

Conclusions

The calculations indicate that the overvoltage and the secondary Townsend coefficient γ govern the shape of the discharge pulse.
If γ is small ($< 10^{-7}$) the streamer-like discharge type occurs even without

overvoltages. For larger values of γ ($\approx 10^{-3}$) Townsend-like discharges occur unless large overvoltages are applied ($>2.5\%$).
It was calculated that the residual voltage across the void is strongly effected by the overvoltage. In the literature this residual voltage is often taken as zero. While this may be true for streamer-like discharges, it certainly is not for Townsend-like discharges. Depending on the overvoltage, the residual voltage can be very close to the initial voltage across the void.

Chapter 6
Diagnostics

6.1 Introduction

The ability to distinguish between the three different stages of the discharge process may be used for diagnostic purposes in practical cases. Especially the detection of the third stage, when the discharge activity is very deleterious, can be of importance. This knowledge could be applied to full-size high voltage components, using ultra-wide band detection (≈ 1 GHz bandwidth). In that case two problems have to be solved:

a. The recognition of the transitions (phase I to phase II and phase II to phase III) can be performed by an observation of the discharge pulse shapes on an oscilloscope. This method however strongly depends on the observer and is therefore regarded as less suitable. Therefore it is proposed in section 6.2 to characterize the stages by statistical distributions of the discharge pulse parameters. This approach is inspired by the success of a similar technique used with classic detection. In section 6.3 results of tests using the *moving median* are presented.
b. The high frequency coupling of the detector to the high voltage component. One has to bear in mind that in practice insulating constructions, like for instance in transformers, are complex systems as opposed to the geometrically simple models used in this thesis; their high frequency transmission characteristics might be unsuitable for time-resolved detection. For other objects, like GIS and high voltage cables of moderate length, this coupling is not very complicated. In 6.4 some examples described in literature are presented.

6.2 Statistical distributions of time-resolved parameters

The time-resolved pulse parameters show a scatter, due to statistical variations in the development of a discharge. Accounting for the statistical nature of the discharge, intensity distributions of the pulse parameters were determined. The interval between the minimum and the maximum value of a pulse parameter was split in N sections. The intensity of the i^{th} section was calculated as the number of pulses occurring in the i^{th} section divided by the total number of pulses in the N sections.

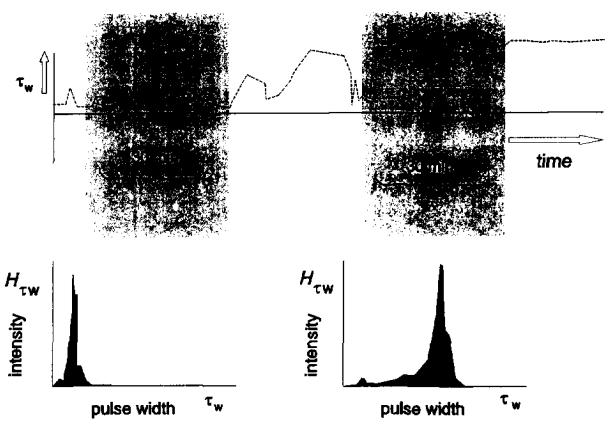

Figure 6.1 Construction of the pulse width intensity distribution $H_{\tau w}$.

The following *intensity* distributions were calculated:

- pulse height, H_I
- pulse width (50%-50%), $H_{\tau w}$
- pulse width (20%-20%)[1], $H_{\tau w,20\%}$
- pulse rise time, $H_{\tau r}$

Figure 6.1 shows as an example the construction of the pulse width distribution $H_{\tau w}$.

[1] See Chapter 2, page 23.

In addition the *phase* distribution of the discharge intensity

$H_n(\varphi)$

was determined. $H_n(\varphi)$ is defined as the total number of discharges occurring in phase interval φ_i.
In the following section the distributions of discharge measurements up to 100 hrs are presented. The samples consisted of a 10 mm diameter, 0.1 mm high void bounded by polyethylene, stressed 50% above the inception voltage. All distributions represent pulse parameters obtained within a 30 minute time interval. In each case distributions are shown that can be considered typical for a specific phase of the ageing process.

Pulse height distribution H_I

Figure 6.2 shows the evolution of H_I. The sharp decrease of the pulse height at the start of the test is remarkable and is typical for the flat voids studied in this thesis. A similar behavior is known from measurements with a classic detection system [35]. After 50...100 hrs discharges of very small pulse height appear. These discharges are of the pitting type described in Chapter 3.

Pulse width distribution $H_{\tau w}$

The pulse width distributions in Figure 6.3 clearly show the evolution of the discharge mechanism from stage to stage. In the first hours of discharge activity there is a clear shift towards a larger pulse width, see Figure 6.3c. The distribution concentrates around the pulse width characteristic for the height of the void. After 50...100 hrs pulses with a small width start to appear. This indicates the occurrence of pitting discharges.

Pulse width distribution $H_{\tau w,20\%}$

The parameter $\tau_{w,20\%}$ is able to detect the Townsend-like pulses which show a significant electron peak due to the ignition at small overvoltages. These pulses are the first Townsend-like pulses to occur; later on the overvoltage decreases resulting in a small electron peak. Therefore the $H_{\tau w,20\%}$ distribution is more suitable for recognizing the transition to the Townsend-like mechanism than the $H_{\tau w}$ distribution. Figure 6.4 shows the evolution of the $H_{\tau w,20\%}$ distribution.

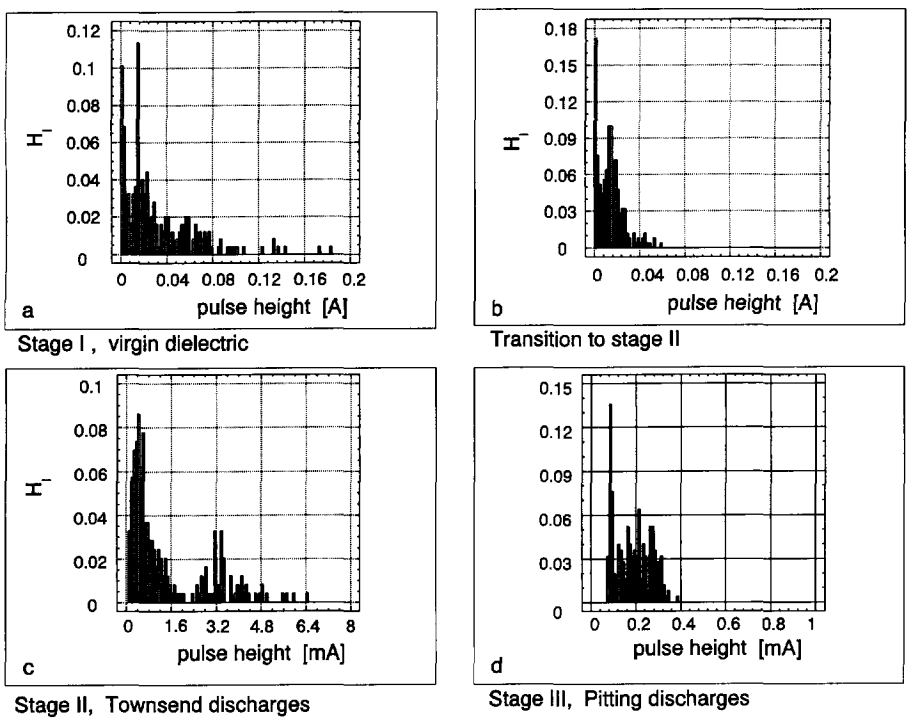

Figure 6.2 Pulse height distribution for
a. $0<t<30$ min b. $30<t<60$ min
c. $7<t<7.5$ hrs d. $99.5<t<100$ hrs

Pulse rise time-phase distribution $H_{\tau\tau}$

The parameter τ_r, like τ_w and $\tau_{w,20\%}$, is sensitive to the transition from streamer-like to Townsend-like pulses as is shown in Figure 6.5. However, the changes of τ_r are relatively small making this parameter less suitable as an indicator for the state of the ageing process.
Furthermore, the ability to discriminate between different values of the rise time is strongly effected by the bandwidth of the measuring system.

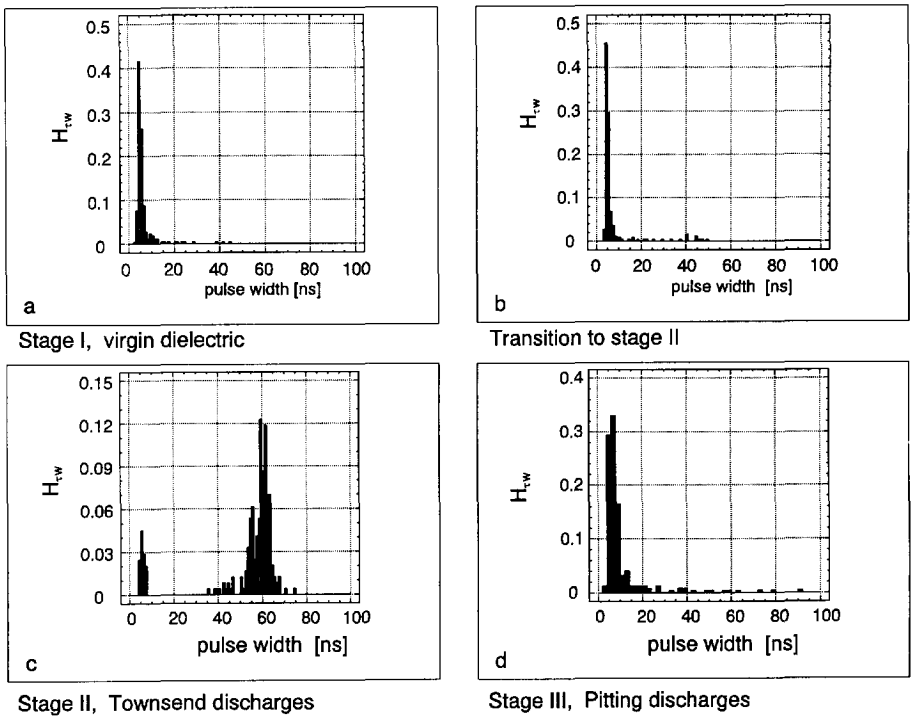

Figure 6.3 Pulse width distribution for
a. $0 < t < 30$ min b. $30 < t < 60$ min
c. $7 < t < 7.5$ hrs d. $99.5 < t < 100$ hrs

Discharge phase distribution $H_n(\varphi)$

The discharge phase distribution is well suited to describe the changes of the discharge mechanism. Figure 6.6 shows the evolution of $H_n(\varphi)$.
At the start of the test, the discharges are scattered over a large part of the voltage cycle because the time-lag, and thus the overvoltage is large. Gradually within the first hour the majority of the discharges starts to occur at distinct phase positions. This is because the time-lag has decreased and the discharges ignite close to the phase corresponding to the minimum or Paschen breakdown voltage. After 50 hours a high discharge intensity is seen at equidistant phase positions, indicating the occurrence of the high intensity pitting discharges.

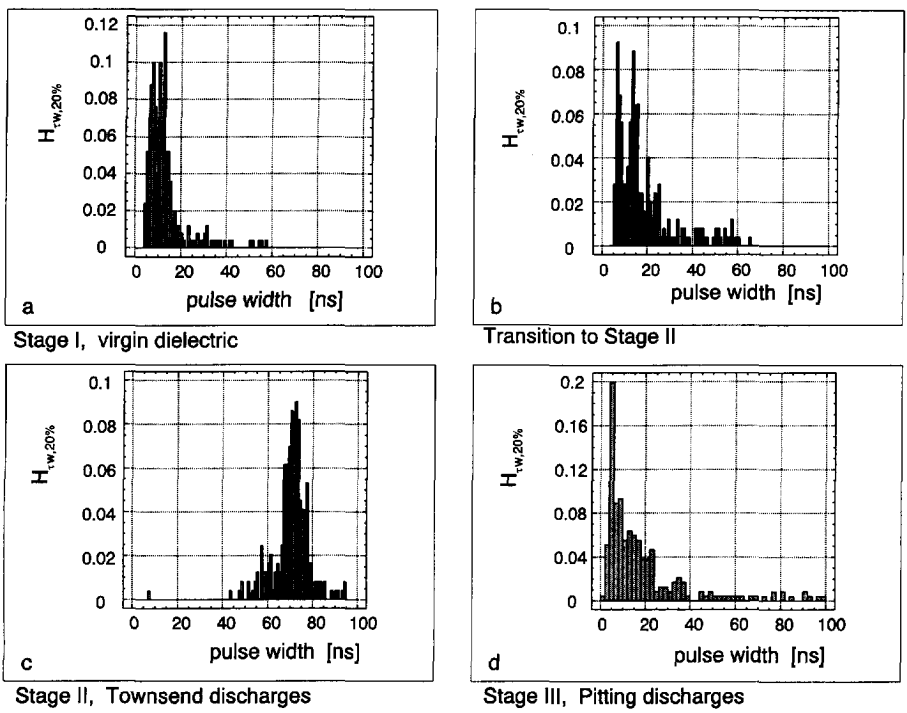

Figure 6.4 Pulse width 20% distribution for
a. $0<t<30$ min b. $30<t<60$ min
c. $7<t<7.5$ hrs d. $99.5<t<100$ hrs

It can be concluded that the intensity distributions of the time-resolved pulse parameters offer significant information on the discharge mechanism and the stage of the ageing process. The diagnostic strength of the distributions was compared on the basis of Figures 6.2-6.6.

The $H_{\tau w,20\%}$ was selected as the most sensitive parameter because the different discharge mechanisms are well marked by different pulse widths. Furthermore, the pulse width in the second stage is strongly correlated with the size of the void, see Chapter 3. The $H_{\tau w}$ distribution is rather slow in detecting the transition to stage II and is therefore disregarded. The changes in $H_{\tau\tau}$ are small, therefore this distribution is considered not to be selective.

The phase distribution $H_n(\varphi)$ is sensitive to the discharge mechanism. With classic detection methods similar distributions are obtained and analyzed [34].

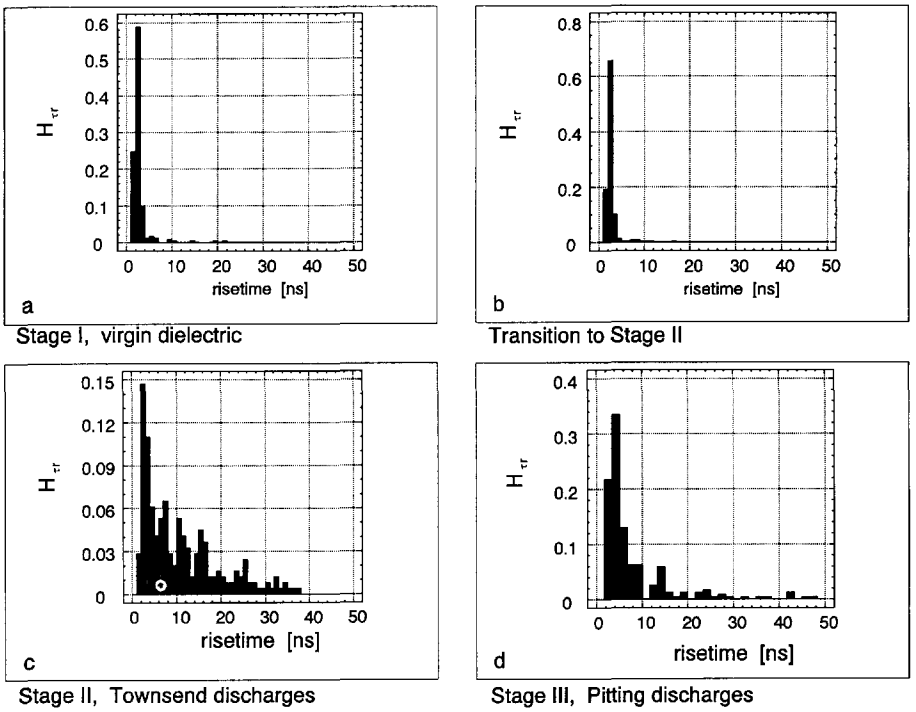

Figure 6.5 Pulse rise time distribution for
a. $0<t<30$ min b. $30<t<60$ min
c. $7<t<7.5$ hrs d. $99.5<t<100$ hrs

In this thesis a choice has been made for $H_{\tau w,20\%}$, i.e. the distribution of a parameter obtained with time-resolved detection and further analysis of $H_n(\varphi)$ is left for the area of classic detection.

6.3 Moving median of the pulse width

The 20% pulse width of the discharge signal is the most characteristic parameter. It undergoes distinct changes when the transitions between stages I, II and III occur. Therefore the moving median of this pulse width was introduced, as described in Chapter 3. If this parameter is determined during monitoring of the discharge signal over a long period, a clear diagnosis of the stage of the ageing process can be possible. To illustrate this

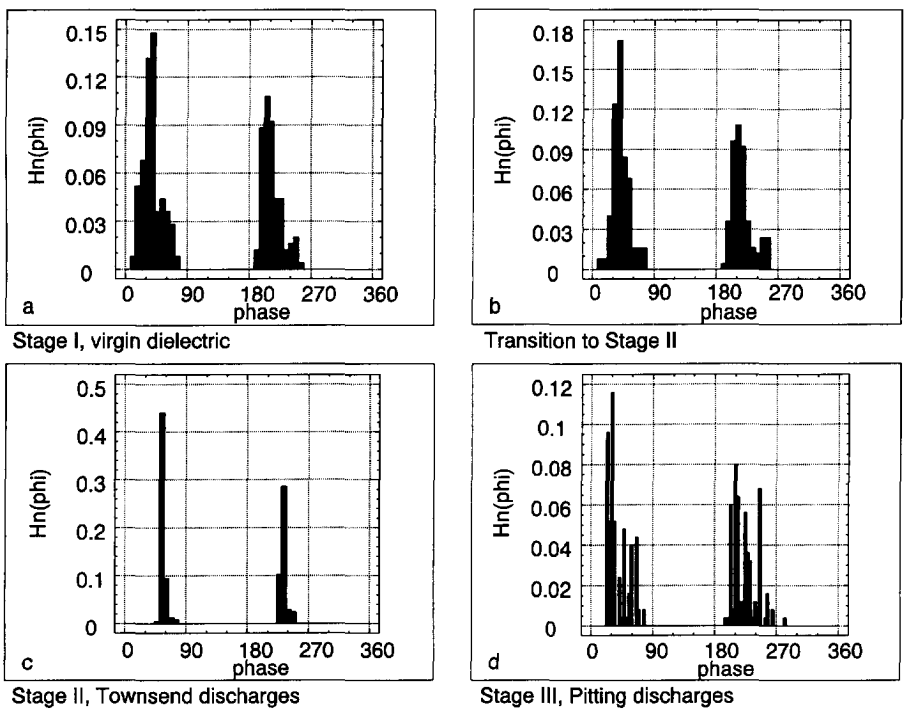

Figure 6.6 Pulse intensity - phase distribution for
a. $0<t<30$ min b. $30<t<60$ min
c. $23.5<t<24$ hrs d. $49.5<t<50$ hrs

Figure 3.27, Figure 6.7a-d shows a typical example of the development of the moving median as a function of the duration of the discharge activity. In Figure 6.7a the transition from the streamer-like to the Townsend-like mechanism can be clearly recognized: the moving median gradually increases until the transition is completed. Figure 6.7b shows a constant median where the Townsend-like regime is present only. The transition to the pitting mechanism is shown in Figure 6.7c, the moving median decreases in an irregular way to a low value. Thereafter it gives a characteristic pattern for tens of hours as can be seen in Figure 6.7d.
Generally speaking, the first transition is characterized by a positive gradient of the moving median and the second transition is characterized by a negative gradient. The onset of significant degradation of the dielectric starts with the second transition and is thus recognized by the moving median.

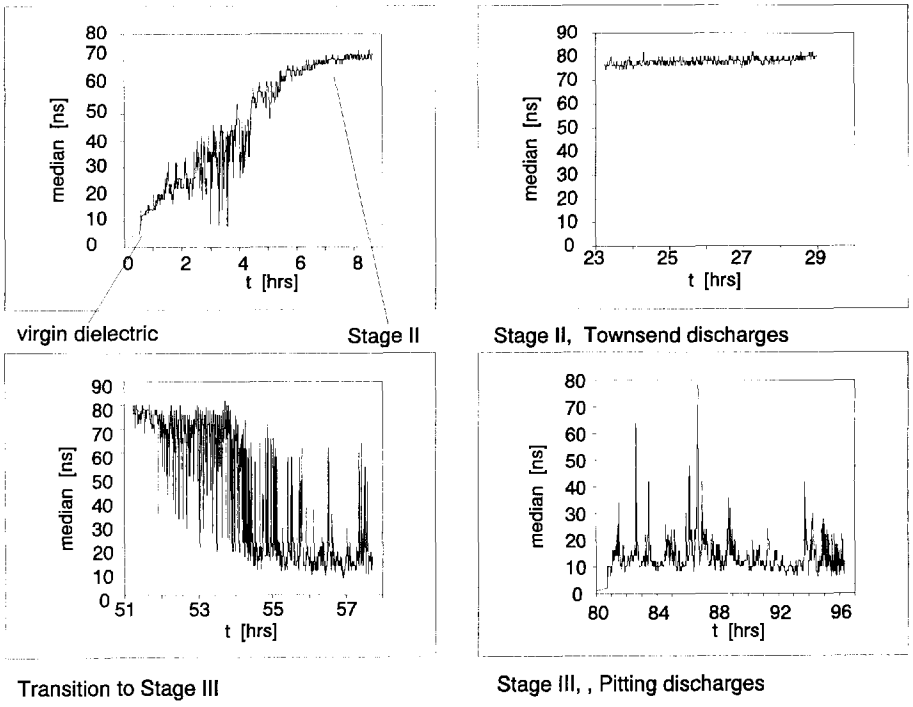

Figure 6.7 Typical behavior of the moving median at different stages of the ageing of the dielectric.

6.4 Time-resolved detection on full-size high voltage components

In literature a number of examples are found of ultra-wide band detection of discharges. In the majority of cases it was not the aim to correlate the shape of the discharge pulse to the physics of the discharge mechanism. However, it *has been* shown that with the right coupling techniques and with a careful lay-out of the measuring system it is possible to maintain the information present in the original discharge signal. In this section examples are given of ultra-wide band measurements on:

- GIS (gas insulated switchgear)
- turbo generators
- electrical machines

For electrical machines the frequency spectrum of the discharge pulses is used to obtain information on the stage of the ageing process.

GIS

GIS (gas insulated systems/substations/switchgear) theoretically are ideal high-voltage components for time-resolved detection of partial discharges [79]. They provide (at least the less complicated GIS) a perfect transmission line to guide the discharge signal from its source to the point of detection. Furthermore, GIS is a fully encapsulated system, shielding external disturbances from its interior.
Partial discharges in SF_6 in GIS generate extremely short electrical pulses with

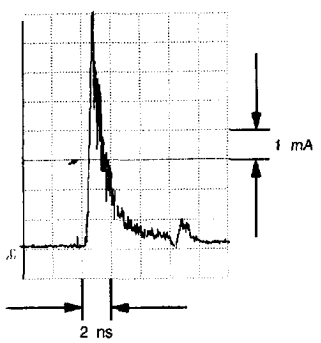

Figure 6.8 Typical partial discharge waveform in a GIS. After Baumgartner [7].

risetimes faster than 1 ns, as is shown in Figure 6.8. These discharges can be modelled by a current source I which injects a charge pulse into the conductors. The result is a travelling wave propagating from the point of injection in both directions of the GIS bus duct. The travelling wave encounters a transmission line impedance Z of 45 to 70 Ω, typical for a GIS bus duct [7]. The injected current is split in two directions, so the ensuing voltage wave is equal to $I/2 \times Z$. Detection of the voltage wave form can take place by capacitive sensors near the enclosure. Königstein [49] describes such a sensor which consists of a metallic ring, insulated from the GIS enclosure, as is shown in Figure 6.9. With an optimal design the frequency response is adapted to the frequency spectrum of the partial discharge pulses.
When the travelling wave arrives at a branching point an impedance mismatch

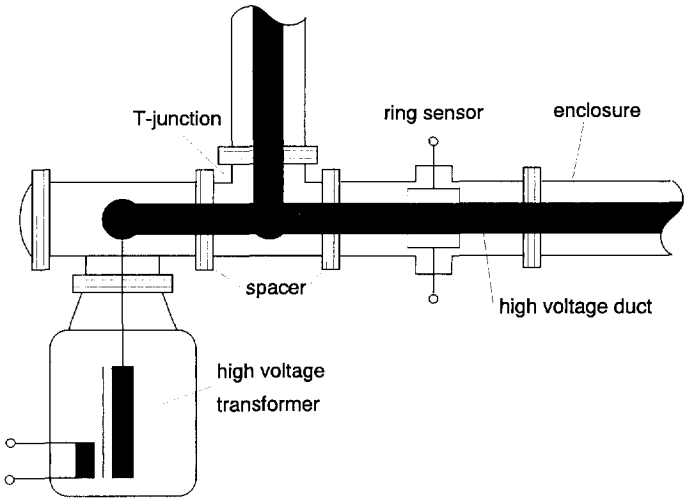

Figure 6.9 Time-resolved partial discharge detection in GIS with a capacitive sensor. After Königstein [49].

occurs, resulting in reflection and refraction. In a complex GIS many interconnections are present and several travelling waves meet at the point where detection takes place. These signals arrive at different times (ns scale), and the detected signal is somewhat distorted.
Time-resolved detection of partial discharges in GIS is used mainly for the assessment of the presence of discharges and for the location of the discharge sites by evaluating the time of arrival of the two waves travelling in opposite directions [1,36].

Stone [79] was able to distinguish two types of discharge pulses in GIS spacers with time-resolved detection. The first type was a narrow pulse with sub-ns to ns risetime and ns duration, the second type had a pulse width of 10-20 ns and a risetime of several ns. The pulse types measured by Stone are possibly the streamer-like and Townsend-like type described in this thesis.
His results are promising for the application of time-resolved detection in GIS.

Turbine generators

Extensive experience has been gathered on the implementation of time-

resolved detection technique on turbine generators [79]. Partial discharge testing is considered to be a valuable tool for the assessment of the insulation condition of stator windings. Here, time-resolved detection is used primarily

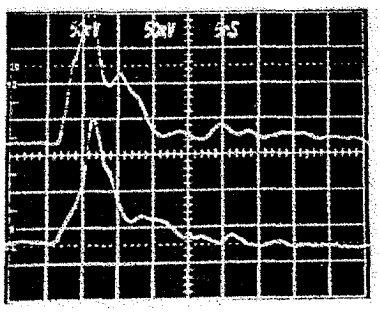

Figure 6.10 Partial discharge pulses measured at Ontario Hydro in an operating 22 kV, 500 MW turbine generator. Timebase = 5 ns/div. Reproduced from [79].

to improve the signal-to-noise ratio when measuring on-line in the noisy environment of turbine generator stations. A coupling device was developed [78] with a bandwidth extending from 10 MHz to more than 1 GHz. Because high frequency signals are heavily attenuated in stator windings [37], the coupler is located in the stator slot, thereby enhancing the sensitivity to partial discharges. As noise signals have to travel some distance before they reach the coupler, their high frequency components are filtered out. Consequently they can be distinguished from the partial discharge signals. The discharge pulses in Figure 6.10, reproduced from [79] originate from an operating 22 kV, 500 MW turbine generator. They prove that, even under non-ideal conditions, time-resolved detection is possible.

Electrical machines

Dejean [21,22] identified different steps in the ageing of a dielectric with void discharges, using a frequency analysis of the discharge current. In order to use this method for medium voltage machines he combined three filters to discriminate discharge pulses of different shapes by their frequency content as is shown in Figure 6.11. Considering that the windings of the electrical machines act as passive linear filters, the original frequency content of the discharge pulse is still present, but attenuated, at the point of detection.
Filter A is a high-pass filter with a cut-off frequency of ≈ 35 MHz, filter B a

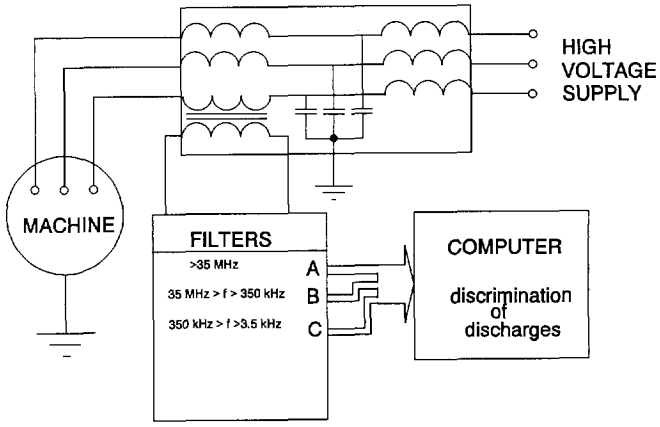

Figure 6.11 Discrimination between discharge pulses of different frequency content.

band-pass filter with cut-off frequencies of 35 MHz and 350 kHz and filter C is a band-pass filter with cut-of frequencies of 350 kHz and 3.5 kHz. By comparing the relative amplitudes of the discharge signal at the output of the three filters a discrimination between different pulse shapes was possible.

High-voltage cables

The pulse width of partial discharges in cables longer than a few meters is small compared to the transit time of the discharge pulse in the axial direction. Therefore the partial discharge signal is considered to act as a travelling wave that encounters a characteristic cable impedance. This characteristic is fruitfully used for the localization of discharge sites using the *travelling wave method.* If the cable is regarded as a loss-free system the discharge signal arrives undistorted at the detection site. With the right coupling method and a high bandwidth detector the high frequency information originally present in the discharge signal is maintained. In high-voltage cables however semi-conducting layers are applied between the insulating dielectric and the conductors. These layers introduce frequency dependent losses, thereby limiting the maximum usable detection bandwidth to about 100 MHz [92].
Wolzak [92] describes a method that was originally introduced by Kreuger [50]. In this method the discharge signal is detected with a measuring resistor

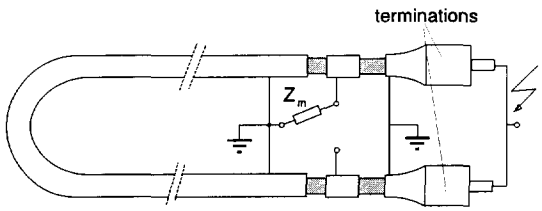

Figure 6.12 Discharge detection circuit using sheath interruptions.

across an interruption of the cable sheath. This procedure may be used for detection or localization of discharges. Figure 6.12 shows a schematic representation of a possible measuring circuit. The detection of the discharges takes place across the measuring impedance Z_m. With a sheath interruption at both ends of the cable the following detection circuits are possible:

- straight detection at one interruption for time-resolved detection of the discharge
- balanced detection, to be used for the suppression of external interference or localization of a discharge site

It is shown in [92] that time-resolved detection is well possible for coaxial cables without semiconducting layers. In 30/50 kV XLPE cables with semiconducting layers high frequency signals were attenuated, but high frequency components up to 100 MHz were still present in the detected signal.

6.5 Summary

The evolution of the discharge mechanism can well be recognized by the shape of the pulse parameter distributions, with an emphasis on $H_n(\varphi)$ and $H_{rw,20\%}$.

A statistical operator was defined, namely the moving median, that describes the temporal change of the 20% pulse width, $t_{w,20\%}$. This operator is very sensitive to the stage of the discharge process. Most important, it recognizes the transition to the pitting mechanism and consequently the onset of intensive degradation.

The possibilities for time-resolved detection applied to full-size high voltage components are promising.

Chapter 7
Conclusions and suggestions

Conclusions

The aim of this study was to describe and to explain the evolution of the discharge process in dielectric bounded voids, with respect to degradation of the dielectric. In this chapter the results of this study are summarized in a number of conclusions.

Extraction of information from the discharge process

1. Information about the discharge mechanism is present in the pulse shape of the discharge current. If a time-resolved detection system is used this information can be extracted from the discharge signal. The bandwidth of the detection system shall be larger than 100 MHz.

2. Optical registration of the discharge images makes it possible to obtain a spatial impression of the discharge.

3. Synchronic detection of the discharge current and optical observation of the discharge image offers additional information about the discharge process.

Discharge stages

4. The discharge mechanism in dielectric bounded voids evolves as a function of the duration of the discharge activity. It was found that this evolution can be divided in three consecutive stages, each stage characterized by a set of electrical and optical parameters: *streamer-like* mechanism, *Townsend-like* mechanism and *pitting* mechanism.

5. *Streamer-like* stage. This stage is present in the first 10 to 60 minutes of the discharge activity. It is characterized by a short discharge current

pulse width of about 1 ns. The void is partially discharged by a number of discharges spatially distributed over the void surface. These discharges ignite in rapid succession, with a time interval between discharges of several tens of nanoseconds down to less than 1 nanosecond. Voids with a large diameter/height-ratio are discharged by a large number of discharges with equal magnitude.
Optically, one single discharge consists of a narrow channel (in analogy with streamers) with some lateral extension at the void surface. There are no preferential locations for discharge ignition when the void surface is smooth.

6. *Townsend-like* stage. This stage is dominant after 10 to 60 minutes of discharge activity and lasts for a period of several days. The discharge current pulses are characterized by a broad pulse width proportional to the height of the void. Single discharges show a large scatter of the pulse height. The maximum pulse height grows with an increasing diameter-/height ratio of the void.
Optically, a single discharge is diffuse and covers a large part of the void surface.

7. *Pitting* stage. This stage starts after some tens of hours of discharge activity, initially parallel with the *Townsend-like* stage. The name *pitting* was chosen because in this stage extensive degradation of the dielectric starts with the creation of *pits*. Pitting discharges are characterized by a high repetition rate of several tens per millisecond and a very small pulse height that shows little scatter. Discharge inception takes place at voltages lower than the inception voltage for streamer-like and Townsend-like discharges.
The discharges are located at preferential spots of the void surface.

Discharge mechanisms

8. The transition between the streamer-like and the Townsend-like mechanism is mainly governed by the state of the interface between the gas and the dielectric. Discharge by-products at this interface influence the emission of electrons from the dielectric surface.

9. It was established that the deposition of *oxidation* products is a necessary

condition for a transition from streamer-like to Townsend-like discharges.

10. The disappearance of oxygen in the gas phase has a minor effect on the transition.

11. The transition to Townsend-like discharges is explained by a reduced time-lag caused by an enhanced availability of secondary electrons. The reduced time-lag results in smaller overvoltages. It was shown by numerical calculations that for small overvoltages the Townsend mechanism is operative.

12. The clustering of *crystals of oxalic acid* is a necessary condition for the occurrence of pitting discharges. This discharge type is induced by a local enhancement of the electric field and by an increase of the surface conductivity of the void.

Discharge diagnosis

13. A tool is presented that recognizes the discharge stage by time-resolved detection: the *moving median* of the width of the discharge pulses.

14. A high repetition rate of discharges with a magnitude smaller than 1 pC predicts the onset of pitting discharges and the start of a severe degradation of the dielectric.

Suggestions for further study

The results of this study lead to the formulation of a number of topics that are interesting for further study. These topics are rather diverse and lead in different directions.

1. The time-resolved tests in this study were performed with models. It would be of great interest to apply the time-resolved concept in tests on real high-voltage equipment. The main obstacle here is the complexity of some equipment (for instance transformers) with respect to the coupling of the detector and the distorted shape of the discharge signal. However, GIS (gas insulated switchgear) and high-voltage cable systems of moderate length are well-suited because of their relative simplicity and well-defined characteristic impedance.

2. With respect to the theory of the transition between the streamer-like and the Townsend-like mechanism it would be worthwhile to probe deeper into the creation of traps at the surface of the dielectric. Techniques are available for the measurement of the depth and the number of traps.

3. The characteristic parameters of the time-resolved method might have a counterpart in parameters obtainable with the classic phase-resolved detection method. In this thesis this topic was dealt with superficially. Preliminary studies, however, indicated that this direction is promising.

4. Further study of the nature of pitting discharges and their effect on ageing will be valuable to understand the ageing mechanism of synthetic dielectrics.

List of symbols

α	Townsend primary ionization coefficient
α_{eff}	effective primary ionization coefficient (α-η)
$\alpha_{eff,cr}$	critical effective primary ionization coefficient necessary for streamer development
γ	Townsend secondary ionization coefficient
γ_i	number of electrons released at the cathode per incident positive ion
γ_{ph}	number of electrons released at the cathode per ionizing collision in the gas
ΔV	overvoltage in a percentage of the minimum breakdown voltage
ΔV_{abs}	overvoltage in volts
ΔV_{cr}	critical overvoltage for streamer development
ϵ_0	permittivity of vacuum
η	electron attachment coefficient
θ	number of photons emitted per ionizing collision
ε_r	relative permittivity of a dielectric
κ	number of electrons released at the cathode per incident photon
λ	wavelength
μ_i	mobility of positive ions

ν_0	phonon frequency
ρ	gas density
ρ_A	surface charge density
ρ_V	volume charge density
τ_s	statistical time-lag
τ_{ave}	average time-lag
τ_c	time constant of the detection circuit
τ_d	time constant of the front of the discharge
τ_{tr}	average life-time of a trapped electron
Φ_{rad}	radiative flux density
ψ	space charge potential
C_{rad}	radiative absorption by matter
d	thickness of the dielectric
D	(a) void diameter (b) diffusion coefficient
D_m	diameter of the measuring electrode
dA	surface element, used in calculation of the space charge induced electric field
d_{tot}	separation between high-voltage electrode and measuring electrode
dv	volume element, used in calculation of the space charge induced electric field

e	atomic charge
E	electric field strength
E_0	Laplace field (electric field without space charge)
E_{space}	space charge induced electric field
E_{tr}	trap depth (the energy needed to free a trapped electron)
f_e	production rate of initiatory electrons
g	geometry factor relating the number of photons impinging on the cathode to the total number of electrons emitted in an avalanche
GIS	(a) Gas insulated substation (b) Gas insulated system
h	void height
H_{rr}	distribution of the discharge pulse rise time
H_{rw}	distribution of the discharge pulse width at the 50% levels of the pulse height
$H_{rw,20\%}$	distribution of the discharge pulse width at the 20% levels of the pulse height
H_I	distribution of the discharge pulse height
$H_n(\varphi)$	phase distribution of the discharge intensity
I	discharge current source
$\hat{\imath}$	discharge pulse height
$i(t)$	discharge current
k	Boltzmann constant

l_{min}	minimum length of the discharge path to obtain a self-sustained discharge at a specified electric field
m	moving median
n	particle number volume density
N_c	number of secondary electrons produced at the cathode by N_{e0} initiatory electrons
N_{cr}	critical number of electrons to obtain a streamer
n_e	electron volume density
N_e	total number of electrons
n_{e0}	initiatory electron density at $t=0$
N_{e0}	number of initiatory electrons
n_i	positive ion volume density
N_i	total number of positive ions
N_{rep}	discharge repetition frequency
P	net particle production per second as the result of ionization, attachment and conversion processes
$P(\mathrm{d}t)$	probability for the occurrence of an initiatory electron during a time interval dt
$P(t)$	probability of an avalanche starting in time t
PE	polyethylene
LDPE	low-density polyethylene
PP	polypropylene

q	discharge magnitude
R	(a) discharge radius (b) resistance
R_d	damping resistor in the high-voltage circuit
R_m	measurement resistance
S_a	avalanche size
t	time
T	absolute temperature
tan δ	dielectric loss factor
t_d	discharge pulse decay time
TIM	image processing software
t_r	discharge pulse rise time
T_{trans}	transition time from streamer-like to Townsend-like mechanism
t_w	discharge pulse width at the 50% level of the pulse height
$t_{w,20\%}$	discharge pulse width at the 20% level of the pulse height
U	test voltage applied to the electrodes
U_e	discharge extinction voltage (the momentary value of the voltage over the void when a discharge has extinguished)
U_i	discharge ignition voltage (the momentary value of the voltage over the void at the moment of occurrence of a discharge)

U_{inc}	discharge inception voltage (the momentary voltage at the electrodes at which the discharge process starts when the test voltage is raised from zero)
$U_{Paschen}$	breakdown voltage of a void between metal electrodes obtained from the Paschen curve
u_t	thermal energy of electrons
V	volume of the void
V_{min}	minimum breakdown voltage of a void
V_{res}	residual voltage over a void after the discharge has extinguished
W	drift velocity
W_e	drift velocity of electrons
W_i	drift velocity of positive ions
x	position along the discharge axis relative to the cathode
x_{cr}	critical discharge length to obtain a streamer
Z	transmission line impedance

References

[1] M. Albiez, M. Leijon, "PD measurements in GIS with electric field sensor and acoustic sensor". Proceedings of the 7th Int. Symp. on High Voltage Eng., Dresden, 1991, 75.08, pp. 185-188.

[2] A.E.W. Austen and S. Whitehead, "Discharges in insulation under alternating current stresses". Journal IEE, Vol. 88, Part II, 1941, pp. 18-22.

[3] S. Badaloni and I. Gallimberti, "Basic data of air discharges". UPee, 72-02, University of Padua, 1972.

[4] R. Bartnikas and J. Levi, "A simple pulse-height analyzer for partial discharge rate measurements". IEEE Trans on Instr. and Meas., Vol. 18, 1969, pp. 341-345.

[5] R. Bartnikas "Note on discharges in helium under ac conditions". Brit. J. Appl. Phys. (J. Physics D.), Vol. 1, 1968, pp. 659-661.

[6] R. Bartnikas and J.P. Novak, "On the spark to pseudoglow and glow transition mechanism and discharge detectability". IEEE Trans. on Electr. Insulation, Vol. EI-27, 1992, pp. 3-14.

[7] R. Baumgartner, B. Fruth, W. Lanz and K. Pettersson, "PD in gas-insulated substations-measurements and practical considerations". IEEE Electr. Insul. Magazine, Vol.8, No.1, 1992, pp.16-27.

[8] M. Beyer, W. Boeck, K. Möller and W. Zaengl, "Hochspannungstechnik", Springer Verlag, 1986.

[9] P. Bezborodko, O. Lesaint and R. Tobazéon, "On the mechanism of partial discharges in gaseous cavities in contact with solid or liquid insulators". Proc. 3rd Int. Conf. on Cond. and Breakdown in Solid Diel., Trondheim, Norway, 1989.

[10] W. Boeck, "Entstehung und Bedeutung von Raumladungen in

Kunststoff-Folien durch Koronaentladungen". PhD-thesis TU Braunschweig, 1967.

[11] S.A. Boggs and G.C. Stone, "Fundamental limitations in the measurement of corona and partial discharge". IEEE Trans. on Electr. Insul. EI-17, 1982, pp. 143-150.

[12] E. Cartier and P. Pfluger, "Detection of hot electron-induced radiation damage in organic dielectrics by exoelectron emission from thin films". IEEE Trans. on Electr. Insul. EI-22, 1987, pp.123-128.

[13] E. Cartier and F. Pfluger, "Charge storage and radiation damage in thin dielectric films studied by electron spectroscopy". Proceedings of the 2nd Int. Conf. on Conduct. and Breakd. in Sol. Diel., 1986, p. 308

[14] L.G. Christophorou and L.A. Pinnaduwage, "Basic physics of gaseous dielectrics". IEEE Trans. on Electr. Insulation, Vol. EI-25, 1990, pp. 55-74.

[15] D.E. Cooper, M. Farber and S.P. Harris, " ". Ann. Rep. Elec. Insul. & Diel. Phenom., 1984, pp. 32-37.

[16] G.C. Crichton, P.W. Karlsson and A. Pedersen, "Partial discharges in ellipsoidal and spherical voids". IEEE Trans. on Electr. Insul. EI-24, 1989, pp. 335-342.

[17] T.W. Dakin et al, "Breakdown of gases in uniform fields - Paschen curves for N_2, air and SF_6". Electra no. 32, 1974, pp. 61-82.

[18] M.G. Danikas, R. Bartnikas and J.P. Novak, "On the spark to pseudoglow and glow transition mechanism and discharge detectability". IEEE Trans. on Electr. Insul. EI-28, 1993, pp. 429-431.

[19] M.G. Danikas and A.M. Bruning, "Comparison of several theoretical sub-corona to corona transition with recent experimental results". Proc. of the 1992 IEEE Int. Symp. on Electr. Insul., Baltimore, 1992, pp. 383-388.

[20] A.J. Davies and C.J. Evans, Proc. IEE, Vol. 114, 1967, p. 1547.

[21] P.P.F. Dejean, "Étude de la dégradation des isolants solides sous moyenne tension alternative en régime de décharges partielles". PhD-thesis Université Pierre et Marie Curie, France, 1991.

[22] H. Dejean, P.P.F. Dejean and M. Goldman, "On site very high frequency PD pulse measurements on full size rotating machine stator for discharge type recognition". Proceedings IEE Int. Conf. on Partial Discharge, No 378, Canterbury, 1993, pp.66-67.

[23] J.C. Devins, "The physics of partial discharges in solid dielectrics". IEEE Trans. on Electr. Insulation, Vol. EI-19, 1984, pp. 475-494.

[24] L.A. Dissado and J.C. Fothergill, "Electrical degradation and breakdown in polymers". Peter Peregrinus Ltd., London, 1992.

[25] B. Fruth and L. Niemeyer, "The importance of statistical characteristics of partial discharge data". IEEE Trans. on Electr. Insulation, Vol. EI-27, 1992, pp. 60-69.

[26] M. Gamez-Garcia, R. Bartnikas and M.R. Wertheimer, "Modification of XLPE exposed to partial discharges at elevated temperature". IEEE Trans. on Electr. Insulation, Vol. EI-25, 1990, pp. 199-205.

[27] M. Gamez-Garcia, R. Bartnikas and M.R. Wertheimer, "Synthesis reactions involving XLPE subjected to partial discharges". IEEE Trans. on Electr. Insulation, Vol. EI-22, 1987, pp. 199-205.

[28] V.R. García Colón, "Evaluacion de superficies de XLPE expuestas a descargas parciales mediante una microsonda electrostatica". IEEE 1th reunion de Verano, capitulo de potencia, Acapulco, 1988.

[29] A. Gemant and von Philippoff, "Die Funken-strecke mit Vorkondensator". Zeitschrift für technische Physik, Vol. 13, 1932, pp. 425-430.

[30] M. Giesselmann, "Kurzzeitoptische Untersuchungen der Entladungsentwicklung in N_2 und SF_6 an Modellanordnungen bei Gleich- und Impulsspannung". PhD-thesis Technische Hochschule Darmstadt, Germany, 1986.

[31] M. Goldman and A. Goldman, "Physical and chemical aspects of partial discharges and their effects on materials". Proceedings IEE Int. Conf. on Partial Discharge, No 378, Canterbury, 1993, pp.11-14.

[32] Y. Gosho and M. Saeki, "Secondary electron emission from dielectric surface under atmospheric air conditions due to UV irradiation". Proc. 5th Int. Symp. on High Volt. Eng., Braunschweig, 1987, 23.24.

[33] B. Gravendeel, "Negative corona discharges. A fundamental study." PhD-thesis Eindhoven University of Technology, 1987.

[34] E. Gulski, "Computer-aided recognition of partial discharges using statistical tools". PhD-thesis Delft University of Technology, Delft University Press, 1991.

[35] E. Gulski, P.H.F. Morshuis and F.H. Kreuger, "Automized recognition of partial discharges in cavities". Japp. Jrnl of Appl. Phys., Vol 29, No 7, 1990, pp. 1329-1335.

[36] B.F. Hampton and R.J. Meats, "Diagnostic measurement at UHF in gas insulated substations". Proc. IEE, Vol. 135, JPt. C, No. 2, 1988.

[37] M. Henriksen, G.C. Stone and M. Kurtz, "Propagation of partial discharge and noise pulses in turbine generators". IEEE Trans. on Energy Conversion, Vol. 1, 1986, pp. 161-166.

[38] M. Hikita, K. Yamada, A. Nakamura, T. Mizutani, A. Oohasi and M. Ieda, "Measurements of partial discharges by computer and analysis of partial discharge distribution by the Monte Carlo method". IEEE Trans. on Electr. Insulation, Vol. EI-25, 1990, pp. 453-468.

[39] J.T. Holbøll, "The resistance of composite materials against electrical discharges". PhD-thesis Technical University of Denmark, 1992.

[40] C. Hudon, R. Bartnikas and M.R. Wertheimer, "Spark-to-glow discharge transition due to increased surface conductivity on epoxy resin specimens". IEEE Trans. on Electr. Insulation, Vol. EI-28, 1993, pp. 1-8.

[41] M. Ieda, "Electrical conduction and carrier traps in polymeric materials".

IEEE Trans. on Electr. Insul. EI-19, 1984, pp. 162-178.

[42] N. Izeki and F. Tatsuta, "Behavior of void discharges in short gaps". 4th Int. Symp. on High-Voltage Eng., Athens, 1983, 22.04.

[43] M.O. Jørgensen, "Experimental investigations regarding the applicability of Lichtenberg figures to voltage measurement". Ingeniørvidenskabelige skrifter, A Nr. 37, 1934, pp. 5-39.

[44] S. Kärkkäinen, "Internal partial discharge pulse distributions. Physical mechanisms and effects on insulations". PhD-thesis Helsinki Institute of Technology, Finland, 1976.

[45] Y. Kitamura and S. Hirabayashi, "Partial discharge deterioration of epoxy resin for electronic parts". Ann. Rep. Conf. Elect. Insul. & Diel. Phenom., 1985, pp. 485-490.

[46] W. Köhrmann, Zeitschr. Angew. Physik, Vol. 7, 1955,p.183.

[47] D. König, "Erfassung von Teilentladungen in Epoxydharzplatten zur Beurteilung des Alterungsverhaltens bei Wechselspannung". PhD. thesis TH Braunschweig, 1967.

[48] D. König, "Impulslose Teilentladungen in Hohlräumen von Epoxydharzformstoff-Isolierungen". ETZ-Archiv, Vol. 90, 1969, pp. 156-158.

[49] D. Königstein, "Advances in partial discharge detection technic". Proc. NordIS, 1992, 2.4:1.

[50] F.H. Kreuger, "Partial discharge detection in high-voltage equipment". Butterworths, London, 1989.

[51] M. Kurrat, "Wideband measurement of partial discharges for fundamental diagnostics". Proceedings of the 7th Int. Symp. on High Voltage Eng., Dresden, 1991, 72.02, pp. 47-50.

[52] G.C. Lichtenberg, "Nova methodo naturam ac motum fluidi electrici investigandi, novi commentarii societatis regiae scientarum Gottingensis". Tomus VIII, Göttingen, 1777, p. 1968.

[53] B. Luczynski, "Partial discharges in artificial gas-filled cavities in solid high-voltage insulation". PhD-thesis Technical University of Denmark, 1979.

[54] J.H. Mason, "Dielectric breakdown in solid insulation", Chapter 1 in Progress in Dielectrics, Vol 1, Heywood, 1959.

[55] C.J. Mayoux, "Partial-discharge phenomena and the effect of their constituents on polyethylene". IEEE Trans. on Electr. Insul. EI-11, 1976, pp. 139-149.

[56] J.M. Meek and J.D. Craggs, "Electrical breakdown of gases". Wiley, 1978.

[57] F.H. Merrill and A. von Hippel, "The atomphysical interpretation of Lichtenberg figures and their application to the study of gas discharge phenomena". Jrnl. of Appl. Phys., Vol. 10, 1939, pp. 873-886.

[58] T. Mizutani, Y. Suzuoki and M. Ieda, "Thermally stimulated currents in polyethylene and ethylene-vinyl-acetate copolymers". J. Appl. Phys., Vol. 48, 1977, pp. 2408-2413.

[59] P.H.F. Morshuis and F.H. Kreuger, "The spatial distribution and electrical parameters of partial discharges in polyethylene insulation during ageing". Proc. 4th Int. Conf. on Cond. and Breakdown in Solid Diel., Sestri Levante, Italy, 1992.

[60] P.H.F. Morshuis and F.H. Kreuger, "A relation between time-resolved discharge parameters and ageing". Proc. 6th Int. Conf. on Diel. Mat., Meas. and Appl., Manchester, UK, 1992.

[61] P.H.F. Morshuis and F.H. Kreuger, "The evolution of the discharge mechanism in a dielectric bounded cavity due to surface effects". Proc. 3rd Int. Conf. on Prop. and Appl. of Diel. Mat., Tokyo, 1991, pp. 672-675.

[62] P.H.F. Morshuis and F.H. Kreuger, "The influence of the dielectric-gas interface on the discharge mechanism in a dielectric bounded cavity". Proc. 7th Int. Symp. on High Voltage Eng., Dresden, 1991, 22.07.

[63] P.H.F. Morshuis and F.H.Kreuger, "Transition from streamer to Townsend mechanisms in dielectric voids". J. Phys. D:Appl. Phys., Vol 23, 1990,pp. 1562-1568.

[64] P.H.F. Morshuis, "Time-resolved discharge measurements". Proc. Int. Conf. on Partial Discharge, No 378, Canterbury, 1993, pp. 43-46.

[65] M. Nagao, M. Kosaki, T. Ishida and Y. Mizuno, "Swarming pulsive microdischarges and internal partial discharge degradation in epoxy resin". 6th Int. Symp. on High-Voltage Eng., New Orleans, 1989, 22.21.

[66] L. Niemeyer, B. Fruth and F. Gutfleisch, "Simulation of partial discharges in insulation systems". Proceedings of the 7th Int. Symp. on High Voltage Eng., Dresden, 1991, 71.05, pp. 24-28.

[67] K.W. Nissen and P. Röhl, "Löschen von Teilentladungen in Hohlräumen in Polyethylen". Siemens Forsch.- und Entwickl.-Ber., Vol. 10, 1981, no. 4, pp. 215-221.

[68] F. Paschen, "Über die zum Funkenübergang in Luft, Wasserstoff und Kohlensäure bei verschiedenen Drucken erforderliche Potentialdifferenz". Annalen der Physik, Vol. 37, 1889, p. 69.

[69] P.O. Pedersen, "On the Lichtenberg figures". Det Kgl. Danske Videnskabernes Selskab. Mat.-fys. Meddelelser, Part 1, 1919, Part 2, 1922, Part 3, 1929.

[70] J. Pfaue, Zeitschrift f. Angew. Physik, Vol 11, 1959, p. 409.

[71] H. Raether, "Electron avalanches and breakdown in gases". Butterworths, London, 1964.

[72] G. Robinson, "Discharges in asymmetric cavities under AC stresses". IEE Proc.A, Vol. 138, 1991, pp. 119-126.

[73] E.C. Rogers, "The self-extinction of gaseous discharges in cavities in dielectrics". Proc. IEE, Vol. 105A, 1958, pp. 621-630.

[74] M. Saeki and Y. Gosho, "Electron emission from dielectric surface due to UV radiation under atmospheric air condition". 2nd Int. Conf. on

Properties and Applications of Dielectric Materials, Beijing, 1988, pp. 172-173.

[75] H. Schering, "Die Isolierstoffe der Elektrotechnik". Verlag Julius Springer, Berlin,1924.

[76] Schlieren,

[77] W. Schockley, "Current to conductors induced by a moving point charge". J. Appl. Phys., Vol. 9, 1938, p. 635.

[78] H.G. Sedding, S.R. Campbell, G.C. Stone and G. Klempner, "A new sensor for detecting partial discharge in operating turbine generators". 1991 IEEE Winter Power Meeting, New York NY, paper 91 WM 065-3-EC, 1991.

[79] G.C. Stone, H.G. Sedding, N. Fujimoto and J.M. Braun, "Practical implementation of ultrawideband partial discharge detectors". IEEE Trans. on Electr. Insul. EI-27, 1992, pp. 70-81.

[80] Y. Suzuoki, K. Yasuda, T. Mizutani and M. Ieda, "The influence of oxidation on thermally stimulated currents from trapped carriers in high density polyethylene". J. Phys.D: Appl. Phys., Vol. 10, 1977, pp. 1985-1990.

[81] Y. Takahashi, S. Kato and S. Kobayashi, "Discharge voltage of dielectric gaps and the generalized secondary ionization coefficient Γ of the dielectric cathode". Proc. 2nd Int. Conf. on Prop. and Appl. of Diel. Mat., 1988.

[82] Y. Takai, K. Mori, T. Mizutani and M. Ieda, "Investigations of traps in γ-irradiated polyethylene by photo stimulated detrapping current analysis". Jap. Jrnl. Appl. Phys., Vol. 15, 1976, pp. 2341-2347.

[83] T. Tanaka, "Internal partial discharge and material degradation". IEEE Trans. on Electr. Insulation, Vol. EI-21, 1986, pp. 899-905.

[84] T. Tanaka and T. Okamoto, "A minicomputer based partial discharge measurement system". 1978 IEEE Int. Symp. on Electr. Insul., Conf. Record 78CH1287-2-EI, Philadelphia, 1978, pp. 86-89.

[85] T.H. Teich and R. Bräunlich, "UV and other radiation from discharges in artificial air and its constituents". Proc. 8th Int. Conf. on Gas. Disch., 1985, p. 441.

[86] J. Tom, H.F.A. Verhaart, A.J.L. Verhage and C.S. Vos, "Photo-emission of charged insulators in insulating gases". Proc. IEEE 2nd Int. Conf. on Cond. and Breakd. in Sol. Diel., Erlangen, 1986, pp. 301-307.

[87] J.S. Townsend, "The theory of ionization of gases by collisions". Constable, London, 1910.

[88] C. Wen, Time-resolved Swarm Studies in Gases with emphasis on Electron Dteachment and Ion Conversion, Ph.D. thesis, Eindhoven University of Technology, 1989.

[89] J.M. Wetzer and P.C.T. van der Laan, "Prebreakdown Currents, basic interpretation and time-resolved measurements, IEEE Trans. on Electr. Insulation, Vol. EI-24, 1989, pp. 297-308.

[90] J.M. Wetzer, A.J.M. Pemen and P.C.T. van der Laan, "Experimental study of the mechanism of partial discharges in voids in polyethylene". Proc. 7th Int. Symp. on High-Voltage Eng., Dresden, 1991.

[91] K.D. Wolter, J. Tanaka and J.F. Johnson, "A study of the gaseous degradation products of corona-exposed polyethylene". IEEE Trans. on Electr. Insulation, Vol. EI-17, 1982, pp. 248-252.

[92] G.G. Wolzak, "The development of high-voltage measuring techniques". PhD-thesis Technische Hogeschool Eindhoven, 1983.

[93] M. Yumoto and T. Sakai, "Photo electron emission from dielectric materials by ultra-violet-ray irradiation". Annual Conf. on Electr. Insul. and Dielectr. Phen., Boston, 1980, pp. 75-80.

[94] K. Züber, "Über die Verzögerungszeit bei der Funkenentladung". Annalen der Physik, Vol. 76, 1925, pp. 231-260.

Appendix A

The Ramo-Shockley theorem[2]

When a charge δq is placed between two electrodes at a fixed potential, charge will be induced on these electrodes. These induced charges can be calculated. Let us consider the arrangement of N electrodes as shown in Figure A.1.

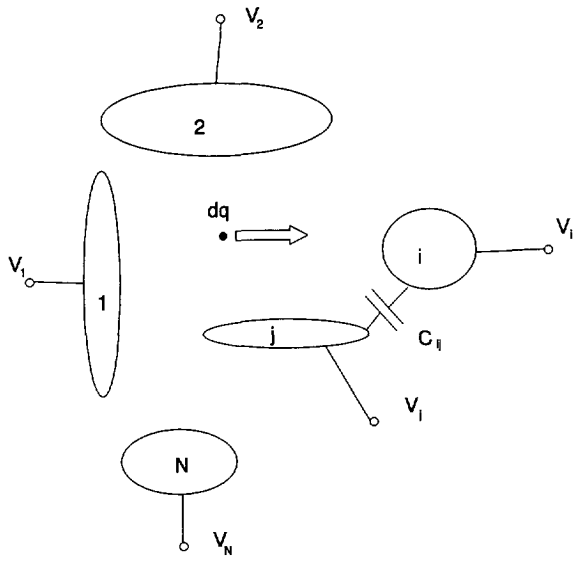

Figure A.1 System of free charges and electrodes. 1,2,i,j,N are electrodes.

The electrodes with indices i have the fixed potential V_i. Q_i is the charge induced on the ith electrode. With electrostatic theory we obtain the charge induced on the ith electrode:

[2] The origin of this theorem dates back to 1938 when W. Shockley calculated the current induced by moving electrons in a vacuum tube [?].

$$Q_i = \sum_{j=1}^{N} C_{ij} \cdot (V_i - V_j) \tag{A.1}$$

with C_{ij} the capacitance between electrodes i and j, depending on the geometry of the system only.
Now the case is considered of a discharge resulting in space charge δq moving in the space between the electrodes. This space charge will electrostatically induce charges on all electrodes.
Two hypothetical situations are described, (I) the situation with space charge and all electrodes at zero potential and (II) the situation without space charge but with all electrodes at zero potential, except the measuring electrode which is at a certain potential. The combination of these two situations delivers, with the use of Green's theorem, delivers the charge induced on the measuring electrode.

Situation (I)
Let us denote the charge δq to a hypothetical conducting sphere k of vanishingly small radius. The charge appearing at electrode l is:

$$\delta Q_l = C_{lk} \cdot V_k \tag{A.2}$$

For k we have:

$$V_k = \delta q / C_{kk} \tag{A.3}$$

so

$$\delta Q_l = C_{lk} / C_{kk} \cdot \delta q \tag{A.4}$$

Situation (II)
Now let us consider the situation without charge on conductor k, δq=0, and all electrodes at zero potential, except the measuring electrode l. In this case, denoting all voltages in this situation with the index °, we get:

$$C_{kl} \cdot V_l^o + C_{kk} \cdot V_k^o = 0 \tag{A.5}$$

so:

$$C_{kl} / C_{kk} = -\left(V_k^o / V_l^o\right) \tag{A.6}$$

with $C_{kl} \equiv C_{lk}$ and combining situation I and situation II (A.4) δQ_l may be written as:

$$\delta Q_l = -\left(V_k^o / V_l^o\right) \cdot \delta q \qquad (A.7)$$

Or, in words: the amount of charge induced on the measuring electrode l can be calculated by solving the Laplace field with all electrodes at zero potential, except the measuring electrode.

Implications for the electrode set-up as described in Chapter 2

The factor relating the induced charge at the measuring electrode to the real charge can be calculated by solving the Laplace equations for the system of electrodes. In this way the relation between the apparent charge measured at the electrodes and the real charge located in the void is obtained. If we call $V_k^o/V_l^o = \lambda$, using the terminology of Pedersen [16], λ can easily be calculated by setting the measuring electrode at a potential "1" and all other electrodes at zero potential.
The same calculations can be made for the guard electrode. The diameter of the measuring electrode has to be chosen large enough so that no charge is induced on the guard electrode. This is easily verified by the above mentioned calculations.
If the thus calculated field along the discharge axis is constant, no charge is induced on the guard electrode, see Figure A.2. This is approximately the case when:

$$d_{tot} \leq 0.25 \cdot (D_m - D) \qquad (A.8)$$

However, if for instance $D_m = D$, the field along the discharge axis is not constant as can be seen in Figure A.3. A considerable amount of field lines ends at the guard electrode and the shape of the measured discharge pulse will be distorted. Wetzer [89] has shown this experimentally.

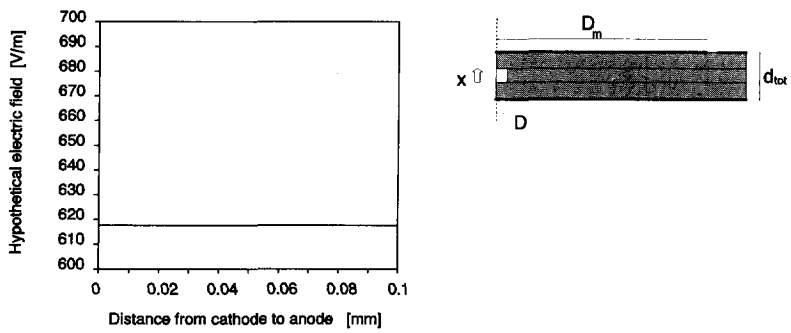

Figure A.2 Hypothetical field along the discharge axis for $d_{tot} \approx 0.25$ $(D_m\text{-}D)$.

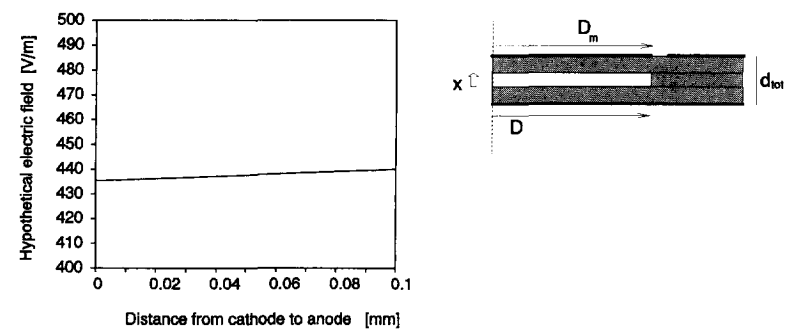

Figure A.3 Hypothetical field along the discharge axis for $D_m = D$.

Appendix B

Procedure for the numerical calculation of the discharge current

A set of three partial differential equations has to be solved with the variables x (location in the void) and t (time). This set consists of two conservation equations to account for the movement and the production of electrons and positive ions, and of the Poisson equation which determines the electric field. In these calculations the effect of negative ions and neutral particles has been neglected.
All important parameters governing the development of the discharge current are electric field dependent, such as

- the electron and ion velocities W_e and W_i
- the ionization coefficient α

Townsends' second coefficient γ is kept constant, independent of the electric field.
The electric field $E(x,t)$ is composed of the Laplace field E_L resulting from the voltage supplied to the electrodes and the charge-induced field $E_Q(x,t)$. The latter can be calculated if the charge densities $n_e(x,t)$ and $n_i(x,t)$ at all locations in the void are known.
The calculation of the charge densities $n_e(x,t)$ and $n_i(x,t)$ is performed as follows:

Initially, at the start of the discharge development, a Gaussian distribution of initiatory electrons is assumed as is shown in Figure B.1. The total number of starting electrons is chosen to be 1.
The first step now is to calculate the electric field in the void using the initial charge density distribution and the Laplace field. In the case of Townsend-like discharges a 1-dimensional Poisson equation was used while in the case of the onset of streamer-like discharges the cylindrical method, discussed in Chapter 5, was used.
Having thus calculated the initial electric field E in the void, in the second step the field dependent parameters can be initialized. In the third step the continuity equations are solved for a sufficiently short time so that the values

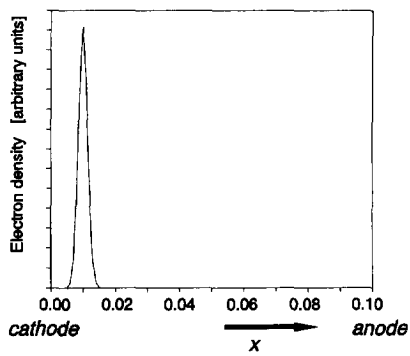

Figure B.1 Initial Gaussian electron distribution in the void.

of the field dependent parameters can be considered constant. Now the process is repeated starting again with the first step of the calculation of the electric field. The calculations are terminated when the current of the moving charges has dropped to 1 promille of its maximum value.

Calculation of Townsend-like discharges

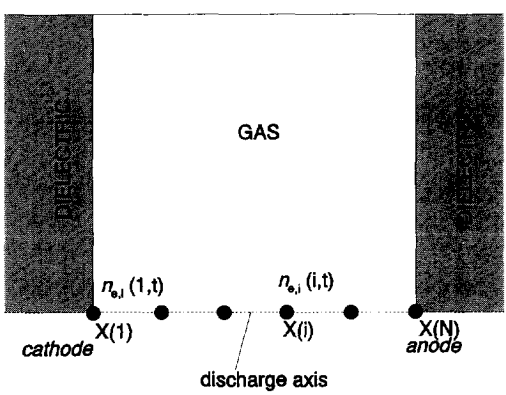

Figure B.2 One-dimensional grid in x used in the calculations.

For the calculations the variations of n_e and n_i with respect to x are considered to take place along a grid in x where a particular value of x is specified in terms of an integer i, as is shown in Figure B.2. Thus X(1) corresponds to $x=0$, or the cathode, and X(N) corresponds to $x=h$, or the anode, where N is the total number of grid points in x. In the method used for the calculation t is treated as a continuous variable.
The partial derivative in x is replaced by an algebraic approximation evaluated at point i. This leads to a system of differential equations in t with t as the only independent variable. Figure B.3 shows a flow diagram of the calculations.
It was assumed that the Townsend-like discharge covers the total surface of the void.

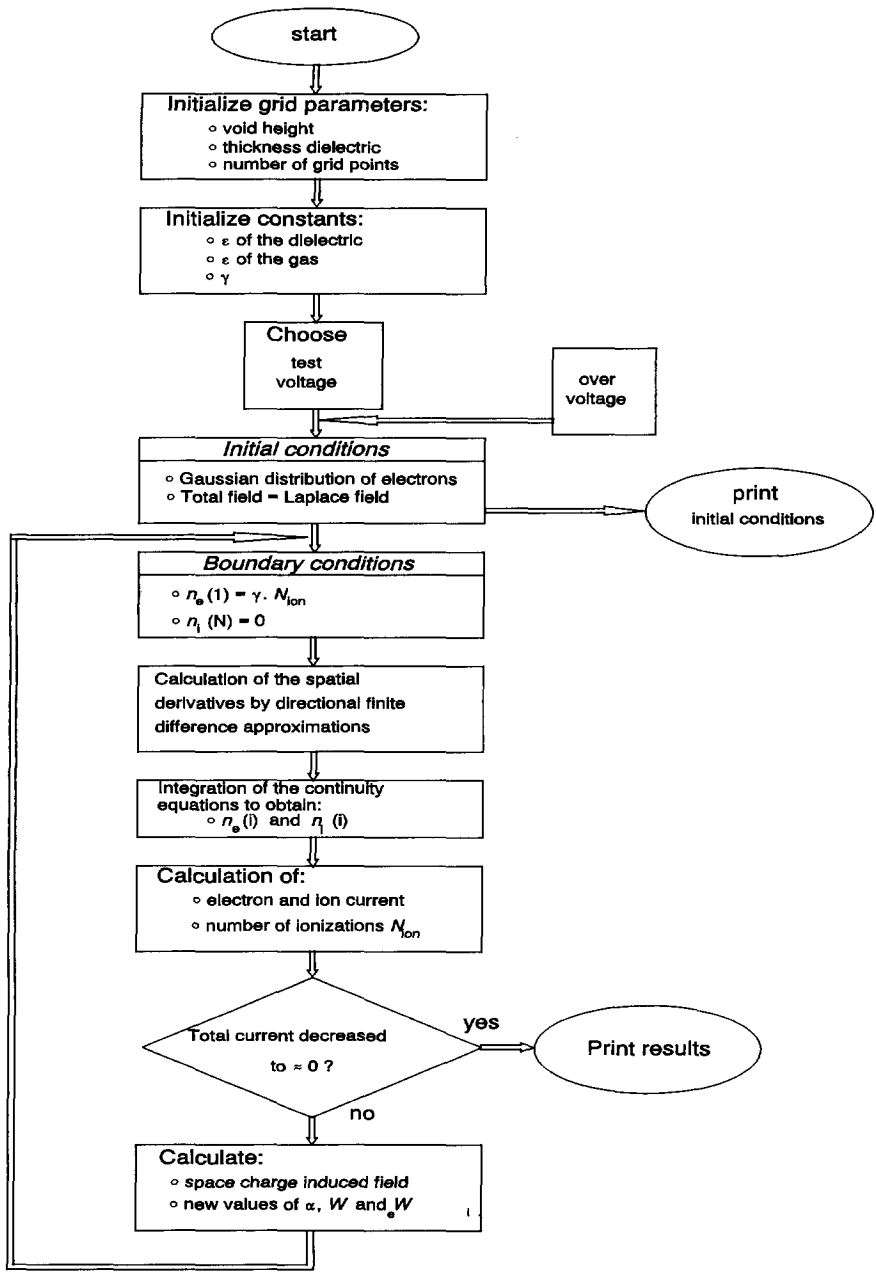

Figure B.3 Flow diagram illustrating the procedure for solving the set of differential equations.

Calculation of the onset of streamer-like discharges

For these calculations the same method was used as described for the Townsend-like discharges, with one exception. The use of the one-dimensional Poisson equation is no longer permitted, the diameter of the discharge is small compared to the height of the void (The diameter is in the order of μms in stead of mms in the case of Townsend-like discharges). Therefore, as an approximation of the two-dimensional case, the cylinder method was adopted. Because these calculations were meant to be indicative only, a further simplification was used: for the calculation of the space charge induced field the presence of the dielectric was disregarded.
An example is shown in Figure B.4 where the electric field of a homogeneous charge distribution (n_e= constant) is plotted against x. Curve *a* represents the field calculated with a two-dimensional finite element program taking into account the presence of the dielectric. Curve *b* represents the field calculated with the method described above. For comparison the profile of the electric field calculated with the one-dimensional Poisson equation is shown as well by curve *c*. This leads to an error in the calculations of some 30%.
The evolution of the discharge current is further calculated using the flow diagram in Figure B.3.

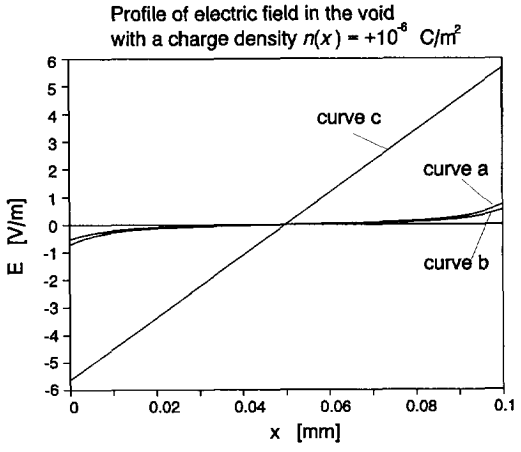

Figure B.4 Profile of electric field of a homogeneous charge distribution calculated using **a.** a two-dimensional field calculation program, **b.** the cylindrical method, **c.** the one-dimensional Poisson equation.

Acknowledgements

I would like to thank my promotor, professor Kreuger, for his continuous encouragement. To my colleagues of the High-Voltage Laboratory I am grateful for their support and understanding in times of thesis-stress.

Samenvatting

Isolatieconstructies in hoogspanningsapparatuur kunnen worden aangetast door partiële ontladingen. Vooral ontladingen in holten, ontstaan door onvolkomenheden in het produktieproces, kunnen de kwaliteit van de isolatie negatief beïnvloeden. De voortdurende inwerking van de ontladingen tijdens de bedrijfsvoering van het hoogspanningsobject kan op den duur leiden tot een complete doorslag van het isolatiemateriaal.

Tijdens dit verouderingsproces is het mechanisme van de ontladingen voortdurend aan veranderingen onderhavig. Dit proefschrift beschrijft de verandering van het ontladingsmechanisme in holten omsloten door een kunststof isolatiemateriaal, met als doel een maatstaf te vinden voor de mate van aantasting.

Hoofdstuk 1 geeft een algemene inleiding waarin ontladingsmechanismen en ontladingsdetektie-methoden worden besproken.

Een specificatie van de toegepaste meetmethoden wordt gepresenteerd in hoofdstuk 2. Hier is gebruik gemaakt van het feit dat belangrijke informatie over het ontladings*mechanisme* besloten ligt in de vorm van de ontladingsstroom. Met behulp van een "time-resolved" ontladingsdetectiesysteem met een bandbreedte van 1 GHz kan deze informatie worden ontsloten. De ruimtelijke uitbreiding van een ontlading kan worden bestudeerd met een optisch registratiesysteem. Door gebruik te maken van een synchrone time-resolved en optische registratie kan een verband worden gelegd tussen de aantasting van het isolatiemateriaal en een aantal ontladingsparameters.

In hoofdstuk 3 worden de resultaten besproken van ontladingsmetingen aan luchtschollen omgeven door een kunststof isolatiemateriaal. De resultaten wijzen op een evolutie van het ontladingsmechanisme als functie van de tijd. Drie opeenvolgende stadia kunnen worden onderscheiden tot aan het moment van significante aantasting van het isolatiemateriaal. Dit zijn het *streamer* mechanisme, het *Townsend* mechanisme en het *pitting* mechanisme.

Een fundamentele discussie van de meetresultaten is te vinden in hoofdstuk 4. Verschillende -experimenteel ondersteunde- theorieën zijn opgesteld om de gevonden ontladingsmechanismen, alsmede de overgangen tussen de mechanismen, te verklaren.

In hoofdstuk 5 worden de resultaten gepresenteerd van berekeningen van de vorm van de ontladingsstroom. Met behulp van een mathematisch model van het ontladingsproces wordt de invloed van een aantal parameters op het verloop van de ontladingsstroom beschreven.

Hoofdstuk 6 gaat tenslotte in op de mogelijkheid de time-resolved detectie-methode toe te passen voor diagnostische doeleinden. Hiertoe is een operator gedefinieerd, de *moving median* van de pulsbreedte, die met succes is aangewend bij het herkennen van het ontladingsmechanisme. Hierdoor kan het stadium waarin het verouderingsproces zich bevindt worden onderkend.

Curriculum vitae

Peter Morshuis was born in The Hague, the Netherlands on December 23, 1959.
In 1978 he obtained the VWO diploma from the Stedelijk Gymnasium in Leiden. He received the M.Sc. degree in electrical engineering in 1986 at Delft University of Technology.
From 1986 to 1988 he was engaged in a research project of NKF Kabel on the influence of contaminations on polyethylene cable life. In april 1988 he joined the High Voltage Laboratory of Delft University of Technology as a staff member. He performed research on the ageing of solid dielectrics due to partial discharges in voids, leading to this thesis.